ROMA TRE
UNIVERSITÀ DEGLI STUDI

Biomedical Sciences and Technologies

XXXVIII cycle

Study of adaptive immune responses induced by viruses in multiple sclerosis

Alice Verdiani

firma

Giovanna Borsellino

firma

Luca Battistini

Docente Guida/Tutor: Prof.

firma

AlessandraSacchi

Coordinatore; Prof.

firma

Index

- **Abstract** 3
- **Summary** 6
- **1. Aims** 9
- **2. Introduction** 10
  - **2.1 Life, death and miracles of T lymphocytes** 10
    - a) *General overview of the immune system* 10
    - b) *Lymphocytes T development, differentiation and functions* 15
    - c) *T cells' contribution in autoimmune diseases* 24
  - **2.2 Multiple Sclerosis** 25
    - d) *Pathology and characteristics of MS* 25
    - e) *Viral infection and their relevance in MS* 28
    - f) *Hints on current treatments and therapies* 30
  - **2.3 Role of T cell activation in MS and other neurological diseases** 31
    - g) *T cells and MS: a long, intertwined story* 31
    - h) *Bystander activation in MS* 32
    - i) *Alzheimer's disease and T cell-driven inflammation* 34
- **3. Materials and Methods** 38
  - **3.1 Study design** 38
  - **3.2 Cell Isolation and counting** 38
  - **3.3 Feeder cells generation** 39
  - **3.4 Cell culture** 39
  - **3.6 Activation Induced Markers (AIM) assay** 40
  - **3.7 Proliferation assay** 40
  - **3.8 Flow cytometry staining and acquisition** 40
  - **3.9 PMA and Ionomycin stimulation assay** 43
  - **3.10 Cell Sorting** 43
  - **3.11 Single cell RNA sequencing** 45
  - **3.12 TCR analysis** 46
  - **3.13 Mice** 48
  - **3.14 Intra Cisterna Magna (ICM) and Intra Venous (IV) mice injection** 49
  - **3.15 T cell isolation and staining from mice brains** 49
  - **3.16 Tissue Preparation** 50
  - **3.17 Immunofluorescence staining** 50
  - **3.18 Confocal microscopy** 51

- **3.19 Statistical analysis** 51
- **4. Results** 52
  - **4.1 Identification and phenotyping of antigen-specific and bystander T cells induced by different viral peptides stimulation in HD and MS patients** 52
    - j) *Identification of virus-specific and bystander AIM+ T cells in both HD and MS patients* ... 52
    - k) *Antigen-specific AIM+ CD4+ T cells exhibit a more central memory phenotype than bystanders in both HD and MS patients* 56
    - l) *Bystander AIM+CD4+ T cells express higher levels of CCR6 than antigen-specific T cells* 58
  - **4.2 Bystander T cells possess inflammatory Th17 and Th1-17 phenotypes *in vitro* experiments** 62
    - m) *Sorted bystander T cells show lower levels of peptide-induced activation than sorted antigen-specific T cells in vitro* 62
    - n) *Bystander CD4+ T cells produce a set of cytokines compatible with Th17 and Th1-17 phenotypes* 64
  - **4.3 Characterization of antigen-specific and bystander T cells in 3 HD and 3 naïve MS patients through scRNAseq** 66
    - o) *Acrtivated bystander T cells are contained within two clusters, characterized by inflammatory and interferon-driven gene expression.* 66
    - p) *CD3 high and cytokine-stimulated samples show higher levels of pro-inflammatory genes* 71
    - q) *MS patients possess some CDR3 sequences specific for myelin-associated proteins.* 77
  - **4.4 Phenotypization of brain-T cells in a mice model of Alzheimer's disease** 82
    - r) *Both CD4+ and CD8+ T cells are present in the brain parenchyma of WT mice* 82
    - s) *5xFAD mice show higher levels of CD8+ T cells infiltration in parenchyma of different brain regions* 84
- **5. Discussion and Conclusion** 89
- **References** 95

Abstract

Titolo: Studio della risposta immunitaria adattativa indotta da virus nella sclerosi multipla

La sclerosi multipla (SM) è una malattia infiammatoria cronica che può portare a una disabilità progressiva nel tempo. L'eziologia della malattia rimane sconosciuta, sebbene una predisposizione genetica e fattori ambientali siano stati associati alla sua insorgenza. Le infezioni virali svolgono un ruolo cruciale nello sviluppo di diverse malattie autoimmuni e la SM non fa eccezione. Un ambiente pro-infiammatorio generato da cellule T virus-specifiche può attivare cellule T autoreattive attraverso meccanismi indipendenti dal TCR. Queste cellule T attivate indirettamente (bystander), cioè attivate dall'ambiente citochinico/infiammatorio generato dalla risposta antivirale e in assenza di riconoscimento diretto dell'antigene non sono state finora ampiamente caratterizzate, e comprendere il loro ruolo nella patogenesi delle malattie autoimmuni è di fondamentale importanza.

L'obiettivo principale di questo progetto è stato quello di ottenere un ritratto fenotipico e trascrittomico completo delle cellule T bystander. È stato messo a punto un sistema in vitro per modellare una risposta immunitaria antivirale, stimolando PBMC con pool di peptidi virali e analizzandole mediante citometria a flusso ad alta dimensionalità. Questo approccio ha permesso di separare le cellule T antigene-specifiche da quelle attivate indirettamente (bystander), sfruttando un principio classico dell'immunologia T: il riconoscimento cognato peptide–MHC induce una rapida modulazione verso il basso del complesso TCR/CD3 (internalizzazione/down-modulation), fenomeno legato al "serial triggering" dei TCR. Pertanto, le cellule T che riconoscono direttamente l'antigene sono state identificate come CD3 low, mentre le cellule che si attivano prevalentemente per effetto del milieu infiammatorio/citochinico mantengono un'espressione CD3 high.

Per ricreare in modo controllato una condizione di attivazione bystander, sono state inoltre stimolate PBMC con un cocktail di citochine definito sulla base dei mediatori presenti nei surnatanti delle colture peptide-stimolate, ottenendo un'attivazione robusta in assenza di stimolo antigene-specifico e con mantenimento di CD3 ad alti livelli (CD3 high), coerentemente con la definizione di bystander activation come attivazione non guidata dal riconoscimento dell'antigene.

Le principali sottopopolazioni (cellule T CD3 low antigene-specifiche; cellule T CD3 high bystander; e una frazione CD69+ attivata all'interno delle CD3high) sono state quindi purificate mediante sorting. Una quota è stata destinata a single-cell RNA-seq integrata con sequenziamento V(D)J/TCR, mentre un'altra quota è stata messa in coltura per stabilire linee e cloni e riesaminarne le proprietà

funzionali, inclusa la produzione di citochine e la capacità proliferativa, in risposta sia a pool peptidici virali sia a stimoli clonali/policlonali.

Sebbene i nostri risultati non abbiano mostrato una maggiore frequenza di cellule T bystander nei pazienti con SM rispetto ai controlli sani, le cellule T bystander hanno espresso livelli più elevati di CCR6, un marcatore associato alle cellule Th17 e Th1-17 patogeniche e all'infiltrazione nel sistema nervoso centrale (SNC). Al contrario, le cellule T CD4+ antigen-specifiche sono risultate principalmente caratterizzate dall'espressione di CD137.

In linea con un fenotipo pro-infiammatorio, gli esperimenti in vitro hanno dimostrato che le cellule T bystander producono una combinazione di citochine associate ai profili Th17 e Th1-17, tra cui IFN-γ, IL-17 e IL-22, dopo stimolazione con phorbol 12-myristate 13-acetate (PMA) e ionomicina, mentre le cellule T antigene-specifiche producono prevalentemente IFN-γ. Inoltre, le cellule T bystander e CD69+ hanno mostrato una capacità proliferativa ridotta rispetto alle cellule T antigene-specifiche in risposta alla stimolazione con pool di peptidi virali.

L'analisi trascrittomica a singola cellula ha identificato due cluster (cluster 0 e 7) arricchiti nei campioni stimolati con citochine e nei campioni bystander. Tali cluster sono caratterizzati da un'elevata espressione di geni associati all'infiammazione, tra cui *ltb, il32, ccr2, ccr6, il22* e *tnfsf13b* (BAFF), coerente con un fenotipo Th17-like attivato. In particolare, il cluster 7 è risultato esclusivo delle cellule T bystander purificate sia da HD sia da pazienti con SM ed è caratterizzato dall'espressione di geni stimolati dall'interferone (IFIT), indicativi di una forte risposta antivirale.

L'analisi del repertorio del TCR ha inoltre evidenziato una maggiore frequenza di clonotipi CDR3 connessi nei pazienti con SM rispetto agli HD, suggerendo una maggiore capacità di riconoscimento antigenico. Inoltre, le cellule T provenienti da persone con SM (pwMS) contenevano clonotipi precedentemente identificati nel tessuto cerebrale e nel sangue periferico di pwMS in tutte le condizioni di stimolazione. Clonotipi specifici per la peripheral myelin protein 22 (PMP-22) un autoantigene coinvolto nella neurite autoimmune sperimentale e nella sindrome di Guillain–Barré—o per la myelin basic protein (MBP) erano condivisi rispettivamente da due e da un paziente con SM della nostra coorte.

In conclusione, i nostri risultati indicano che i linfociti T che, dopo stimolazione con peptidi virali, aumentano i marker di attivazione pur mantenendo elevata l'espressione di CD3 e senza la firma canonica del riconoscimento antigenico rappresentano una popolazione verosimilmente bystander. Questa popolazione è arricchita in cellule con un profilo nettamente proinfiammatorio e con marcate

capacità di migrare nei tessuti, e si concentra in specifici cluster trascrizionali caratterizzati dall'espressione di mediatori infiammatori e di molecole che sostengono l'attivazione e il reclutamento di altre cellule immuni.

Dal punto di vista immunologico, il dato più rilevante è che queste cellule non vanno interpretate solo come effettrici transitorie dell'infiammazione, ma come potenziali promotrici di microambienti meningei favorevoli all'organizzazione di tessuto linfoide terziario. In questo modo possono contribuire a mantenere nel tempo condizioni permissive per l'espansione e la selezione di risposte autoreattive nel sistema nervoso centrale, offrendo una chiave di lettura unificante tra attivazione innescata da stimoli infettivi, persistenza dell'infiammazione e cronicizzazione della malattia.

Summary

Multiple sclerosis (MS) is a chronic inflammatory disease that can lead to progressive disability over time. The etiology of the disease remains unknown, although genetic predisposition and environmental factors have been associated with its onset. Viral infections play a crucial role in the development of several autoimmune diseases, and MS is no exception. A pro-inflammatory environment generated by virus-specific T cells can activate autoreactive T cells through TCR-independent mechanisms. These indirectly activated (bystander) T cells—i.e., cells activated by the cytokine/inflammatory milieu generated by the antiviral response in the absence of direct antigen recognition—have so far not been extensively characterized, and understanding their role in the pathogenesis of autoimmune diseases is of fundamental importance.

The main objective of this project was to obtain a comprehensive phenotypic and transcriptomic portrait of bystander T cells. An in vitro system was established to model an antiviral immune response by stimulating PBMCs with pools of viral peptides and analyzing them using high-dimensional flow cytometry. This approach made it possible to distinguish antigen-specific T cells from indirectly activated (bystander) cells by exploiting a classic principle of T-cell immunology: cognate peptide–MHC recognition induces rapid down-modulation of the TCR/CD3 complex (internalization/down-modulation), a phenomenon linked to "serial triggering" of TCRs. Accordingly, T cells directly recognizing antigen were identified as CD3 low, whereas cells activated predominantly by the inflammatory/cytokine milieu retained high CD3 expression (CD3 high).

To reproducibly generate a condition of bystander activation, PBMCs were also stimulated with a cytokine cocktail defined on the basis of mediators present in the supernatants of peptide-stimulated cultures. This resulted in robust activation in the absence of antigen-specific stimulation and with maintenance of high CD3 expression (CD3 high), consistent with the definition of bystander activation as antigen-independent activation.

The main subpopulations (CD3 low antigen-specific T cells; CD3 high bystander T cells; and a CD69+ activated fraction within the CD3 high population) were then purified by cell sorting. A fraction of the cells was subjected to single-cell RNA sequencing integrated with V(D)J/TCR sequencing, while another fraction was cultured to establish lines and clones and to reassess their functional properties, including cytokine production and proliferative capacity, in response to both viral peptide pools and clonal/polyclonal stimuli.

Although our results did not show an increased frequency of bystander T cells in patients with MS compared with healthy donors, bystander T cells expressed higher levels of CCR6, a marker associated with pathogenic Th17 and Th1-17 cells and with infiltration into the central nervous system (CNS). In contrast, antigen-specific CD4+ T cells were mainly characterized by expression of CD137.

Consistent with a pro-inflammatory phenotype, in vitro experiments demonstrated that bystander T cells produce a combination of cytokines associated with Th17 and Th1-17 profiles, including IFN-γ, IL-17, and IL-22, following stimulation with phorbol 12-myristate 13-acetate (PMA) and ionomycin, whereas antigen-specific T cells predominantly produce IFN-γ. In addition, bystander and CD69+ T cells displayed a reduced proliferative capacity compared with antigen-specific T cells in response to stimulation with viral peptide pools.

Single-cell transcriptomic analysis identified two clusters (clusters 0 and 7) enriched in cytokine-stimulated samples and in bystander samples. These clusters are characterized by high expression of inflammation-associated genes, including *ltb, il32, ccr2, ccr6, il22,* and *tnfsf13b* (BAFF), consistent with an activated Th17-like phenotype. Notably, cluster 7 was exclusive to purified bystander T cells from both healthy donors and patients with MS and was characterized by the expression of interferon-stimulated genes (IFIT), indicative of a strong antiviral response.

Analysis of the TCR repertoire further revealed a higher frequency of connected CDR3 clonotypes in patients with MS compared with healthy donors, suggesting greater antigen recognition potential. Moreover, T cells from people with MS (pwMS) contained clonotypes previously identified in brain tissue and peripheral blood of pwMS under all stimulation conditions. Clonotypes specific for peripheral myelin protein 22 (PMP-22)—an autoantigen involved in experimental autoimmune neuritis and Guillain–Barré syndrome—or for myelin basic protein (MBP) were shared by two and one patients with MS in our cohort, respectively.

In conclusion, our results indicate that T lymphocytes which, following stimulation with viral peptides, upregulate activation markers while maintaining high CD3 expression and lacking the canonical signature of antigen recognition represent a likely bystander population. This population is enriched in cells with a strongly pro-inflammatory profile and marked tissue-migratory capacity and is concentrated in specific transcriptional clusters characterized by expression of inflammatory mediators and molecules that support activation and recruitment of other immune cells.

From an immunological perspective, the most relevant finding is that these cells should not be interpreted merely as transient effectors of inflammation, but rather as potential promoters of meningeal microenvironments conducive to the organization of tertiary lymphoid tissue. In this way, they may contribute to the long-term maintenance of permissive conditions for the expansion and selection of autoreactive responses within the central nervous system, providing a unifying framework linking infection-triggered activation, persistence of inflammation, and disease chronicity.

1. Aims

The aims of this study are to unravel how viral infections impact T lymphocytes, particularly in the context of brain inflammation and MS. Our hypothesis is that an infection-derived inflammatory environment might induce the TCR-independent activation of pathogenic T cells, known as bystander T cells. This work is primarily focused on finding biological markers to unmistakably identify and phenotype bystander T cells, and to study their immunologic potential and antigen reactivity.

To accomplish this goal and achieve the most comprehensive characterization possible, we employed several techniques, including multicolour flow cytometry, *in vitro* assays, and single-cell RNA sequencing (scRNA-seq). Then, the last part of this project focus on T cell characterization in the context of another neurodegenerative disease: Alzheimer's.

2. Introduction

2.1 Life, death and miracles of T lymphocytes

General overview of the immune system

1. What's the immune system?

The immune system is a sophisticated defence mechanism that protects us against pathogen invasion, thereby ensuring -in most cases- our survival.

Host protection has been essential ever since the appearance of the first living organisms. To preserve cellular integrity, homeostasis, and survival, various strategies have evolved, beginning with restriction enzymes and clustered regularly interspaced short palindromic repeats (CRISPRs) in prokaryotic cells, and then progressively increasing in complexity and efficiency alongside the evolution of eukaryotic cells [1].

Phagocytosis, for example, is a highly conserved ability of certain immune cells and was first acquired by unicellular amebae[2]. However, a true game changer in host protection -and reproduction- was the acquisition of the capacity to discriminate "self" and "non-self", a property found in both unicellular and multicellular organisms. This ability relies on cellular receptors that bind, engulf, phagocytose, or kill invading agents [3].

Then, another major evolutionary breakthrough was the acquisition of jaws in vertebrates. This event led to the almost coincident emergence of the adaptive immune system in these animals, and it is also referred to as the "immunological big bang". The adaptive immune system likely evolved exclusively in jawed vertebrates due to their newly acquired predatory lifestyle, which resulted in increased injuries in the feeding apparatus and greater microbial exposure through the ingestion of diverse prey species - factors that created the need for a more specific, efficient and -most importantly- memory protective system [4]. The ability to recognize already encountered pathogens and rapidly respond to their invasion is a key feature of adaptive immunity.

What makes this development even more remarkable is that it required additional prerequisites: the presence of an ancestral immunoglobulin (Ig) molecule and the enzymes necessary for DNA recombination, known as RAGs [5].

2. How is the immune system composed?

In humans, as well as in most of the other mammals, the immune system can be divided in two major branches: the innate and the adaptive immune system. The former is the most ancient, non-specific and fast-acting; the latter is pathogen-specific and slower.

The immune system can also be divided into cellular components -comprising several subsets of specialized cells- and humoral components, which include the complement system and the various pro- and anti-inflammatory cytokines produced by immune cells[6,7]. In this section, the main cell subsets, along with a brief explanation on their purposes and characteristics, composing both the innate and adaptive immune system will be discussed.

The innate immune system is extremely heterogeneous, comprising several subsets of cells with distinct origins, wide-ranging functions and capabilities:

- Granulocytes (neutrophils, eosinophils, basophils and mast cells)

These cells are characterized by the presence of cytoplasmic granules containing proteinases and other degradative enzymes. Neutrophils represent the vast majority of granulocytes in our bodies and constitute the first line of defense against pathogenic microorganisms, as they are the first cells to arrive at sites of infection. Neutrophils possess phagocytic and killing abilities, mediated through granule function and secretion. Among the other subsets, the primary function of eosinophils is protection against parasitic infections, while basophils and mast cells play central roles in allergic immune reactions[8,9].

- Dendritic cells (DCs)

DCs are a heterogeneous family of immune cells that can be broadly categorized by ontogeny into conventional DCs (cDC1 and cDC2), which mainly arise from myeloid progenitors, and plasmacytoid DCs (pDCs), which develop from lymphoid progenitors.
The primary function of DCs is antigen uptake and presentation to T cells, making them professional antigen-presenting cells (APCs). Moreover, DCs produce several cytokines and chemokines, thereby regulating the outcome of immune responses, inducing immune tolerance, and driving negative selection of T cells in the thymus[10].

- Monocytes and macrophages

Monocytes derive from myeloid progenitors in the bone marrow and represent the immature form of tissue macrophages. They circulate in the bloodstream for several days before migrating into tissues, where they differentiate into resident macrophages. The central role of macrophages in homeostasis is highlighted by their tissue-specific differentiation, which grants them distinct names according to their organ of residence - for example, microglia in the brain and Kupffer cells in the liver. Both

monocytes and macrophages can phagocytose, process antigens, and act as APCs. They also express a wide variety of pattern recognition receptors (PRRs) and antigen-presenting molecules, produce cytokines, and participate in inflammation and immune regulation[11,12].

- Natural Killer cells (NKs)

NK cells derive from lymphoid progenitors in the bone marrow but do not express antigen-specific receptors. Their name reflects their intrinsic ability to kill virus-infected and cancer cells through the secretion of cytotoxic granules and the production of pro-inflammatory cytokines. Human NK cells can be categorized based on expression levels of CD56, the 140-kDa isoform of neural cell adhesion molecule (NCAM), into the younger CD56bright ($CD56^{br}$) and the more mature CD56dim ($CD56^{dim}$) subsets. Several studies have demonstrated that $CD56^{br}$ cells are potent cytokine producers, particularly of interferon-γ (IFN-γ), whereas $CD56^{dim}$ NK cells possess greater cytolytic capacity against tumor cells. $CD56^{dim}$ cells also express the low-affinity Fcγ receptor IIIA (CD16), which binds to the Fc region of Igs, thereby activating $CD16^{+}$ NK cells. This activation induces target cell killing through NK-mediated degranulation and perforin release, a process known as antibody-dependent cellular cytotoxicity (ADCC)[13,14].

- Innate Lymphoid Cells (ILCs)

ILCs are a fascinating subset of lymphocytes that lack TCR and BCR but nonetheless play a central role in tissue homeostasis and protection, especially in the intestine, lungs, and adipose tissue. ILCs are divided into three groups (group 1, 2, and 3), containing two, one, and three subsets, respectively. Each group includes cells that share similar cytokine profiles and dependencies on specific transcription factors (TFs) for development and differentiation. Notably, ILC1 cells and conventional NK cells coexist in group 1; group 2 includes only ILC2; and group 3 consists of natural cytotoxicity receptor $(NCR)^{-}$ ILC3, NCR^{+} ILC3, and lymphoid tissue inducer (LTi) cells. ILCs are activated early during immune responses by recognizing signals or cytokines released by tissue-resident cells. They can also express major histocompatibility complex (MHC) class II and process antigens, thereby modulating T-cell responses. ILC1, ILC2, and ILC3 are considered the innate counterparts of $CD4^{+}$ T cells, resembling Th1, Th2, and Th17 cells, respectively (see next chapter: *T Lymphocyte development, differentiation and functions*, section 4)[15].

In contrast to the large number of subsets within the innate immune system, the adaptive system relies primarily on two main components, both of which are lymphocytes. Nevertheless, their specialized

functions and diverse differentiation capacities make this group essential for a fully effective immune response:

- T Lymphocytes

  T cells are the main component of the adaptive immune system, protecting the body against pathogenic invasion and tumour cell proliferation. T lymphocytes are characterized by the expression of the T cell receptor (TCR), which allows them to recognize antigens presented by APCs and subsequently specialize and expand to combat infection. T cells are divided into two major subsets: $CD4^+$ and $CD8^+$ T cells. $CD4^+$ T cells, also called T helper (Th) cells, produce pro- and anti-inflammatory cytokines and assist in B-cell activation, whereas $CD8^+$ T cells generally specialize in cytotoxicity and directly kill infected or cancerous cells[16].

- B Lymphocytes

  B cells represent the second major component of the adaptive immune system. Although less numerous than T cells, they play a fundamental role in host protection. B cells can differentiate into multiple subtypes, and their final maturation step leads to the generation of memory B cells or antibody-secreting cells (ASCs), which produce antigen-specific antibodies and contribute to pathogen clearance, also through cytokine production[17].

3. How the immune response actually works

While the focus of this thesis is on T lymphocytes, their role can only be understood within a broader context. As a matter of fact, no cell works alone, and this is even more true for the immune system. Every member of this wonderful tree is in constant dialogue, generating a complex yet extraordinary symphony of protection.

As previously mentioned, the immune system acts in concert to protect the host from pathogen invasion and other harmful molecules. Innate immune cells represent the first line of defense, acting rapidly and recognizing a wide variety of danger signals through their PRRs and metabolic sensors (MS)[18]. Danger signals can be classified as exogenous, or pathogen-associated molecular patterns (PAMPs), when produced by invading microorganisms, or endogenous, or damage-associated molecular patterns (DAMPs), when derived from injured self-cells, damaged tissues, or metabolic stress[6,7,18,19]. Recognition of DAMPs or PAMPs by PRRs on innate immune cells induces cell activation and results in tissue inflammation due to the release of pro-inflammatory mediators, such as tumor necrosis factor α (TNFα), reactive oxygen species (ROS), and various other cytokines[6,18].

Different PAMPs or DAMPs bind different PRRs, leading to a kind of "danger-specific" cytokine or signaling molecule production by activated innate cells. This results in a tailored immune response through recruitment of specialized immune cells, while also triggering common systemic effects, such as fever[7].

For example, viral infections induce the activation of NK cells and pDCs, through PRRs such as Toll-like receptor 3 (TLR3), TLR7 and TLR9, leading to the production of interleukin 12 (IL-12), IL-15, IL-18, and interferons (IFNs), which activate and recruit NK cells and cytotoxic T cells establishing an anti-viral state; [20] by contrast, extracellular bacteria activate tissue macrophages and classical DCs through PRRs such as TLR2, TLR4 and NOD-like receptors, inducing the production of TNF, IL-1β, IL-6, IL-23 and chemokines (e.g. CXCL8/IL-8), which drives neutrophil and inflammatory monocyte recruitment and a strongly phagocytic response.

While most innate immune cells are engaged in pathogen elimination, some function as APCs, a critical step for the activation of adaptive immunity. APCs capture antigens -specific, unique short peptides released by invading microorganisms - process them, and present them to T cells in the lymph nodes. This allows the maturation of highly specialized, antigen-specific lymphocytes capable of eliminating the particular pathogen[6,7,18]. Simultaneously, a subset of T cells called T follicular helper (Tfh) cells interacts with B cells in the lymph nodes, supporting their differentiation into plasma cells.

Adaptive immune cells require several days to fully differentiate. Once mature, they exit the lymph nodes and migrate to the site of infection, where they help clear pathogens through cytokine production, release of cytotoxic molecules, and generation of antibodies. After the invading microorganism is eliminated, some differentiated antigen-specific T and B cells become memory cells, remaining in the bloodstream ready to respond rapidly to subsequent encounters with the same pathogen[6,7,18]. This process is summarized in Fig.1

Lymphocytes T development, differentiation and functions

1. Where do T cells come from?

T cell development begins in the thymus, a small gland in the lymphatic system, from $CD34^+$ bone marrow-derived thymus progenitors (TPs). In the thymus, human TPs undergo a series of four developmental stages, ranging from double negative 1 (DN1) to DN2, DN3, and DN4, based on CD38 and CD1a expression[21]. In particular, the DN2 and DN3 stages are crucial for commitment to either the conventional αβ or γδ T cell lineages. During the DN2 stage, TCRγ and TCRδ chains begin to

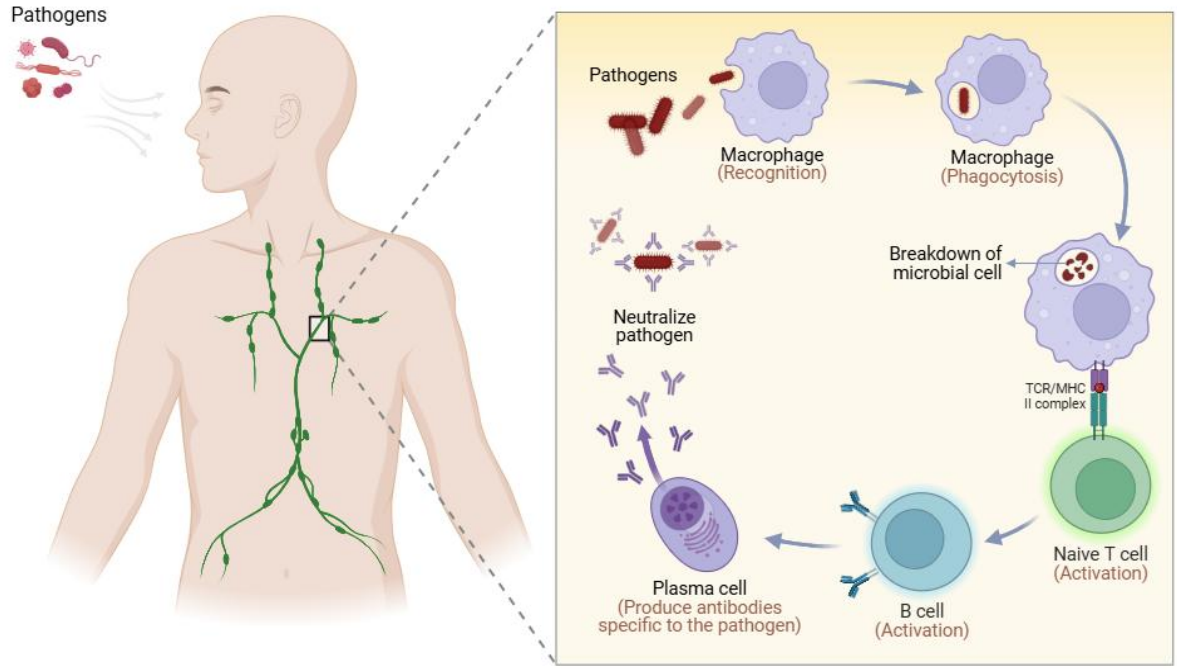

Figure 1. Example of the immune response. Pathogens invade the organism, activating innate tissue-resident cells, in this case a macrophage. The macrophage recognizes and phagocytoses a pathogen, processing and presenting the antigen on its MHC class II. The macrophage functions as an APC for naïve T cells in the lymph node, activating pathogen-specific $CD4^+$ T cells, which then expand and proliferate. A specialized subset of $CD4^+$ T cells, called Tfh cells, interacts with B cells to fully activate them, inducing plasma cell differentiation and antigen-specific antibody production. Both antigen-specific T and B cells subsequently migrate to the site of infection, where they help eliminate the pathogen. Figure template obtained from Biorender.com.

rearrange to form the pre-TCR complex. If a non-functional δ-chain is produced, the T cell will proceed with TCRβ rearrangements[22]. Only DN3 thymocytes expressing a rearranged TCRβ together with an invariant pre-TCRα and CD3 molecules can successfully progress to the DN4 stage and differentiate into conventional αβ T cells; otherwise, they are directed toward the γδ T cell lineage[23,24]. This process, known as β-selection, represents a major checkpoint in T cell development.

A combination of pre-TCR and Notch signalling is required for DN4 thymocytes to transition into Double Positive (DP) CD4+ CD8+ cells[16,23]. In humans, T cells undergo a $CD4^+$ single-positive stage before becoming DP cells, during which TCRα rearrangements occur. DP cells expressing an αβ heterodimer then undergo positive selection, which selects cells capable of binding self-MHC molecules[25].

The final, critically important process that immature T cells encounter is negative selection, during which DP $CD4^+$ and $CD8^+$ T cells bearing high-affinity autoreactive TCRs are eliminated - or at least should be - from the pool of new lymphocytes. This process allows T cells to maintain extensive clonality while keeping the host safe from potentially harmful T cells[26]. Approximately 95% of T cells fail this checkpoint and undergo apoptosis.

Following positive and negative selection, DP cells differentiate into either $CD4^+$ or $CD8^+$ single-positive (SP) cells, depending on the class of MHC (human leukocyte antigen or HLA in humans) expressed - MHC class I for $CD8^+$ and MHC class II for $CD4^+$ - and the strength of their TCR signaling. Strong TCR signaling drives thymocytes toward a $CD4^+$ fate, whereas weak TCR signaling induces $CD8^+$ differentiation. This fate choice is finely regulated by the balance between two antagonistic TFs: Thpok and Runx3, which induce the $CD4^+$ and $CD8^+$ lineages, respectively[16,27]. Described process is recapitulated in Fig. 2.

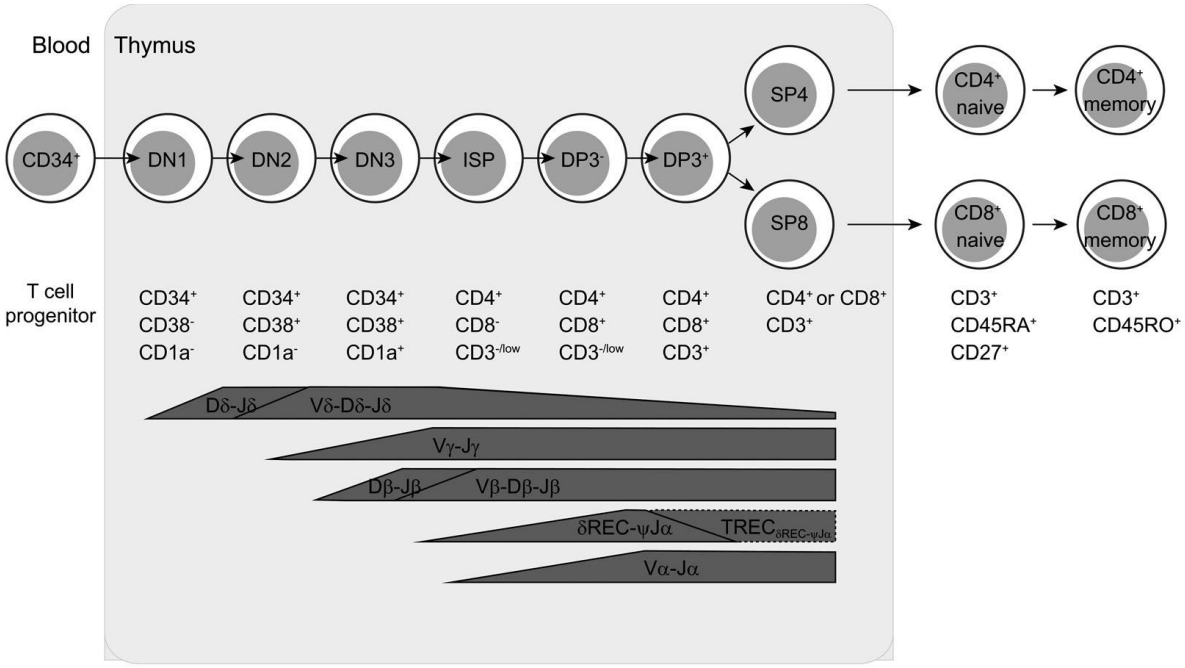

Figure 2. Overview on human T cell development. CD34+ bone-marrow derived progenitors migrate into the thymus, where they undergo a series of developmental stages, beginning from DN1 cells. The most important markers, as well as rearranged chains expressed at each stage, are summarized in the figure. Positive and negative selection occur at the DP3+ stage. Following CD4+ or CD8+ fate decision, naïve T cells are ready to migrate to the periphery.

2. The TCR and T cell activation process

The TCR is a heterodimer composed of two single TCR chains, the most common pairing being TCRα/TCRβ, while only a small percentage (0.5–5%) of T cells express the TCRγ/TCRδ combination[28].

All heterodimers form an octameric complex with the invariant CD3γ, CD3δ, CD3ε, and CD3ζ chains, assembling with a 1:1:1:1 stoichiometry (TCRαβ:CD3δε:CD3γε:CD3ζζ).

The TCR can be divided into an extracellular region, a transmembrane domain, and a cytoplasmic tail, each with specific functions. The extracellular domain binds specific antigens, the transmembrane domain anchors the TCR to the cell membrane, and the cytoplasmic tail transduces signals into the T cell, activating it[29]. Specifically, the extracellular domain contains six hypervariable regions in the paired TCR chains, known as complementarity-determining regions (CDRs), which bind and recognize peptides/antigens loaded on a suitable MHC (pMHC) presented by an APC.

Regarding the cytoplasmic tail, only the CD3 chains contain signaling domains called Immunoreceptor Tyrosine-based Activation Motifs (ITAMs). Each TCR complex contains ten ITAMs distributed among the CD3 subunits. In the absence of pMHC contact, the intracellular regions of the CD3 chains adopt a closed conformation that blocks Lck tyrosin-kinase access to the

ITAMs. Lck-mediated ITAM phosphorylation triggers recruitment and phosphorylation of ZAP-70, activating multiple signaling cascades, including Ca^{2+}–calcineurin–NFAT, PKCθ–IKK–NFκB, RASGRP1–RAS–ERK1/2, and TSC1/2–mTOR. These cascades regulate different aspects of T cell biology, impacting proliferation, differentiation, and cytokine production[28,30].

As previously mentioned, T cells express either CD4 or CD8 on their surface. These co-receptors each consist of extracellular, transmembrane, and cytoplasmic domains. Although they share functional roles, CD4 and CD8 differ structurally: CD4 acts as a monomer, whereas CD8 can form a homodimer or a heterodimer composed of its two isoforms, CD8α and CD8β. The role of these co-receptors is to bind the TCR/pMHC complex, enabling the Lck protein tyrosine kinase to phosphorylate specific ITAMs and initiate signal transduction[31].

Interestingly, following ligation by TCR/pMHC, the TCR complex is rapidly internalized - a phenomenon known as “CD3 downregulation”. This can be observed by flow cytometry and marks recently activated T cells. Resting T cells quickly re-express the TCR complex[32–34].

However, TCR/pMHC/CD4 or CD8 engagement alone is insufficient for full T cell activation, as it only provides signal 1. Two additional signals are required. Signal 2 is mediated by interaction between T cell CD28 and co-stimulatory molecules, such as CD80 or CD86, on the APC surface. Signal 3 is provided by cytokines in the microenvironment[35].

The precise balance and timing of these three signals is crucial for directing T cell differentiation into effector and memory subsets, each with distinct characteristics tailored to specific immune challenges.

3. V(D)J recombination in lymphocytes T

When we think about T cells, we generally associate them with TCR-dependent antigen specificity. Antigen specificity is an extremely powerful capability, allowing fully differentiated T cells to eliminate any invader bearing a particular antigenic sequence. However, without the extremely wide clonality that already exists in naïve T cell subsets, antigen specificity would not be possible.

V(D)J recombination - where V(D)J stands for variable (V), diversity (D), and joining (J) regions of the TCR - is the process that generates the slightly different TCRs that make up the T cell repertoire. V(D)J recombination is a site-specific process that occurs only in developing T lymphocytes and only between TCR gene segments flanked by recombination signal sequences (RSSs)[36]. The enormous diversity of the TCR repertoire primarily arises from the random combination of pre-existing V, D, and J segments. Specifically, the exons of TCRβ and TCRδ chains are assembled from V, D, and J segments, whereas the exons of TCRα and TCRγ chains are assembled from V and J segments.

Briefly, recombination begins with a cleavage in the DNA at the RSS regions, a highly regulated process mediated by lymphocyte-specific recombination-activating genes (RAG1 and RAG2). The V, D, and J segments are then stochastically rearranged using common cellular DNA repair mechanisms (Fig. 3). The DNA portion between the rearranged exons is excised from the genome as a circular signal joint. The number of different TCRs produced by this process depends not only on the combinatorial diversity of the rearranged fragments but also on junctional modifications and the subsequent pairing of the two fully formed TCR chains, resulting in an extraordinary potential of 10^{16} possible combinations in humans[36,37].

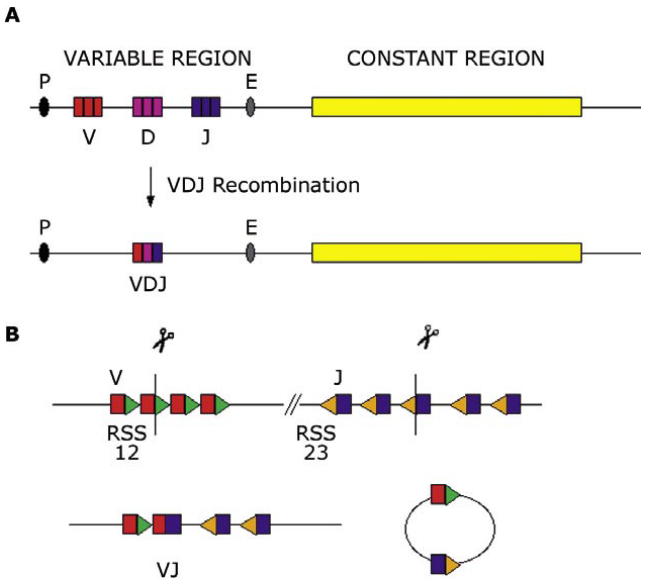

Figure 3. V(D)J recombination. (A) Schematic representation of a V(D)J locus flanking a constant region, shown before and after V(D)J recombination. (B) VJ recombination: V segments are colored in red, while their RSSs, along with 12-bp spacers, are green. J segments are blue, with their RSSs and 23-bp spacers shown in orange. An example of a VJ junction (bottom left) and the resulting circular signal joint (bottom right) is also illustrated. Abbreviations: P, promoter; E, enhancer. Adapted from Market and Papavasiliou, 2003.

4. T cell classification and differentiation

T lymphocytes can be classified based on their differentiation and function. One common classification divides both $CD4^+$ and $CD8^+$ T cells according to their seniority, ranging from naïve to terminally differentiated effector cells.

Following antigen engagement, both naïve $CD4^+$ and $CD8^+$ T cells - generally identified by the expression of CD45RA and CD27 - mature into memory T cell subsets, progressing through several stages during their lifespan, each with distinct functions and capabilities.

The first maturation stage is central memory (CM; $CD45RA^-$ $CD27^+$). These cells are not yet committed to any specific effector phenotype, allowing them to be influenced by the cytokine milieu once they reach the site of infection. They express markers that permit entry into lymph nodes from the peripheral blood (PB), where they are likely to be re-activated[38,39].

The second stage is effector memory (EM; CD45RA$^-$ CD27$^-$). EM cells are the main effectors for fighting infection, being highly efficient at producing pro-inflammatory cytokines and, in some cases, directly killing target cells[16,38,39].

At the end, T cells differentiate into terminal effector memory cells (TEMRA; CD45RA$^+$ CD27$^-$). As the name suggests, this stage characterizes aged EM cells expressing senescence markers, such as KLRG1, and producing high levels of cytotoxic molecules and cytokines[40,41].

Furthermore, once the infection has been cleared, memory T cells can remain in tissues for local immune surveillance. These cells are called tissue-resident memory (Trm) Trm cells and are identified by CD69 expression, an early activation marker also upregulated following antigen recognition. Trm CD8$^+$ T cells additionally express the integrin CD103, which contributes to their tissue retention[38,39].

T cells can also be grouped by their specific phenotypes and effector functions. As concerns CD4+ T cells, also referred to as Th cells, these are a heterogeneous group of lymphocytes that play central roles in immunity and defense against infectious diseases. Following antigen recognition, naïve CD4$^+$ T cells can differentiate into multiple subsets, historically defined by their cytokine production profiles. Expression of specific surface markers and TFs can also be used to distinguish them. Th specialization is driven by particular stimuli present in the microenvironment, as summarized in Table 1.

Subset	Main functions	Differentiation factors	Key TFs	Surface Markers	Cytokines produced
Th1	Protect host against intracellular bacteria and viruses[16]	IFN-γ, IL-12	Tbet	CXCR3+ CCR6-	IFN-γ, IL2
Th17	Protect host against extracellular pathogens, especially at mucosal tissue, and contribute in chronic inflammation and autoimmune diseases[16,42,43]	IL-6, TGF-β	RORγT	CCR6+ CXCR3- CCR4+	IL-17A-F, IL-22, IL-10, IL-23, IL-21

Th1-17	Mostly found in autoimmune diseases[42,43]	IL-12	RORγT, Tbet	CXCR3+ CCR6+	IFN-γ, IL-17, GM-CSF
Th22	Protective role in mucosal inflammation, tissue repair but also involved in autoimmune diseases[44,45]	IL-1β, IL-6, IL-21, IL-23, TNF-α	AHR+,	CCR6+, CCR4+ CCR10+	IL-22, IL-13, TNF-α
Th2	Protect the host against helminth infections, contribute to tissue repair and also chronic inflammation as in allergic reactions[16]	TCF-1, IL-2, IL-4	GATA-3	CRTH2+ CCR4+ CCR6- CXCR3-	IL-4, IL-5, IL-13
T regulatory (Treg)	Maintain immune tolerance by suppressing the immune response[46]	TGF-β, IL-2	FoxP3	CD25high, CD127-	IL-10, IL-35, TGF-β
Tfh	Interaction with B cells, promoting their maturation and proliferation[47]	IL-6, IL-21	Bcl-6	CXCR5+	IL-21, IL-4
Th9	Roles in infectious diseases, allergy, cancer, and autoimmune immunity[16]	IL-4, TGF-β,	PU.1., IRF4, GATA-3	CCR4+, CCR6-	IL-9, IL-10, IL-21

Table 1. CD4+ Th cells subsets characteristics

$CD8^+$ T cells, on the other hand, specialize in the elimination of intracellular pathogens, such as viruses, and malignant cells. EM $CD8^+$ T cells, also referred to as cytotoxic T lymphocytes (CTLs), can directly induce target cell death through both CD95 or Fas/Fas ligand interactions and the combined secretion of cytolytic mediators, such as perforin and granzymes[16]. Although most memory

$CD8^+$ T cells function as CTLs, recent studies have identified additional $CD8^+$ T cell subsets that share transcriptional profiles and cytokine production patterns similar to those of $CD4^+$ T cells, as summarized in Table 2.

Subset	Main functions	Differentiation factors	Key TFs	Surface Markers	Cytokines produced
CTL or Tc1	Antitumoral and antiviral response[48,49]	IL-12	Tbet, EOMES, STAT4	CD49d, IL18R	IFN-γ, Perforin, Granzyme B, TNF-α
Tc17	Contribute to immune response against pathogens such as bacteria and fungi[48,49]	IL-6, TGF-β	RORγT, STAT3	CD161, CD26, CD6, CD39, CD69, CD120b, PD-1	IL-17A
Tfc	Enhancing B responses and antitumoral activity[48,49]	IL-6, IL-21, IL-23, TGF-β	Bcl-6, TCF-1, RUNX3	CXCR5	IFN-γ, IL-4, IL-21
Tc22	Tumor control, some reports protective role in viral infections[48,49]	IL-1β, IL-6, IL-21, IL-23, TNF-α	AHR, STAT1, STAT3, STAT5	IL6R	IL-22, TNF-α
Tc2	Asthma, allergic reactions[48,49]	IL-4	GATA-3, STAT6	CysLT1, BLT-1	IL-4, IL-5, IL-13
CD8+ Treg	Immunosuppressive functions[48,49]	TGF-β	FoxP3	CD103	IL-10, TGF-β
Tc9	Allergic reactions[48,49]	IL-4, TGF-β,	IRF4, STAT6	IL9R	IL-9

Table 2. CD8+ T cells subsets characteristics

5. T cell activation markers

Activated antigen-specific T cells are characterized by the upregulation of a series of surface markers, which can be monitored using flow cytometry. This section provides a summary of some of the most important activation markers.

CD154 (CD40L) is a transiently expressed costimulatory molecule rapidly upregulated on $CD4^+$ T cells after TCR engagement. By binding CD40 on APCs and B cells, CD154 functionally activates DCs, promotes cytokine production, and drives B cell proliferation and class-switching[50,51].

CD137 (4-1BB)**,** a member of the TNF receptor superfamily, is upregulated following TCR stimulation. CD137 provides costimulatory signals for T cell proliferation and cytokine secretion, while also promoting T cell memory and effector differentiation[52].

CD25 (IL-2Rα) is the α chain of the IL-2 receptor. While constitutively expressed at high levels on Tregs, CD25 is also rapidly upregulated in both $CD4^+$ and $CD8^+$ T cells upon activation. IL-2-mediated STAT5 signalling sustains and maintains high CD25 expression on activated T cells[51].

CD69, a type II C-lectin receptor, is implicated in lymphocyte migration and retention within lymph nodes or inflamed tissues. Like CD25, CD69 is an early activation marker following TCR engagement.

CD38 is a nicotinamide adenine dinucleotide (NAD^+) enzyme upregulated during some chronic viral infections, such as HIV-1. CD38 reduces $CD4^+$ T cell death, induces Ca^{2+} influx, and promotes cytokine production. However, CD38 is also highly expressed on exhausted $CD8^+$ T cells and in various malignancies, and its precise role in T cells remains incompletely understood[53].

Interestingly, activated T cells can also express MHC class II molecules, particularly HLA-DR, mainly on CTLs and effector subsets[54,55]. Co-expression of CD38 and HLA-DR on $CD8^+$ T cells has been associated with worse prognosis and reduced survival in patients with COVID-19 and cirrhosis[56,57].

CD278 (ICOS) is another costimulatory molecule expressed by $CD4^+$ T cells after activation. CD278 sustains CD154 upregulation, is highly expressed on Tfh cells, and promotes B cell maturation and survival. Additionally, CD278 plays a key role in modulating Th differentiation and immune tolerance[58].

Finally, activated T cells upregulate checkpoint inhibitors or immunosuppressive markers, such as CD39 and Programmed cell Death 1 or PD-1 (CD279). CD39 is an ectoenzyme that, together with CD73, converts ATP to adenosine, promoting immunosuppression. On activated T cells, CD39 is expressed by Tregs and Th17 cells. $CD39^+$ $CD8^+$ T cells are considered terminally exhausted in chronic viral infections and are associated with poor survival in tumors[59]. PD-1 is one of the most well-known checkpoint inhibitors expressed on activated T cells. During acute infections, PD-1 is transiently upregulated on antigen-specific $CD4^+$ and $CD8^+$ T cells to control immune responses and

prevent autoimmune damage. In chronic infections, continuous antigen exposure leads to sustained PD-1 expression, correlating with T cell dysfunction and exhaustion[60].

T cells' contribution in autoimmune diseases

1. When the immune response becomes pathogenic: autoimmunity

The immune system functions like an orchestra, finely tuned and regulated in all its movements. It is therefore not difficult to imagine what happens when something falls out of balance - this is part of what autoimmunity represents: a disruption. An autoimmune disease (AID) a condition in which the body's immune system attacks its own tissues.

The mechanisms underlying autoimmunity are not yet fully understood. Several predisposing factors have been identified, including an altered microbiome, female sex, specific genetic backgrounds, epigenetic modifications, and even viral infections[61].

Although AIDs can involve both T and B cells, this thesis will focus exclusively on T cell–driven autoimmunity to avoid unnecessary digression.

2. Autoreactive T cells

Autoreactive T cells, as the name suggests, are T cells specific for a "self" antigen. Their pathogenic role has been demonstrated in several AID, such as MS, rheumatoid arthritis (RA), systemic lupus erythematosus (SLE), and type 1 diabetes (T1D)[16].

Interestingly, autoreactive T cells can also be found in healthy donors (HD), although they are more activated and produce higher levels of pro-inflammatory cytokines in AID patients[62,63].

Normally, when a T cell continuously encounters its antigen -as occurs in chronic viral infections or cancer- it becomes exhausted, a state characterized by loss of cytokine secretion, reduced proliferative potential, and upregulation of inhibitory receptors, also called immune checkpoints[64]. It has been hypothesized that autoreactive CD4+ T cells in AID may evade exhaustion, thereby fueling inflammation and also supporting B cells in autoantibody production[61]. Moreover, checkpoint inhibitors - such as PD-1, CTLA-4, LAG-3, VISTA, TIGIT, and TIM-3 - are expressed by both autoreactive and normal T cells, helping suppress excessive immune reactions in HD. Not surprisingly, deficiencies in some of these molecules leads to AID[62,65].

Another theory suggests that peripheral autoreactive T cells are less activated in HD because they rarely encounter their specific self-antigen, which may be sequestered in immune-privileged tissues such as the eye or testis. This quiescent state can be disrupted by infection - for example, by Epstein-

Barr virus (EBV) - or by tissue damage that exposes self-antigens, leading to activation of autoreactive cells and disease development[62].

Among the most pathogenic CD4+ T cell subsets in AID are Th17 and Th1-17 cells. Th17 cells promote inflammation by recruiting pathogenic myeloid subsets and producing pro-inflammatory cytokines in SLE, MS, and RA. Th1-17 cells have also been shown to secrete pro-inflammatory cytokines and cross the blood–brain barrier (BBB) in MS[16,42,66].

Tregs are another CD4+ subset often dysregulated in AID. Both MS and SLE patients exhibit Tregs with dysfunctional phenotypes[67].

Regarding autoreactive CD8+ T cells, they have been implicated in several AID, including Crohn's disease, MS, and T1D[68–70]. These cells produce high levels of cytotoxic molecules, such as IFN-γ, TNF-α, granzyme B, and perforin, resulting in self-tissue damage.

Taken together, these findings highlight the pivotal role of autoreactive T cells in autoimmunity and emphasize the importance of deepening our understanding of their development and functions in both HD and AID patients to improve treatment and prevention strategies.

2.2 Multiple Sclerosis

Pathology and characteristics of MS

1. What's MS?

MS is one of the most common chronic, inflammatory, and demyelinating diseases of the central nervous system (CNS) in young adults, typically presenting in individuals between 20 and 40 years of age. It affects nearly three million people worldwide, particularly in Western countries, and no definitive cure is currently available[71,72].

Although many candidate autoantigens -mainly myelin proteins- have been identified, no single disease-defining autoantigen or autoantibody has been identified.

The first reports of what is now recognized as MS date back to the 19th century. The first accurate description of MS plaques was provided by the eminent neurologist Jean-Martin Charcot in 1868. During that century, many other physicians identified the disease in multiple patients; however, without a deeper understanding of its biology, they were unable to fully treat or comprehend it[73].

Advancing to 1935, Dr. Thomas Rivers at the Rockefeller Institute in New York City induced an MS-like disease in mice by injecting them with myelin under controlled laboratory conditions. This animal model, known as Experimental Autoimmune Encephalomyelitis (EAE), would later become one of the most important tools for studying MS[73].

2. Diagnostic criteria

The diagnosis of MS relies on the McDonald criteria, which combine radiological, clinical, and laboratory features[74]. In particular, magnetic resonance imaging (MRI) and cerebrospinal fluid (CSF) analysis play pivotal roles in MS diagnosis. MS is characterized by the presence of lesions in the brain and spinal cord: oval or round hyperintense areas, or plaques of demyelinated and inflamed white or grey matter, which can be detected by MRI. MRI is also essential for monitoring disease progression over time.

When MRI criteria are not fully met, the presence of IgG oligoclonal bands (OCBs) in the CSF serves as an additional important biomarker for MS diagnosis. At present, MS remains essentially a diagnosis of exclusion, requiring the careful ruling out of alternative diseases, such as Neuromyelitis Optica (NMO) or MOG Antibody Disease (MOGAD), through a thorough assessment of all symptoms and clinical features[74].

3. Pathology and classification of MS

MS manifests with acute neurological symptoms, or relapses, which reflect the localization of lesions within the CNS. The most common initial symptom is unilateral visual impairment or optic neuritis, but MS can also present with unilateral sensory or motor deficits, diplopia, imbalance, or vertigo. Clinical events typically last days to weeks, and recovery from a relapse is generally partial, resulting in the progressive accumulation of disability over time. Other non-specific symptoms include fatigue, mood disturbances, and cognitive dysfunction[72].

MS is traditionally subdivided based on disease activity and clinical progression:

- Relapsing-remitting MS (RRMS): the most common form, characterized by acute relapses followed by remission, during which symptoms partially or completely resolve. Periods of disease inactivity occur between relapses.
- Primary progressive MS (PPMS): affects approximately 10% of patients and is characterized by steady disease progression from onset.

- Secondary progressive MS (SPMS): develops in 50–80% of RRMS patients over 15–20 years, marked by gradual and continuous worsening of symptoms in the absence of relapses.
- Clinically Isolated Syndrome (CIS): represents a first clinical manifestation that does not fulfill all diagnostic criteria for MS; it may or may not evolve into RRMS.

The Expanded Disability Status Scale (EDSS) is a widely used non-linear scale for assessing disease severity and disability in people with MS (pwMS) at onset and during follow-up. Scores range from 0 ("normality") to 10 ("death caused by MS"). EDSS calculation relies on functional system scores, evaluating impairments in areas such as bladder-bowel function, motor performance, and sensory deficits[75]. EDSS, along with MS subtype, clinical manifestations, and diagnostic criteria, is crucial for tracking patients and monitoring neurodegeneration over time.

MS plaques are areas in the CNS where myelin loss impairs neuronal function and signal transmission. In early inflammatory phases, active lesions are characterized by infiltration of T and B lymphocytes. Cortical regions of RRMS plaques also contain activated innate immune cells, including macrophages, microglia, and reactive astrocytes, which contribute to inflammation and tissue damage. In contrast, PPMS and SPMS lesions show lower lymphocyte infiltration, although demyelination persists, likely driven by microglial activation and chronic inflammation[71,76].

Traditionally, RRMS was considered to be inactive between relapses, but recent evidence suggests that disability can accumulate also during periods free of clinical symptoms. This phenomenon, termed Progression Independent of Relapse Activity (PIRA), accounts for MS worsening in nearly 50% of RRMS patients and is thought to result from chronic inflammation driven by innate immune cells in inactive lesions, called "smouldering lesions"[77–79].

4. Environmental and genetic risk factors

The aetiology of MS remains unknown, but several risk factors associated with both disease onset and progression have been identified. Like many other AIDs, MS is strongly linked to specific genetic backgrounds, particularly certain HLA class II regions. Among the HLA alleles most predisposing for MS onset are HLA-DRB1*15:01 and HLA-DQB1*06:02[80]. MS is notably more prevalent in certain geographic regions, such as Northern Europe and Sardinia (Italy). This distribution may be explained by the historical advantages conferred by HLA-DRB1*15:01, which likely protected ancient carriers from novel pathogens as they adopted a pastoral lifestyle[81]. Interestingly, in Sardinia, HLA-DRB1*1501 appears to have a protective effect, while MS susceptibility is associated with other HLA alleles, such as DQB1*03:01[82].

Epidemiologically, MS is more frequent in women than in men, with a female-to-male ratio ranging from 2:1 to 4:1[83].

However, genetic predisposition alone is not sufficient to trigger the disease. Specific environmental factors are crucial for MS onset. Studies have shown that vitamin D deficiency, smoking, Western diet -high in fats and carbohydrates and low in fiber-, gut dysbiosis, and obesity are all important risk factors. The common denominator among these elements is low-grade but persistent inflammation[72].

Among all environmental triggers, viral infections have emerged as particularly significant. In particular, EBV infection has been strongly associated with MS onset, and it has become a major focus of research worldwide due to its ubiquitous presence and potential role in triggering autoimmunity[84].

Viral infection and their relevance in MS

1. Virus-related mechanisms of AIDs induction

Let's take a step back to broaden our perspective: viral infections can trigger several AIDs, not only MS. In this section, the proposed mechanisms by which viruses induce autoimmunity are described.

First, viruses generate inflammation through activation of both innate and adaptive immune responses. Chronic viral infections may contribute to AIDs through three main mechanisms: epitope spreading, molecular mimicry, and bystander activation[85].

- Epitope spreading: During viral infection, hidden or cryptic self-antigens may be released by damaged infected cells. These newly available antigens may be captured by APCs and presented to naïve T cells, thereby recruiting additional autoreactive clones and progressively broadening the autoimmune repertoire[86].
- Molecular mimicry: In this model, TCRs generated against viral epitopes also recognize structurally similar self-peptides. Such cross-reactivity can break tolerance and drive autoimmune pathology when anti-viral T cells engage homologous self-antigens [87,88].
- Bystander activation: Here, the inflammatory milieu generated by virus-specific lymphocytes can activate nearby T cells that are not specific for the infecting virus, independently of cognate antigen recognition. These bystander activated, potentially autoreactive lymphocytes may release cytotoxic molecules and pro-inflammatory mediators, contributing to tissue injury [89]. As this concept is central to this thesis, it will be further explored in the next chapter.

All three mechanisms have been implicated in MS onset. For instance, epitope spreading against proteolipid protein (PLP) and myelin basic protein (MBP) was first demonstrated in EAE, a mouse

model of MS[90]. Furthermore, molecular mimicry between EBV antigens, such as Epstein–Barr nuclear antigen 1 (EBNA-1), and host proteins like GlialCAM has been shown to contribute to MS development. Finally, bystander activation of CD4+ T cells has been linked to enhanced autoimmune pathogenesis in EAE(Lanz et al.; Van Aalst et al.).

2. EBV and MS

Evidence linking viral infections to MS is accumulating, but EBV stands out as the most prominent candidate. EBV is a ubiquitous, double-stranded DNA gamma-herpesvirus, infecting more than 90% of the human population. Primary EBV infection is usually asymptomatic, but the virus has been implicated in a wide range of diseases, from lymphomas to autoimmunity, including MS[93,94].

EBV primarily infects memory B cells, where it establishes a latent state, occasionally reactivating. This reactivation can promote B cell transformation or trigger autoimmunity through molecular mimicry. EBV may also facilitate the generation of myelin autoantigen-recognizing B cell receptors (BCRs), which can capture antigens from the CNS and activate autoreactive CD4+ T cells[95]. High serum titers of EBV-specific antibodies were found in MS patients and both humoral and cellular immune responses towards EBNA-1 were correlated to MS onset[96–98]. Additionally, antibodies targeting the EBV latent membrane protein 1 (LMP1) were shown to cross-react with MBP[99]. Clinically, Infectious Mononucleosis, the symptomatic form of EBV infection, has been associated with a five-fold increase in MS risk[100]. Lastly, a recent pivotal study demonstrated that EBV infection is required for MS onset, showing that EBV-seroconversion precedes disease development by 5-20 years[84].

Research has also focused on EBV-specific T cells, particularly CD8+ subsets. Angelini et al. reported that during MS relapses, there is a selective expansion of $CD8^+$ T cells targeting EBV lytic antigens, coinciding with expression of the same viral proteins in CNS lesions, suggesting a link between intracerebral EBV reactivation and disease exacerbation[101].

Similarly, lesions from MS patients appear enriched with EBV-specific CD8+ T cells[102].

Collectively, these findings underscore the critical need to study EBV-specific T cells in MS, to better understand their role in disease initiation and progression.

3. Other viruses linked to autoimmunity and MS

Other viruses have also been linked to MS or, more broadly, to autoimmunity, including cytomegalovirus (CMV), SARS-CoV-2, and influenza (H1N1) virus.

The impact of CMV on MS remains controversial, with some studies even suggesting a protective role. In MS patients, CMV-associated TCRs appear reduced compared to healthy donors, and CMV seropositivity has been correlated with decreased MS severity[93]. Further research is needed to clarify whether CMV truly confers a protective effect in MS and to elucidate the underlying mechanisms.
Although not directly linked to MS, SARS-CoV-2 - the viruses responsible for COVID-19 - and H1N1 influenza virus have been associated with the onset of several autoimmune diseases, including Guillain-Barré Syndrome, T1D, RA, Narcolepsy type 1, and acute myelitis[103,104].

Hints on current treatments and therapies

1. Treatment of acute disease

The primary goal of MS treatment is to reduce or prevent relapses, while acute therapies are necessary to accelerate symptom recovery and remission. Acute relapses are typically managed with high-dose systemic corticosteroids, which act as immunosuppressive agents, administered for a few days depending on the severity of the episode[72].

2. Disease Modifying Therapies (DMTs)

MS relapses and disease progression are generally managed with DMTs. Currently, 27 DMTs have been approved, differing in their mechanisms of action, clinical efficacy, safety profiles, and routes of administration[72,105].
DMTs can be divided in three main groups:

- Immuno-sequestration – these therapies prevent immune cells from entering the CNS. For example, natalizumab, a monoclonal antibody targeting the integrin VLA-4, blocks lymphocyte migration, while spingosine-1-phosphate (S1P) modulators trap T cells in lymph nodes, preventing their egress.
- Immuno-depletion – these treatments reduce or eliminate entire immune cell subsets. Anti-CD20 monoclonal antibodies deplete B cells, and Cladribine markedly reduces both T and B cell numbers.
- Immuno-modulation – these drugs aim to regulate the immune system and promote less inflammatory phenotypes. Dimethyl fumarate is a representative example[106].

The choice of DMT depends on disease severity, relapse frequency, and drug availability, and must be tailored to each patient[107].

2.3 Role of T cell activation in MS and other neurological diseases

T cells and MS: a long, intertwined story

1. Role of T cells in MS

MS has long been considered a T cell-mediated disease, a view initially supported by data from EAE models. While the T cell-centric perspective has since expanded to include other immune populations, T lymphocytes remain central to MS pathogenesis. Both CD4+ and CD8+ clonally expanded T cells have been identified in lesions and CSF of MS patients, indicating a role for antigen-specific T cells in the disease[108]. Despite extensive research, the precise epitopes recognized by these cells remain largely unknown[109,110]. Earlier studies showed that myelin-reactive T cells exist in both MS patients and HD. The crucial difference is that T cells from MS patients typically display a Th memory phenotype, whereas in HD they are mostly naïve[111]. In EAE models, disease was ameliorated by delivering of altered MBP peptide ligands, mutated at the TCR-binding sites. However, similar experiments in humans only exacerbated the symptoms[112].

CD4+ T cell subsets are strongly implicated in MS. Increased frequencies of both Th1 and Th17 CD4+ T cells have been found in CSF and lesions derived from pwMS, with increased Th17 frequency in CSF during relapses[113]. The role of Th1 and Th17 subsets in human MS is controversial due to the EAE animal model, where genetic depletion of IFN-γ enhances the severity of the disease thus supporting the belief that IL-17 is the principal mediator of EAE[114,115]. Nonetheless, data in humans show a pathogenic role for both IFN-γ and IL-17 in MS.

IL-17 production has been strongly linked to MS activity by several studies. IL-17 messenger RNA (mRNA) has been found in MS plaques and T cells able to secrete IL-17 are enriched in active lesions compared to inactive brain regions[116,117]. Furthermore, elevated levels of IL-17 and IL-22, both produced by Th-17 subsets, in the CSF of pwMS correlate with neutrophil expansion, BBB disruption and lymphocyte infiltration in the brain[111]. Th17 cells can also secrete GM-CSF, which activates CNS myeloid cells and exacerbates inflammation[118]. Th1 cells produce IFN-γ, associated with microglial activation and lesion activity, though some reports remain controversial.[111,114]. Notably, Th1-17 cells have been found to be enriched in EAE and human MS[119].

In the EAE model, which is mainly driven by an inflammatory CD4+ T cells response, CD8+ T cells play a suppressive role[120]. However, in human MS, CD8+ T cells are linked to axonal injury and relapses[121]. Moreover, some CD8+ subsets can produce IL-17, suggesting a more central pathogenic role than previously thought[116]. Lastly, CD8+ T cells produce a wide range of cytotoxic molecules,

such as granzymes and perforins, which correlate to neurologic disability and axonal injury[122]. These findings highlight the involvement of CD8+ T cells in both acute inflammatory and progressive phases of MS.

Overall, while T cells clearly play a pivotal role in MS, further research is needed, particularly to understand their contribution to disease onset. A model summarizing MS immunopathogenesis is presented in Fig. 4.

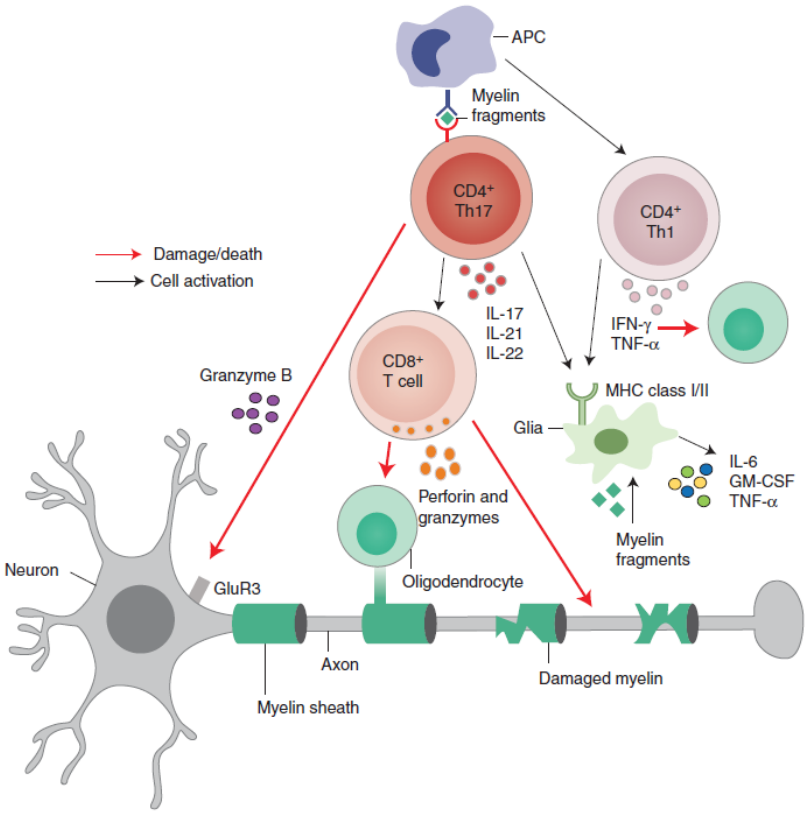

Figure 4. Model of MS immunopathogenesis. An APC presents myelin antigens to CD4+ T cells, including Th17 and Th1 subsets, which secrete pro-inflammatory cytokines such as IL-17, IL-22, TNF-α, and IFN-γ. This inflammatory environment activates microglia and CD8+ T cells, which release additional pro-inflammatory cytokines and cytotoxic molecules, leading to oligodendrocyte death and myelin damage. Th17 cells can also directly contribute to neuronal loss. Adapted from Kaskow and Baecher-Allan, 2018.

Bystander activation in MS

1. Theories on MS onset

Theories on the initiation of MS can be broadly divided into two major groups:

- Outside-in, peripheral activation of CNS-specific immune cells: In this model, self-reactive lymphocytes are first activated outside the CNS. Their activation may be driven by molecular mimicry, epitope spreading or bystander activation. Once activated, these cells migrate across the BBB, produce pro-inflammatory cytokines and chemokines, disrupt astrocyte homeostasis, and recruit additional innate and adaptive immune subsets into the CNS[110,123].
- Inside-out, primary CNS insult: According to this theory, a local insult - likely an infection - triggers microglial activation and local inflammation. This initial event then recruits adaptive

and innate immune cells to the CNS. Subsequently, CNS antigens, possibly transported by DCs, reach peripheral lymph nodes and activate autoreactive lymphocytes in the periphery[110,124].

2. Bystander activation in AIDs and MS

The term "bystander activation" refers to a TCR-independent activation of T cells that are not specific for the pathogen currently being fought but happen to be present in, or recirculate through, the inflamed tissue. In this context, inflammatory cytokines and other soluble mediators released during infection (e.g. type I IFNs, IL-12, IL-15, IL-18) can activate these fortuitously located T cells in the absence of cognate antigen recognition (Fig. 5).

During acute viral infections, bystander-activated $CD8^+$ T cells have been reported to contribute to tissue damage rather than to pathogen clearance, primarily through the unspecific release of cytotoxic granules[125–127]. In contrast, bystander $CD4^+$ T cell activation has mostly been observed post-vaccination, and its functional consequences remain unclear(Li Causi et al.; Di Genova et al.; Van Aalst et al.). Studies in healthy infections show no direct contribution of bystander T cells to pathogen clearance, although their presence may suggest potential antitumoral roles[131].

Several cytokine cocktails can induce bystander activation. Bystander CD8+ T cells have been reported to be activated by IL-15, IL-12 and IL-18. In particular, IL-15 seems to be a crucial cytokine in the CD8+ bystander context[132]. Activated bystander CD8+ express CCR5, cytotoxic molecules such as granzyme B and perforin, and also NK-like markers as NKG2D[131,132]. Notably, bystander activation in CD4+ T cells seems to be related to slightly different cytokines, such as IL-1 family, IL-2, IL-12, IL-23 and IL-27[133]. At the moment no specific set of markers is able to precisely identify bystander -especially CD4+- T cells.

Bystander activation is a proposed model of virus-induced autoimmunity and it has been reported in several AIDs. In autoimmune hepatitis, influenza infection triggered CD8+ T cell activation that damaged the liver in absence of the virus[134]. Multiple microbes, such as *Porphyromonas gingivalis*, *Proteus mirabilis*, EBV, and *Mycoplasma* contributed in RA development and exacerbation[135]. In celiac disease, dysregulated IL-15 expression lead to the activation of NK-like bystander CD8+ T cells[136]. Conversely, in SLE NKG2D+ CD4+ bystander T cells had a protective role and produced anti-inflammatory cytokines such as IL-10 and TGF-β[137].

In the EAE model, CNS-infiltrating effector CD4+ cells were reported for being non-specific for myelin oligodendrocyte glycoprotein (MOG) and that these T cells expressed high levels of pro-inflammatory IL-17, GM.CSF and IFN-γ, suggesting that non-antigen-specific CD4+ T cells might

contribute to CNS inflammation[138]. Bystander CD4+ T cells isolated from MS patients expressed IL-1 receptor 1 (IL1R1), TLR2 and TLR4, normally associated with innate immune cells. Stimulation of these receptors led to increased production of IL-6, IL-17A, IFN-γ, and GM-CSF[139]. Moreover, systemic LPS injection was shown to trigger EAE relapse via bystander activation[140].

These findings support a role for bystander activation in both MS onset and progression. However, a comprehensive phenotypic and functional characterization of bystander T cells is still lacking and is necessary to fully understand their contribution to disease pathogenesis.

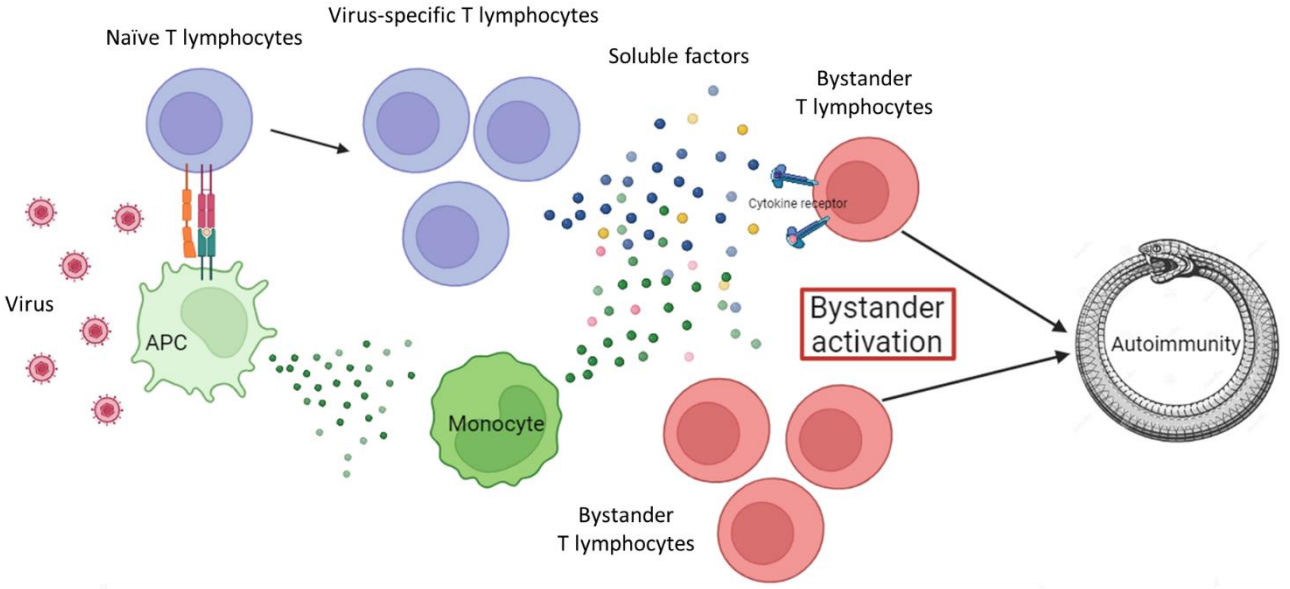

Figure 5. Bystander activation. A viral infection induces naïve T cells activation by APCs antigen-presentation. Antigen-specific T lymphocytes fight the virus producing cytokines and other soluble factors. Non-specific T lymphocytes, or bystander, gets activated by the cytokines present in the inflammatory environment. The unspecific nature of bystander T cells prompt them to even attack healthy cells, thus leading to autoimmunity. Bystander T lymphocytes can also be low-affinity autoreactive T cells whose only need signal 3 to fully activate. Made with Biorender.com

Alzheimer's disease and T cell-driven inflammation

Beyond multiple sclerosis, we asked whether analogous mechanisms of T cell activation and tissue entry might also operate in other chronic neuroinflammatory settings. Alzheimer's disease has increasingly been linked to immune-driven pathology, including the presence of peripheral T cells in the central nervous system and their potential contribution to local inflammation and neurodegeneration. In this perspective, shifting to Alzheimer's disease is not meant as a change of topic, but as an opportunity to interrogate similar immunological questions in a different, non-autoimmune context of persistent brain inflammation.

As part of the PhD training abroad, a research period was carried out in Colonna's laboratory to gain hands-on expertise with animal models and in vivo immunological approaches. This experience made it possible to complement the human data with mechanistic experiments in mice, focusing on the origin, localization and phenotypic features of brain-associated T cells, and offering an experimental framework to study how peripheral immune cells can access and persist in the central nervous system during chronic neuroinflammation.

1. Alzheimer's disease (AD) characteristics and inflammation

AD is a neurodegenerative disorder characterized by the extracellular deposition of amyloid-β (Aβ) plaques and intracellular accumulation of hyperphosphorylated tau protein. Clinically, AD manifests as memory loss, cognitive decline, confusion, and disorientation, which are caused by regional brain atrophy accompanied by synaptic and neuronal loss[141,142].

AD can be broadly classified in two main types:

- Familial AD (FAD): This form represents 1 to 5% of AD cases and it is caused by autosomal dominant genetic mutation in amyloid precursor protein (APP), presenilin 1 (PS1, PSN1 gene) and presenilin 2 (PS2, PSN2 gene) genes. It usually manifests at a young age -between 30 to 65 years- and progresses rapidly[141].
- Sporadic AD (SAD): SAD represents 95% of all AD cases and it is also called "late-onset" AD, with first symptoms usually appearing after 65 years of age. This cause of this type of AD is not known but it is probably induced by a combination of mutation in specific genetic loci, environmental factors, and some comorbidities[141].

The heterogeneous nature of AD -its varying clinical presentations and triggers- makes understanding its pathology particularly challenging.

Accumulation of Aβ is a hallmark of AD and can begin as early as 20 years before symptom onset[142]. Aβ originates from the abnormal processing of the transmembrane glycoprotein APP. Normally, APP is cleaved by β- and γ-secretases, in which PS1 and PS2 are key components, explaining why a mutation in genes encoding these proteins is directly associated with AD. Increased aggregation and reduce clearance of Aβ plaques is also associated with apolipoprotein E (APOE) gene mutations. Accumulation of Aβ aggregates is believed to trigger tau phosphorylation, mitochondrial dysfunction, microglia activation, inflammation and synaptic damage, ultimately leading to neurodegeneration[143].

Intracellular accumulation of tau protein, which forms neurofibrillary tangles (NFTs), is another key feature of AD pathology. In healthy neurons, tau is a tightly regulated microtubule-associated protein essential for maintaining microtubule stability and integrity, as well as proper intracellular transport

and neuronal function. In AD, tau is abnormally phosphorylated, making it prone to forming insoluble aggregates that accumulate within neurons, causing cellular damage and promoting inflammation[143]. Notably, tau accumulation, rather than Aβ plaque formation, correlates more closely with brain atrophy and cognitive impairment.

Chronic neuroinflammation is also consistently observed in AD patients and contributes to disease progression. Aβ plaque formation activates microglia, which initially phagocytose Aβ. However, in AD, prolonged phagocytosis causes microglia to become enlarged and dysfunctional, reducing their ability to clear plaques[144]. In addition, chronically activated microglia also produce pro-inflammatory cytokines and toxic products, such as ROS and nitric oxide. As microglia become less efficient, peripheral macrophages may be recruited to support plaque clearance. Nevertheless, these macrophages likely exacerbate brain inflammation, as mutations in Triggering Receptor Expressed on Myeloid Cells 2 (TREM2) - a receptor expressed by macrophages - have been linked to increased AD risk[145,146]. Furthermore, several pro-inflammatory cytokines secreted by activated innate immune cells, including IL-1β, IL-6, and TNF-α, have also been associated with AD progression[144].

Recent studies suggest that adaptive immunity, particularly T cells, may also play a role in AD neuroinflammation. AD patients exhibit changes in T cell numbers and distribution, such as reduced $CD8^+$ counts in PB and increased $CD3^+$ infiltration in the brains of animal models[147]. Additionally, higher numbers of Th1 and Th17 $CD4^+$ T cells have been detected in AD brains[148]. Interestingly, these two subsets seem to exert opposite effects in AD pathology. Th-1 mediate IFN-γ production was associated to activation of MHC-II+ microglia that exhibited stronger phagocytic ability[149]. Conversely, Th17 were found to be detrimental through release of IL-17 and IL-22, thus increasing neuronal apoptosis[150]. Moreover, Treg cells, and IL-10 production, were also found to be detrimental in AD, with reports showing that transient depletion in mice model of AD ameliorated Aβ clearance[151,152].

In summary, while innate immune cells clearly contribute to AD pathology, the role of T cells remains controversial, and further studies are needed to clarify how adaptive immunity influences disease progression.

2. AD mice models

As with many human diseases, the study of AD is limited by ethical constraints and the scarcity of pathological tissue, making appropriate animal models essential for understanding disease mechanisms. Wild-type (WT) mice do not develop Aβ plaques or tau aggregates, even at old age.

Therefore, transgenic mice carrying human mutated APP and PSN1 genes have been generated, which can begin accumulating Aβ as early as 2–3 months of age[153].

For example, 5xFAD mice, a widely used model for recapitulating early AD phases, are characterized by co-expression of 5 FAD mutations in the APP/PSN1 genes. 5xFAD mice develop Aβ plaques at young age -around 2 months old- and already exhibit widespread brain deposition by 6–9 months, accompanied by cognitive impairment[154].

Other AD mouse models focus on tau overexpression, mimicking later stages of the disease. Generally, tauopathy models exhibit more severe motor and behavioural deficits compared to Aβ-focused models[153].

3. Materials and Methods

3.1 Study design

- Donor enrolment

For this study a cohort of 52 donors, composed of 26 untreated MS patients and 26 HD, was enrolled from three different hospitals in Rome: San Camillo Forlanini, Santa Lucia Foundation and Sant'Andrea Among these donors, samples from 6 individuals - 3 HDs and 3 MS patients - were also used for single-cell RNA sequencing experiments. For *in-vitro* experiments requiring extended culture periods (2–3 weeks), leukopack (LP) units from 5 anonymous HDs were obtained from San Camillo Forlanini Hospital in Rome. All donors signed informed consent forms approved by the Ethical Committee of Santa Lucia Foundation (Table 3).

	HD	**MS**
Number of donors	26	26
Mean Age in years	41	40
Gender: - **Male (n, %)** - **Female (n, %)**	 M (8, 30.8) F (18, 69.2)	 M (10, 38.5) F (16, 61.5)

Table 3. Age and sex distribution of the donors

- Whole blood collection

Venous blood (30–80 mL) from MS patients or HDs was collected into heparinized tubes (BD Biosciences) and processed on the same day when intended for short-term assays or single-cell RNA sequencing (scRNA-seq). The use of freshly isolated blood cells allowed the detection of fragile markers and prevented biases introduced by freeze/thaw procedures.

3.2 Cell Isolation and counting

Peripheral blood mononuclear cells (PBMCs) were isolated by density-gradient centrifugation using standard procedures (Ficoll-Paque Plus, GE Healthcare). Freshly isolated PBMCs were then resuspended in a suspension cell culture medium consisting of RPMI (Sigma) supplemented with 5% human serum (HS; Sigma), 1% HEPES (Gibco), 1% MEM Non-Essential Amino Acids (Gibco), 1% Sodium Pyruvate (Gibco), and 0.1% 2-mercaptoethanol (Gibco). When PBMCs were used for short-term assays, RPMI was supplemented only with 5% HS.

Following resuspension, cells were counted using a disposable Improved Neubauer chamber (NanoEntek).

3.3 Feeder cells generation

Half of each LP collected for the study was irradiated with an X-ray source to generate cells non-proliferating feeder cells. Feeder cells are essential for the generation of primary T cell lines, as they provide lymphocytes with the growth factors, cytokines and stimuli necessary for their expansion. Feeder cells were stored frozen at -80°C until use.

3.4 Cell culture

All cell cultures were maintained in an incubator at 37 °C and 5% CO_2.

For cultures lasting longer than 18 hours, 20 U/mL IL-2 (Miltenyi Biotec) was added to the complete medium and replenished every 2 days.

3.5 Primary T Cell lines

Primary sorted T-cell lines derived from activated PBMCs (5 HDs) were plated in U-bottom 96-well plates at a density of either 10 or 500 cells per well.

For each donor, the number of primary cell lines generated depended on the frequency of activated $CD4^+$ and $CD8^+$ T cells obtained by cell sorting (Table 4).

Donor ID	N. of cell lines CD4+	# N. of cell lines CD8+
L06M	CD3 low = 6 CD3 high = 5 CD69+ = 0	CD3 low = 2 CD3 high = 0 CD69+ = 0
F06M	CD3 low = 2 CD3 high = 3 CD69+ = 2	CD3 low = 1 CD3 high = 0 CD69+ = 2
G84F	CD3 low = 4 CD3 high = 3 CD69+ = 2	CD3 low = 3 CD3 high = 2 CD69+ = 2
L04F	CD3 low = 6 CD3 high = 3 CD69+ = 4	CD3 low = 7 CD3 high = 5 CD69+ = 3
L07F	CD3 low = 1 CD3 high = 3 CD69+ = 4	CD3 low = 10 CD3 high = 5 CD69+ = 3

Table 4. Number of CD3 low, CD3 high and CD69+ cell lines obtained from each HD

3.6 Activation Induced Markers (AIM) assay

In vitro stimulation of freshly obtained PBMCs was performed as previously described[155–157].

Briefly, 200 µl of cell suspension (2×10^6 cells/well) was seeded in U-bottom 96-well plates and stimulated for 18 hours in incubator at 37°C and 5% CO_2 with either a pool or individual viral peptides (PepTivator EBV, CMV pp65, H1N1 NP and SARS-CoV-2 protein S, S1, and S+ peptide pools; 1 mg/ml each; Miltenyi Biotec) or with an equal volume of water (unstimulated control).

For scRNA-seq experiments, an additional stimulation condition using a custom cytokine cocktail (IL-2, 20 U/mL; TNF-α, 50 U/mL; IL-12, 50 U/mL; Miltenyi Biotec) was included.

Purified αCD40 (0.5 µg/µl; Miltenyi Biotec) was added at the beginning of the culture. At the end of the stimulation period, cells were collected for flow cytometry analysis.

3.7 Proliferation assay

Feeder cells were thawed and stimulated for 2 hours in an incubator with either a pool of viral peptides (CMV pp65, EBV, SARS-CoV-2 S, S+, and S1) or PHA-L (1 µg/mL, Biochrome GmbH), supplemented with 20 U/mL IL-2. An unstimulated control, in which an equal volume of sterile filtered water was added, was included in each experiment.

After the initial stimulation, both LP-derived cell lines and feeder cells were labelled with CellTrace Violet (CTV, Invitrogen) or CFSE (Invitrogen), respectively, following the manufacturer's instructions.

Cells were then plated in U-bottom 96-well plates at the following densities: 100,000 feeder cells and 10,000 cell-line cells per well.

Cultures were maintained for 5 days in an incubator, after which cells were stained using a dedicated flow cytometry antibody panel. Samples were acquired fresh on a fully equipped CytoFLEX LX cytometer.

3.8 Flow cytometry staining and acquisition

Cells were pelleted in V-bottom 96-well plates and resuspended in 30 µl of antibody mixes prepared at pre-optimized concentrations and diluted in Brilliant Stain Buffer (BD Biosciences). Cells were incubated for 20 minutes at room temperature (RT). After staining, cell pellets were fixed in 3,6% formaldehyde (Sigma) in phosphate-buffered saline (PBS).

When required, intracellular staining was performed by incubating cells with 30 µL of cytokine-specific antibodies in 0.25% (w/v) saponin (Sigma-Aldrich) following fixation.

Samples were acquired on a fully equipped CytoFLEX LX within 6 hours from staining and fixation. Quality control beads (Beckman Coulter) were used daily to check and standardize instrument performances. Data were analyzed with FlowJo v.10.8.1

Absolute counts of T lymphocytes were obtained using a volumetric, lyse-no-wash flow cytometry approach. A defined volume of whole blood (50 µL) was reverse-pipetted into a tube and directly stained with 15 µL of an optimized antibody cocktail. After 20 minutes of incubation at RT, fluorescence-activated cell sorting lysing solution (BD Biosciences) was added. Following complete red blood cell lysis, samples were acquired on a CytoFLEX equipped with a volume-calibrated peristaltic pump. The number of cells per microliter automatically provided by the instrument was multiplied by 1000 to determine absolute $CD4^+$ and $CD8^+$ T-cell counts per microliter.

Absolute counts of AIM^+ subsets were calculated by multiplying their frequencies by the absolute counts of their parental lineages.

A complete list of antibodies used for absolute count, surface staining and intracellular staining is provided in Table 5. Antibodies were purchased from BD Biosciences, Beckman Coulter, SONY, Miltenyi, AAT Bioquest and BioLegend. Live/Dead ViaKrome 808 was purchased by Beckman Coulter.

Marker	**Fluorophore**	**Concentration**	**Staining type**
CD137	PE	1:80	Surface
CD137	BUV395	1:30	Surface
CD69	PCF594	1:200	Surface
CD69	BB700	1:100	Surface
CD154	PE	1:30	Surface
CD161	PE-Cy7	1:100	Surface
CD161	BUV661	1:80	Surface
CD278 (ICOS)	APC	1:100	Surface
CD20	PE-Cy5	1:30	Surface
CD38	PE-Cy5.5	1:100	Surface
CCR7	PE-Cy7	1:30	Surface
CD25	Alexa 700	1:60	Surface
CD25	BV650	1:30	Surface
CD25	BUV661	1:40	Surface
CD25	BB515	1:80	Surface
CD8	APC-Vio770	1:120	Surface

CD8	BV605	1:30	Surface
CD8	iFluor594	1:100	Surface
CD8	BUV496	1:30	Surface
CD95	BV785	1:120	Surface
CD95	BB515	1:60	Surface
CXCR5	APC-R700	1:60	Surface
CD19	BV650	1:40	Surface
HLA-DR	APC-Vio770	1:120	Surface
CD3	BUV661	1:100	Surface
CD45RA	BV480	1:200	Surface
CD3	BUV496	1:30	Surface
CD4	iFluor810	1:50	Surface
CD4	BB700	1:100	Surface
CCR6	PCF594	1:100	Surface
CXCR3	Alexa 647	1:40	Surface
TCR Vδ2	BV421	1:60	Surface
CD73	PE	1:30	Surface
CD73	BB515	1:30	Surface
TIM-3	RB613	1:30	Surface
CD127	PE-Cy5	1:150	Surface
CD127	BV785	1:30	Surface
CD39	PE-Cy5.5	1:80	Surface
CD39	BV605	1:30	Surface
CD71	APC-R700	1:100	Surface
KLRG1	APC-Vio770	1:100	Surface
CD96	BV421	1:30	Surface
TIGIT	BV480	1:30	Surface
CD57	BV605	1:100	Surface
CCR5	BV650	1:30	Surface
CD27	BV786	1:30	Surface
CD27	PCF-594	1:600	Surface
CD279 (PD-1)	BUV661	1:60	Surface
CD279 (PD-1)	BV421	1:50	Surface

Live Dead ViaKrome 808	IR840	1:300	Surface
IL-17	Alexa 488	1:50	Intracellular
IL-10	PE	1:400	Intracellular
IL-2	APC-R700	1:100	Intracellular
GM-CSF	PCF-594	1:100	Intracellular
IL-22	PE-Cy7	1:90	Intracellular
IFN-γ	APC	1:100	Intracellular
TNF-α	BUV395	1:100	Intracellular
CD45	FITC	1:50	Absolute Count
CD20	PE	1:80	Absolute Count
CD56	PCF-594	1:50	Absolute Count
CD16	BB700	1:100	Absolute Count
CD14	PE-Cy7	1:200	Absolute Count
CD8	APC	1:50	Absolute Count
CD11c	APC-Alexa700	1:100	Absolute Count
CD3	APC-Vio770	1:100	Absolute Count
CD19	BV421	1:30	Absolute Count
CD123	BV605	1:100	Absolute Count
CD4	BV650	1:100	Absolute Count
HLA-DR	BV786	1:100	Absolute Count

Table 5. Antibodies used for flow cytometry staining of human samples

3.9 PMA and Ionomycin stimulation assay

At least $5x10^5$ cells from cultured T cell lines were collected and incubated for 5 hours at 37 °C and 5% CO_2 in the presence of brefeldin A (10 µg/mL, Sigma), PMA (20 ng/mL, Sigma), and ionomycin (200 µg/mL, Sigma). An unstimulated control, in which only brefeldin A was added, was included for each sample. After stimulation, cells were pelleted and processed for flow cytometry staining. Only cells derived from four healthy donors (F06M, G84F, L04F, and L07F) were included in this experiment.

3.10 Cell Sorting

Stimulated or unstimulated PBMCs were stained for 20 minutes at RT with a specific panel of fluorescent monoclonal antibodies diluted in sterile Brilliant Stain Buffer (BD Biosciences). Samples

were then washed with 1X PBS, filtered, and resuspended in 1X PBS + 0.5% BSA for sorting on a CytoFLEX SRT.

The complete list of antibodies used for sorting and the gating strategy are provided in tables 6 and figure 6, respectively. All antibodies were obtained from BD Biosciences or Beckman Coulter. Live/Dead Aqua dye was purchased from Invitrogen.

Purity of sorted samples (average purity >90%) was confirmed through flow cytometry (Beckman Coulter Cytoflex LX).

Marker	**Fluorophore**	**Concentration**
CD154	BB515	1:30
CD69	BB700	1:30
CD8β	PE	1:15
CD3	BV786	1:30
CD4	PE-Cy7	1:30
CD8	APC-Alexa700	1:30
CD137	BV421	1:30
CD16	PE-Cy5	1:30
CD14	PE-Cy5	1:30
CD19	Bv650	1:30
Live Dead Aqua	BV480	1:100

Table 6. Antibodies used for sorting of T lymphocytes

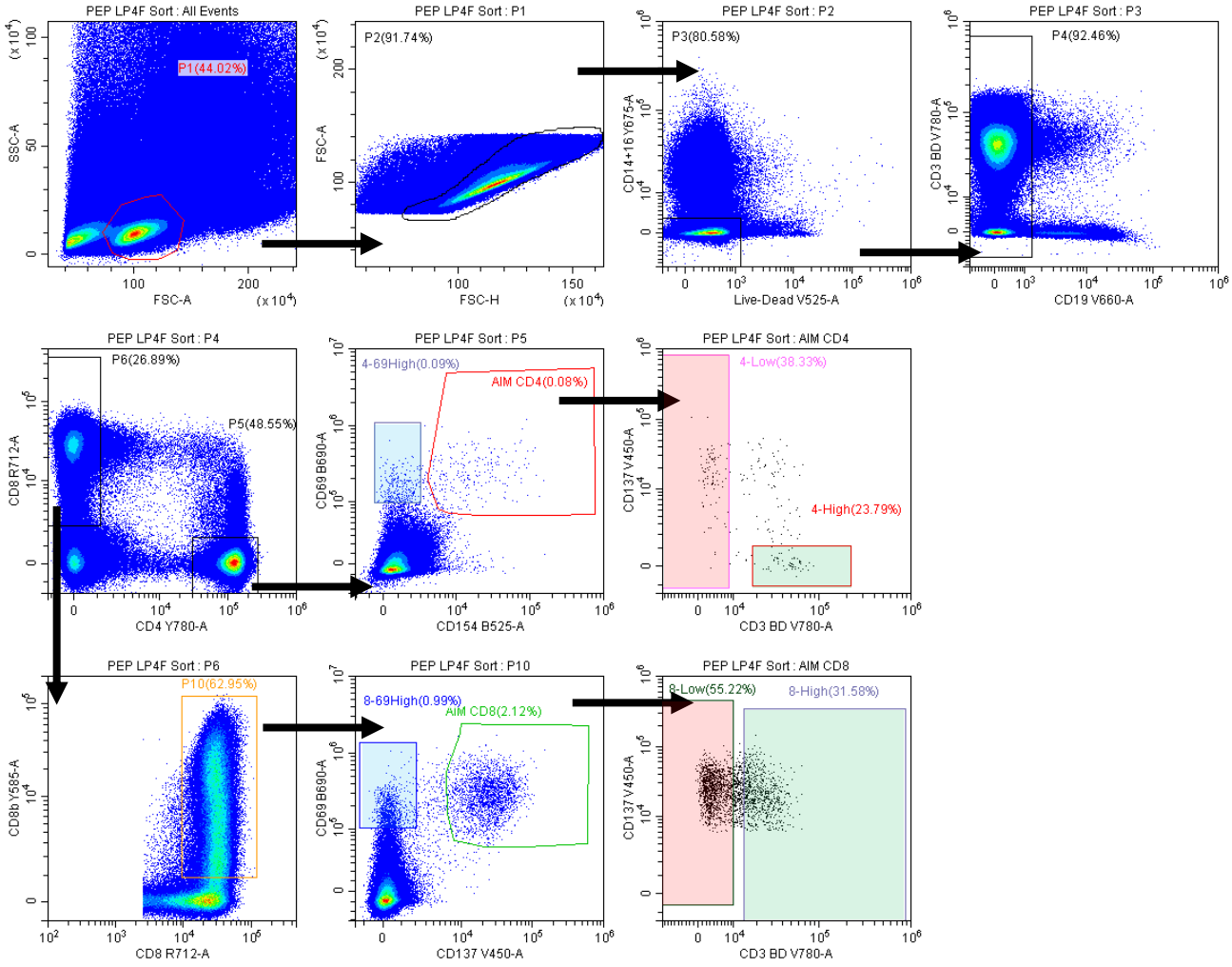

Figure 6. Gating strategy used for sorting both CD4+ and CD8+ AIM+ CD3 high, CD3 low and, in some experiments, CD69+ cells. Sorted gates are evidenced in different colours, red for CD3 low, green for CD3 high and light blue for CD69+.

3.11 Single cell RNA sequencing

A large number of PBMCs (100 x10^6) is required for this preparation. Approximately three quarters of the cells were stimulated with the pool of viral peptides and the remaining part with the cytokine cocktail. A small fraction (4 to 5 x10^6) was left unstimulated as controls (Specific viral peptides and cytokines used are indicated in 3.6 Activation Induced Markers (AIM) assay section).

Stimulation was performed as described in section 3.6 (AIM assay). After stimulation, cells were stained and AIM + CD4+ and CD8+ T cells were sorted based on their CD3 downregulation. Approximately 6,000 cells per sample were obtained. Cell viability (>90%) was verified using a light microscope. Sorted cells were loaded onto a compatible 10X Genomics Chromium chip within one hour. The kits used were the 10X Genomics Chromium Next GEM Single Cell 5' v2 and the 10X

Genomics Chromium Next GEM UCM Single Cell 5' v2. Library preparation for both whole transcriptome and TCR sequences followed the manufacturer's instructions.

Libraries were sequenced using Illumina platforms: NextSeq 550 and NovaSeq X. Sequencing depth was set at 50,000 reads per cell for the whole transcriptome and 5,000 reads per cell for TCR libraries.Analysis of the sequenced data was performed with Cell Ranger software, R package Seurat[158] and Python package scirpy[159].

Briefly, FASTQ files were processed with the cellranger multi pipeline (10X Genomics). RNA expression matrices were analyzed using the Seurat package[158] for the R programming language. After QC and removal of low quality, highly stressed and contaminants – such as monocytes, platelets, and B cells, a total of 39887 cells were retained from 3 MS patients and 5838 from 3 HD. Raw counts were scaled and normalized using the SCTransform function[160,161] and integrated across samples for batch effect removal via Canonical Correlation Analysis (CCA). Unsupervised clustering using the Leuven algorithm with resolution = 0.3 identified 9 clusters, and the FindAllMarkers function with the Wilcoxon test was used to identify top upregulated genes in each cluster. Cluster annotation was manually performed examining the marker lists with the help of Gemini 3 Pro AI (Google). The clusters were visualized in 2D with the Uniform Manifold Approximation and Projection (UMAP) algorithm, setting the min dist parameter to 1.

Statistical testing of differential expression across conditions was performed by grouping all data by subject and condition (pseudobulk) with the AggregateExpression function and the DESeq2 package[162].

3.12 TCR analysis

- T-cell receptor repertoire data statistics and visualization

Statistical analysis of TCR sequencing data was performed using the statistical programming environment R[163]. Data were analyzed with Kruskal-Wallis or one-way ANOVA, followed by the post-hoc Tukey's test, according to data distribution. P-values were adjusted for multiple comparisons. TRBV family frequencies were normalized and visualized as z-score values. Data were shown as mean ± standard error of the mean (SEM). Statistical significance was considered when $p\text{-value}<0.05$.

Graphs were generated using the R packages ggplot2[164], ggpubr[165], RColorBrewer[166], igraph[167], ggbeeswarm[168]. The package pheatmap[169] was used to represent, as heatmap, the most frequent sequences shared across datasets and the TRBV genes frequency. Repertoire architecture networks were visualized using Cytoscape[170].

- TCR architecture analysis

TCR architecture was analyzed through the visualization of clone networks, according to literature[171]. The network was drawn for each repertoire by the R package igraph[167] based on the top 10,000 CDR3s-a.a. or less, if fewer clones were found. Within each network, each node represents a CDR3-a.a.; links, or "edges", were made between similar CDR3s-a.a., based on a Levenshtein distance (LD) of 1 (=1 a.a. sequence change).

- Public datasets

We enclosed in our analysis TCR data from published studies. These included TCR repertoires from MS patients, from HD, and from publicly available TCR datasets that classify published sequences based on a potential antigen association. All the TCR data selected for our analysis were generated with comparable procedures by high-throughput sequences (HTS) platforms.
MS TCR data were retrieved from the following studies: Amoriello et al., 2021[172]; Planas et al., 2018[173], and Salou et al., 2015[174]. These datasets included 37 MS peripheral blood (PB) repertoires, 21 MS CSF repertoires, and 9 MS repertoires from brain white matter lesions[173,174]. Details about patients' characteristics and TCR datasets can be found in the original studies.
HD TCR data of the PB of 30 subjects were retrieved from Hamm DE, 2020, on the immunoSEQ platform, host by Adaptive Biotechnologies, USA, at the following link: https://clients.adaptivebiotech.com/pub/tcrbv4-control (Table 7)[175].
To analyze the possible antigen association of sequences, we used the publicly available TCR datasets McPAS-TCR[176], VDJdb[177], and the Immune Epitope Database (IEDB; iedb.org/). McPAS-TCR and VDJdb are two manually curated databases encompassing TCR sequences from published studies. McPAS-TCR classifies the sequences based on association with diseases or pathogens. VDJdb classified the sequences based on association with pathogen epitopes. For the use in this study, McPAS-TCR and VDJdb were downloaded on October 2023 and September 2025, respectively.
Similarly, IEDB classifies published TCR sequences based on the pathogen-associated antigen specificity. IEDB provides the tool TCRMatch (tools.iedb.org/tcrmatch/), hereby used to find similar CDR3s, in terms of a.a. composition, to input sequences of our interest from the patients' repertoires. TCRMatch attributes a similarity score between the input and output CDR3s-a.a. ranging from 0 to 1, where 1 signifies a perfect a.a. match, thus identical sequences.

Sample ID	Total CDR3s-a.a.	Age	Sex
Subject_156	89058	34	F

Subject_87	253005	20	M
Subject_154	89742	24	F
Subject_26	141537	50	F
Subject_61	267661	21	M
Subject_155	92776	30	M
Subject_94	248572	49	M
Subject_73	285250	27	M
Subject_15	211252	30	M
Subject_19	250957	20	M
Subject_12	272694	30	F
Subject_75	340.188	32	M
Subject_24	183191	24	F
Subject_44	231769	57	F
Subject_99	367869	33	F
Subject_65	231684	24	M
Subject_70	301871	29	M
Subject_56	328855	30	M
Subject_54	333442	59	F
Subject_39	145113	30	F
Subject_86	226912	32	M
Subject_50	327551	57	F
Subject_91	275259	23	M
Subject_102	279364	30	M
Subject_60	245635	57	F
Subject_62	235883	42	M
Subject_98	451853	52	M
Subject_45	191514	53	F
Subject_52	360739	38	M
Subject_158	122581	36	F

Table 7. Characteristics of the 30 healthy donors selected from Hamm DE, 2020. Mean age of donors is 35.77. Ratio Female (F) to Male (M) is 13:17.

3.13 Mice

All mice were bred and housed in specific pathogen-free (SPF) facilities at Washington University in St. Louis, under controlled temperature and humidity, with a 12-h light/dark cycle and ad libitum access to food and water. All animal experiments were conducted in compliance with institutional regulations, under authorized protocols approved by the Institutional Animal Care and Use Committee.

Both WT with genetic background C57BL/6J and 5xFAD mice were generated and provided by The Jackson Laboratory[154]. WT and 5xFAD mice were sacrificed between 3 to 6 months of age. Mice used for experiments were age and sex matched mice.

Cd40lg-cre mice were crossed with the Rosa26-tdTomato reporter line to visualize T cells in the healthy mouse brain. Male Cd40lg-cre;Rosa26-tdTomato mice were analyzed at 14 weeks of age[178].

3.14 Intra Cisterna Magna (ICM) and Intra Venous (IV) mice injection

Anesthetized mice were injected with 2 µL of CD45 Alexa 647 directly into the cisterna magna (ICM) by a specialized technician. After 1 hour at room temperature, mice received an intravenous (IV) injection of 20 µL of CD45 PE. Mice were then sacrificed via perfusion to proceed with brain T cell isolation and flow cytometry staining, as described in section 3.15.

3.15 T cell isolation and staining from mice brains

Anesthetized mice were perfused with at least 20 mL of ice-cold PBS (1X). Brains were collected into DMEM and mechanically dissociated using a Dounce homogenizer. Myelin was removed by density gradient centrifugation using 30% isotonic Percoll (GE Healthcare).

The resulting cell suspensions were incubated with an antibody cocktail and Fc block for 30 minutes on ice. For intracellular FoxP3 staining, BD Pharmingen Transcription Factor Buffer Set was used according to manufacturer's instructions. The antibodies used for staining are listed in Table 8 and were purchased from BD Biosciences, SONY, and BioLegend. Live/Dead Aqua dye was obtained from Invitrogen.

Cell suspensions were acquired on a BD FACSymphony A3 flow cytometer.

Marker	Fluorophore	Concentration
TCRγδ	FITC	1:50
CD3	PE	1:100
CD127	PE-Dazzle 594	1:50
CD19	PE-Cy7	1:50
NK1.1	PE-Cy7	1:50
NK1.1	PerCP-Cy5.5	1:100
CD11b	APC	1:50
CD4	Alexa 700	1:50
CD4	APC-Cy7	1:300

CD103	APC-Cy7	1:50
CD69	BV421	1:50
Live Dead Aqua	BV480	1:1000
CD25	BV650	1:50
CD8a	BUV395	1:25
CD8a	FITC	1:300
CD45	BUV563	1:50
CD45.2	PE-Cy7	1:100
Thy1	PB	1:300
FoxP3	APC	1:50

Table 8. Antibodies used for flow cytometry staining of mice brains

3.16 Tissue Preparation

After perfusion, brains were isolated and fixed in 4% paraformaldehyde (PFA) in PBS overnight at 4°C. Samples were then transferred in 30% sucrose in PBS for 48 hours at 4°C.

Brain tissues were embedded in Tissue-Plus O.C.T. Compound (Thermo Fisher Scientific) and frozen. Longitudinal sections of 60-µm thickness were obtained using a Cryostat (CM1950; Leica). Sections were blocked and permeabilized by 5% BSA and 0.5% Triton-X100 in PBS solution for 2 hours at RT.

3.17 Immunofluorescence staining

Free-floating 60-µm longitudinal brain sections were permeabilized and blocked in 5% BSA in PBS with 0.5% Triton X-100 for 2 hours at room temperature.

Because CD8 staining required a biotin–streptavidin detection system, endogenous binding sites were blocked using the Streptavidin/Biotin Blocking Kit (Vector Laboratories) by applying 2 drops of streptavidin solution for 15 minutes, washing in PBS 1X, and then applying 2 drops of biotin solution for 15 minutes, following the manufacturer's instructions.

Sections were incubated with the necessary primary antibodies diluted in 1% BSA in PBS with 0.5% Triton X-100 for 48 hours at 4 °C under gentle shaking.

Primary antibodies used for immunofluorescence staining: Rat anti-CD8 (1a200, purified), Rabbit anti-Collagen IV (1:200, Millipore), Mouse anti-CD3 (1a200, Millipore).

Sections were then washed once in PBS 1X + 0.5% Tween-20 and then twice in PBS for 5 minutes. When necessary, sections were incubated with biotinylated anti-rat secondary antibody (1:200) for 1 h at RT under gentle shaking. After 3 more washes in PBS 1X for 5 minutes, sections were then incubated with appropriate secondary antibodies for 2 h at RT.

List of secondary antibodies used: Donkey anti-rabbit Alexa Fluor 488, 1:1000, Streptavidin-Alexa Fluor 647, 1:1000, Goat anti-mouse Alexa Fluor 647, 1a1000 and Methoxy-X04 1:3,000 (3 mg/ml; Tocris).

Protocol proceeded then with one wash in PBS 1X and DAPI incubation (1:1000 in PBS) for 5 min. Sections were then washed 3 more times for 5 minutes each (once in PBS 1X + 0.5% Tween-20 and twice in PBS 1X). Lastly, sections were mounted on glass slides using ProLong Gold (Thermo Fisher Scientific) and cured before imaging.

3.18 Confocal microscopy

Images were acquired on a Zeiss LSM880 laser-scanning confocal microscope equipped with Airyscan (Carl Zeiss Inc., Thornwood, NY). The system includes 405-nm diode, 488-nm Argon, 543-nm HeNe, and 633-nm HeNe lasers and a 32-channel GaAsP detector.

Z-stacks were collected using a Plan-Apochromat 40× oil-immersion objective (NA 1.4). Image acquisition was performed using ZEN Black software (version 2.1 SP3) with identical settings within each experiment.

3.19 Statistical analysis

Statistical analyses were performed with GraphPad Prism 10. Details of the statistical tests applied for each experiment are illustrated in the respective figure. Different variables were compared by Kruskall-Wallis, ordinary 2-way ANOVA or Mann-Whitney test. Multiple comparisons were corrected by Dunn's, Sidak's or Tukey's post hoc. Uncorrected Fisher LSD's test was also used. Statistical significance was inferred if $P < 0.05$. In all figures, P values are indicated by *$P < 0.05$; **$P < 0.01$; ***$P < 0.001$; ****$P < 0.0001$. No symbol, no statistical significance.

4. Results

4.1 Identification and phenotyping of antigen-specific and bystander T cells induced by different viral peptides stimulation in HD and MS patients

Identification of virus-specific and bystander AIM+ T cells in both HD and MS patients

The first question we aimed to address in this study was how to identify bystander T cells and distinguish them from their antigen-specific counterparts through flow cytometry. To recreate an antiviral-like immune response in vitro we collected whole blood from a cohort of 52 individuals, matched for age and sex, consisting of 26 HD and 26 MS patients. PBMCs isolated from each donor were stimulated for 18 hours with peptide pools specific for SARS-CoV-2 Spike (HD =26, MS = 25), EBV consensus (HD =26, MS = 26), pp65 CMV (HD =26, MS = 26) and H1N1 NP proteins (HD =18, MS = 19) in the AIM assay (as described in section 3.6).

AIM+ CD4+ T cells were defined by the combined upregulation of CD69+ and CD154+, whereas AIM+ CD8+ T cells were defined as CD69+ and CD137+ (Fig.7A and B) [179–181]. The key principle behind our gating strategy is that cognate TCR engagement induces a rapid down-modulation of the TCR/CD3 complex on the surface of recently activated antigen-specific T cells[34]. Accordingly, within AIM^+ T cells we operationally defined antigen-specific cells as those showing reduced CD3 expression (CD3 low), whereas T cells that became activated indirectly, driven by the inflammatory/cytokine milieu rather than direct peptide recognition, retained high CD3 levels (CD3 high) and were classified as bystander-activated.

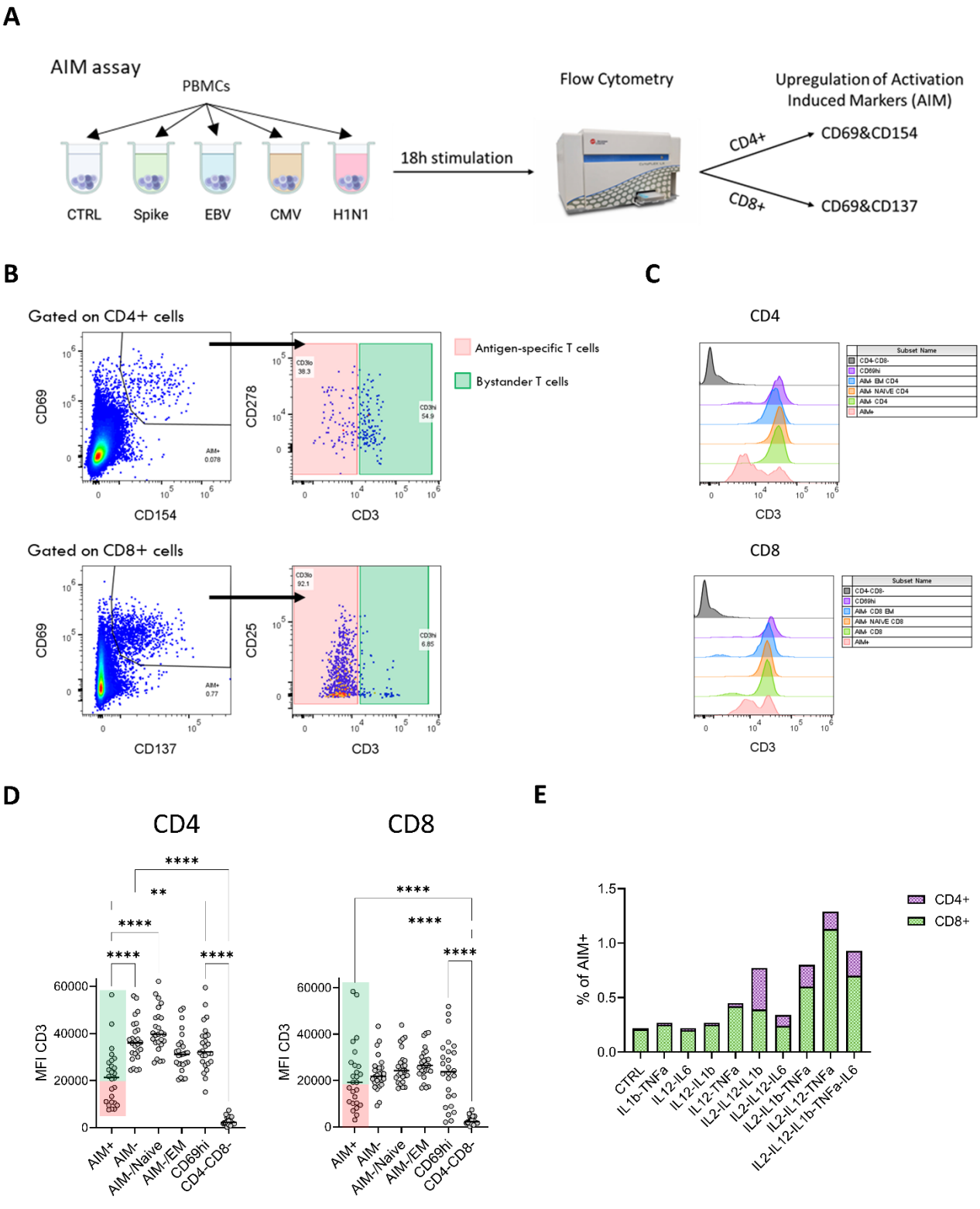
A
AIM assay
PBMCs
CTRL
Spike
EBV
CMV
H1N1
18h stimulation
Flow Cytometry
Upregulation of Activation Induced Markers (AIM)
CD4+
CD69&CD154
CD8+
CD69&CD137
B
Gated on CD4+ cells
CD69
CD154
CD278
CD3
Antigen-specific T cells
Bystander T cells
Gated on CD8+ cells
CD137
CD25
C
CD4
CD8
Subset Name
CD4-CD8-
CD69hi
AIM- EM CD4
AIM- NAIVE CD4
AIM- CD4
AIM+
AIM- CD8 EM
AIM- NAIVE CD8
AIM- CD8
D
CD4
CD8
MFI CD3
AIM+
AIM-
AIM-/Naive
AIM-/EM
CD69hi
CD4-CD8-
E
% of AIM+
CD4+
CD8+
CTRL
IL1b-TNFa
IL12-IL6
IL12-IL1b
IL12-TNFa
IL2-IL12-IL1b
IL2-IL12-IL6
IL2-IL1b-TNFa
IL2-IL12-TNFa
IL2-IL12-IL1b-TNFa-IL6

Figure 7. *Identification of virus-specific and bystander AIM+ T cells in both HD and MS patients*. A) Schematic representation of the AIM assay used in this study. B) Representative plots showing the gating strategy used to distinguish CD3 low antigen-specific and CD3 high bystander CD4+ (top) and CD8+ (bottom) T cells. C) Representative plots of one HD showing the median fluorescence intensity (MFI) of CD3 in virus-activated CD4+ (top) and CD8+ (bottom) populations. A negative CD3 control was also included as CD4-CD8-. D) Dot plots showing the MFI of CD3 in Spike-activated CD4+ and CD8+ T cells in 26 HD. A negative CD3 control was also included as CD4-CD8-. The green and red boxes respectively represent bystander (higher MFI of CD3) and antigen-specific (lower MFI of CD3) T cells within the peptide-stimulated condition. The populations in the graphs were compared using nonparametric Friedmann test followed by Dunn's multiple comparison test; lines represent median with interquartile range. *P < 0.05; **P < 0.01; ***P < 0.001; ****P<0.0001; no symbol, not significant. E) Bar plot graph showing the total frequency of AIM+ T cells obtained after stimulation with different cytokine cocktails.

To further support our hypothesis, we examined the median fluorescence intensity (MFI) of CD3 in Spike-stimulated $CD4^+$ and $CD8^+$ T-cell subpopulations, including bystander and antigen-specific T cells within the AIM+ compartment, as well as non-activated T cells within the AIM-negative (AIM^-) compartment, in our cohort of 26 HD (Fig. 7C and D). We also included a CD3-negative control, defined as CD4−CD8− cells. Our data clearly show a downregulation of CD3 in antigen-specific $CD4^+$ and $CD8^+$ T cells compared with non-stimulated AIM^- T cells and with effector memory AIM^- (AIM^-/EM) and naïve AIM^- (AIM^-/Naïve) subpopulations, while retaining a slightly higher intensity than $CD4^-CD8^-$ cells. Moreover, although the MFI of CD3 in $CD4^+$ bystander T cells is high, it is marginally lower than that observed in AIM^- $CD4^+$ T cells, suggesting that these cells underwent a milder activation compared with truly antigen-specific $CD4^+$ T cells.

Considering that it is widely accepted that bystander activation is cytokine-dependent[132,133], we investigated whether different homemade cytokine cocktails could induce the upregulation of AIM markers on PBMCs derived from a single HD (Fig. 7E). Several combinations of pro-inflammatory cytokines at pre-optimized concentrations were tested to mimic an inflamed T cell environment, including cytokines produced by both the innate immune system, such as IL-12, IL-1β, IL-6, and TNF-α, and the adaptive immune system, namely IL-2 and TNF-α. Notably, stimulation with cytokines alone was sufficient to induce the upregulation of AIM markers, which are typically considered antigen-specific. Among all the combinations tested, IL-2 + IL-12 + TNF-α was selected for subsequent experiments, as it induced the highest frequency of AIM^+ T cells compared with the other conditions.

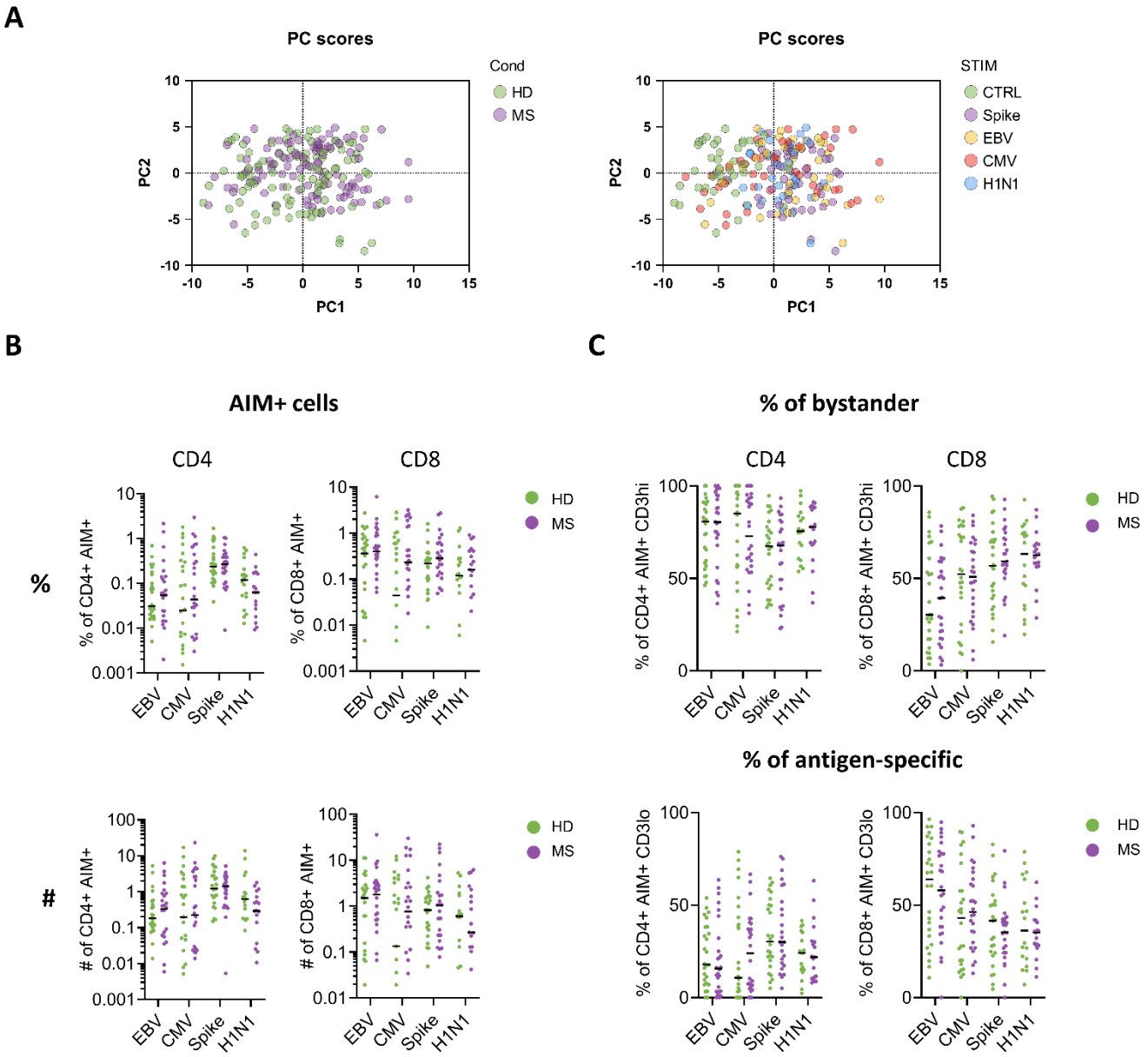

Figure 8. *Identification of virus-specific and bystander AIM+ T cells in both HD and MS patients*. A) Principal Component Analyses (PCA) of the complete AIM assay dataset. The top panel compares HD (green) and MS (purple) patients, while the bottom panel highlights the different stimulation conditions: CTRL (green), Spike (purple), EBV (yellow), CMV (red), and H1N1 (light blue). B) Dot plots showing frequencies (top) and absolute cell counts (bottom) of AIM+ CD4+ and CD8+ T cells for each viral peptide. HD and MS were compared using ordinary 2-way ANOVA followed by Sidak's multiple comparison test; lines represent median with interquartile range. no symbol, not significant. C) Dot plots showing fractions of CD4+ and CD8+ bystander (top) and antigen-specific (bottom) T cells for each viral peptide, within AIM+ cells. HD and MS were compared using ordinary 2-way ANOVA followed by Sidak's multiple comparison test; lines represent median with interquartile range. no symbol, not significant.

The gating strategy shown in Figure 7B was than applied to each stimulation condition, followed by Principal Component Analysis (PCA) to visualize the dataset (Fig. 8A). The PCA is represented in two ways: the first comparing HD and MS, and the second highlighting the different viral stimulation conditions. No differences between HD and MS were observed in the PCA, whereas the unstimulated control group (CTRL) appeared slightly separated from the stimulated conditions. Peptide-stimulated data (Spike, EBV, CMV, and H1N1) largely overlapped in the PCA, suggesting that the AIM+ T cell response is comparable across these viruses. Subsequently, we compared HD and MS responses by analyzing both the frequencies and absolute cell counts of AIM+ CD4+ and CD8+ T cells for each virus (Fig. 8B), as well as the frequency of bystander (CD3 high) and antigen-specific (CD3 low) CD4+ and CD8+ T cells (Fig. 8C). Frequencies were background-corrected by subtracting, for each donor, the unstimulated AIM+ frequency from the stimulated condition.

No significant differences were observed between HD and MS patients in terms of the magnitude of the AIM+ response or its composition - bystander versus antigen-specific T cells.

These results prompted a deeper exploration of the data, suggesting that in both HD and MS, bystander T cells likely differ from antigen-specific T cells in other, more subtle characteristics.

Antigen-specific AIM+ CD4+ T cells exhibit a more central memory phenotype than bystanders in both HD and MS patients

In literature, bystander T cells - particularly CD8+ - are often described as highly differentiated memory cells, capable of expressing granzymes and other cytotoxic molecules, corresponding to an "older" EMRA phenotype[89]. To determine whether bystander T cells are indeed more differentiated than antigen-specific T cells, we analyzed the differentiation status of the cells responding to each virus, and compared HD and MS patients to identify potential differences in the phenotype of activated T cells.

Naïve T cells were defined as CD45RA+CD27+, central memory (CM) as CD45RA−CD27+, effector memory (EM) as CD45RA−CD27−, and EMRA as CD45RA+CD27−. Both antigen-specific and bystander AIM+ CD4+ T cells predominantly displayed a CM phenotype across all viral reactivities, although bystander cells had significantly fewer CM cells and more naïve and EM cells than the antigen-specific subset (Fig.9A). In MS patients, CMV-stimulated antigen-specific CD4+ T cells exhibited a higher proportion of EM cells compared to HD, suggesting a stronger response of this subset to CMV.

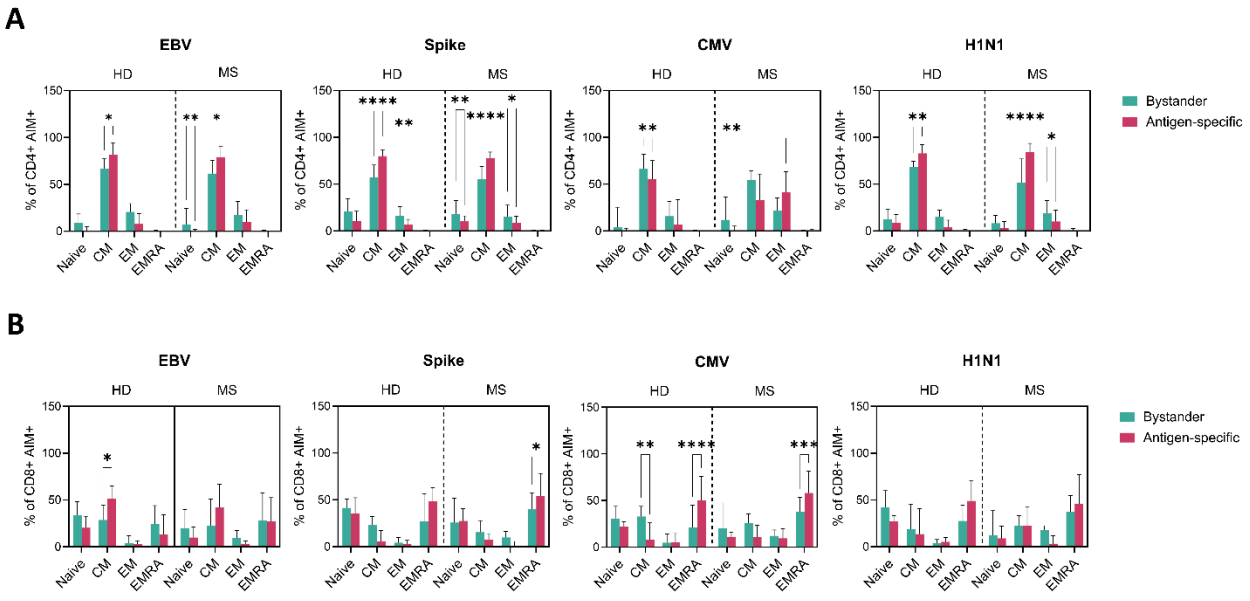

Figure 9. *Antigen-specific AIM+ CD4+ T cells exhibit a higher central memory (CM) phenotype than bystander cells in both HD and MS patients*. A) Graphs showing the distribution of differentiation subsets (Naïve, CM, EM, EMRA) among CD4+ AIM+ bystander and antigen-specific T cells across different stimulation conditions (EBV, Spike, CMV, and H1N1) in both HD and MS patients. Statistical analysis was performed using ordinary 2-way ANOVA with Tukey's multiple comparison test; lines represent median with interquartile range. *P < 0.05; **P < 0.01; ****P<0.0001; no symbol, not significant. B) Graphs showing the distribution of differentiation subsets (Naïve, CM, EM, EMRA) among CD8+ AIM+ bystander and antigen-specific T cells across the same stimulation conditions in HD and MS patients. Statistical analysis was performed using ordinary 2-way ANOVA with Tukey's multiple comparison test; lines represent median with interquartile range. *P < 0.05; **P < 0.01; ***P < 0.001; ****P<0.0001; no symbol, not significant.

For AIM+ CD8+ T cells, antigen-specific cells reactive to Spike, CMV, and H1N1 primarily displayed an EMRA phenotype, whereas EBV-specific AIM+ CD8+ T cells were mainly CM (Fig.9B). In contrast, within bystander AIM+ CD8+ T cells we found a less skewed distribution across the four differentiation stages, with relatively less enrichment in EMRA compared with antigen-specific cells, suggesting that bystander activation recruits a more heterogeneous and overall less terminally differentiated CD8+ pool.

Overall, these data show that antigen-specific (CD3 low) AIM+ CD4+ T cells are largely skewed toward a central memory phenotype across most viral stimuli, whereas bystander (CD3 high) CD4+ T cells display a relatively more differentiated effector profile. In CD8+ T cells, the same trend is weaker and more variable, indicating that the bystander versus antigen-specific separation is most robust for CD4+ responses and is associated with distinct memory/effector programming.

Bystander AIM+CD4+ T cells express higher levels of CCR6 than antigen-specific T cells

To further characterize both bystander and antigen-specific T cells, we measured the expression of activation, co-stimulatory, and chemokine receptors on AIM+ CD4 and CD8 T cells from HD and MS patients across all stimulation conditions (Fig. 10). The radar plots in Fig. 10A (CD4+) and 10C (CD8+), summarise these data by showing, for each marker, the median percentage of AIM^+ cells that express that marker across all viral stimulations. This approach provides a compact overview of the global phenotypic profile in HD versus MS.

For most markers, no significant differences were observed between HD and MS cohorts. PD-1, a major inhibitory checkpoint, appeared to be more highly expressed in HD than in MS patients. However, when analysing virus-specific datasets, this difference was confined to H1N1 stimulation in both bystander and antigen-specific $CD4^+$ T cells (Fig. 10B). In $CD8^+$ T cells, PD-1 expression was higher only in H1N1-bystander T cells (Fig. 10D). No other virus-specific, cohort-dependent differences were observed.

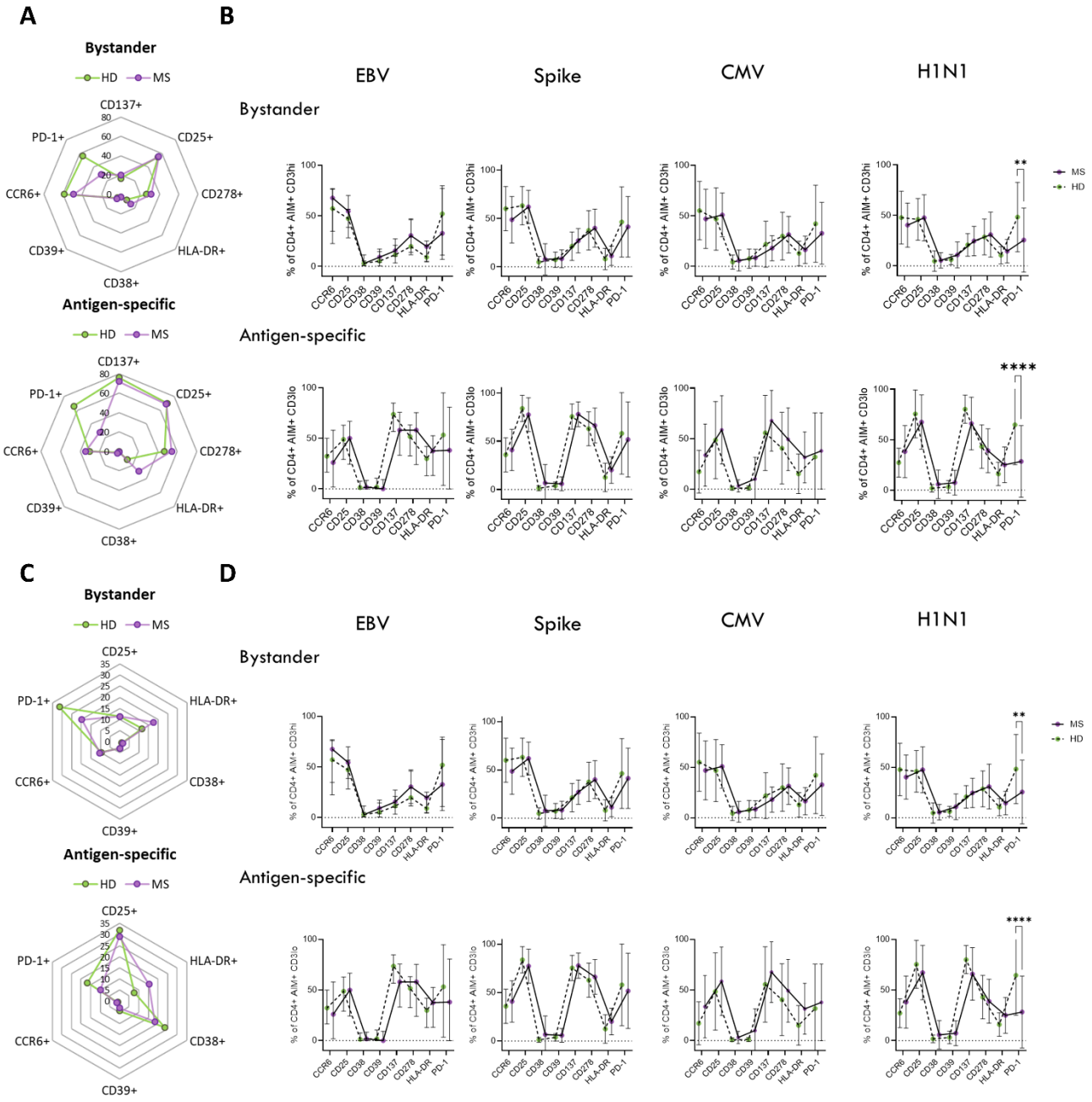

Figure 10. *AIM+ HD and MS patients do not differ in activation markers upregulation.* A) Radar plots summarizing the medians of bystander (top) and antigen-specific (bottom) $CD4^+$ AIM^+ activation markers across all viruses (EBV, Spike, CMV, H1N1). Medians from HD (green) and MS (purple) patients are visually compared using dots connected by lines. B) Expression of activation markers by $CD4^+$ AIM^+ activation marker plots separated by virus. Each dot represents the median plus interquartile range for each dataset subset. Dots are connected by lines to facilitate visualization and direct comparison between cohorts. HD (green) and MS (purple) were compared using ordinary two-way ANOVA with Sidak's post-hoc correction. **P < 0.01; ****P < 0.0001; no symbol = not significant. C) Radar plots summarizing the medians of bystander (top) and antigen-specific (bottom) $CD8^+$ AIM^+ activation markers across all viruses (EBV, Spike, CMV, H1N1). D) $CD8^+$ AIM^+ activation marker plots separated by virus. Each dot represents the median plus interquartile range for each dataset subset. Dots are connected by lines to highlight differences. HD (green) and MS (purple) were compared using ordinary two-way ANOVA with Sidak's post-hoc correction. **P < 0.01; no symbol = not significant.

We then repeated this analysis, now directly comparing bystander and antigen-specific AIM+ T cells within each cohort (Fig. 11). The radar plots for $CD4^+$ and $CD8^+$ T cells use the same virus-aggregated medians as in Fig.10. These plots highlight higher CCR6 expression in bystander $CD4^+$ T cells, and increased expression of CD137 in $CD4^+$ T cells and CD25 in $CD8^+$ T cells (Fig. 11A and C). The accompanying line plots (Fig. 11B, D) resolve these patterns by viral specificity. Across all virus stimulation, we confirmed that antigen-specific $CD4^+$ T cells generally expressed higher levels of CD137, as well as CD278 and CD25, in both HD and MS patients (Fig. 11B); these markers are usually induced by strong, TCR-dependent stimulation. Interestingly, CCR6 was the only marker more strongly upregulated in bystander than in antigen-specific $CD4^+$ T cells, although in MS patients CCR6 this difference was modest. CCR6 was also expressed on bystander $CD8^+$ T cells across all viruses, although without reaching significance (Fig. 11D). Antigen-specific $CD8^+$ T cells showed higher levels of the activation markers CD25 and CD38 compared with bystander T cells.

Taken together, these results confirm that antigen-specific T cells undergo stronger activation than bystander T cells. Additionally, CCR6 upregulation in bystander T cells suggests a preferential skewing of these cells toward a Th17-like phenotype.

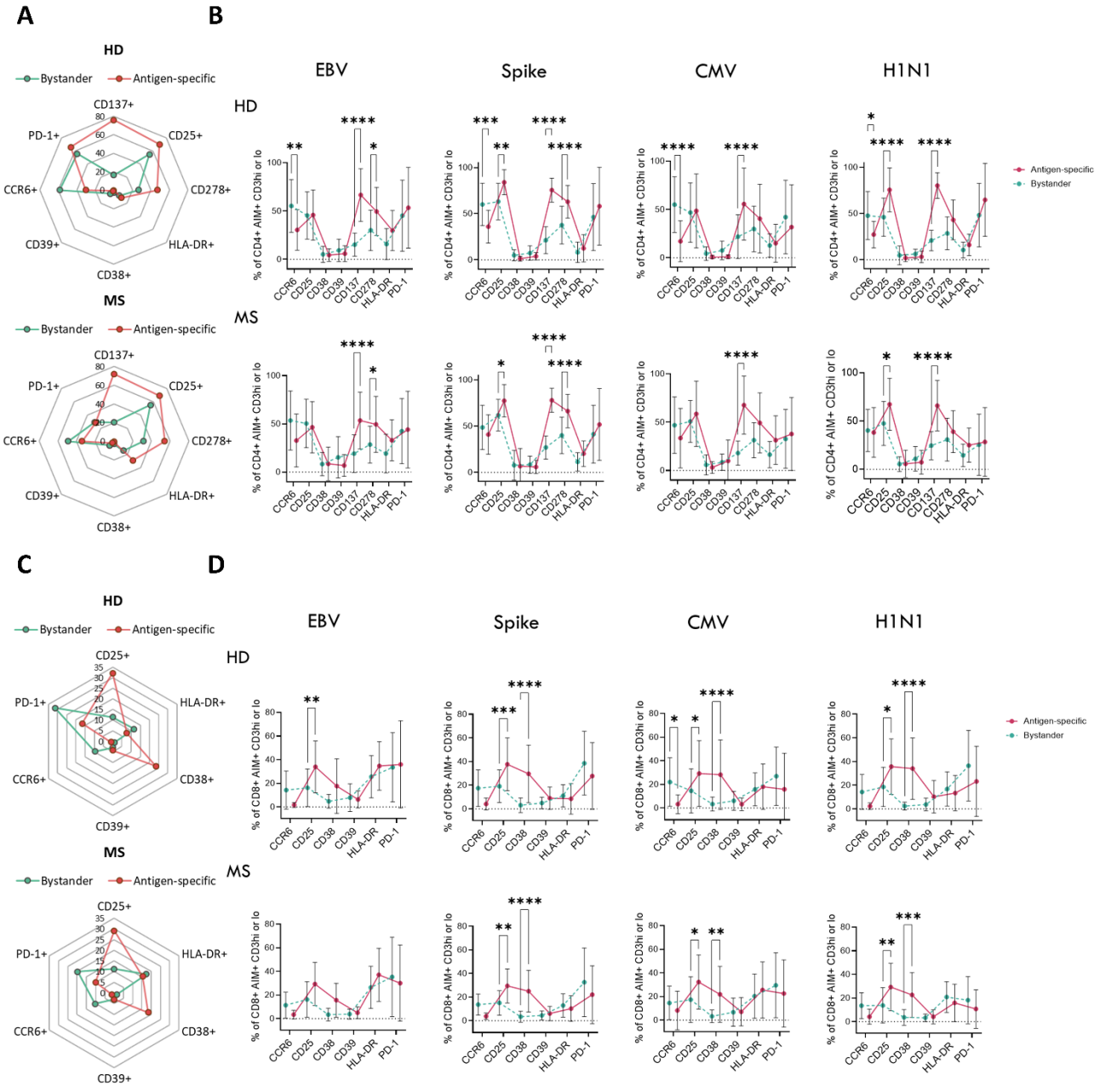

Figure 11. *Bystander AIM+CD4+ T cells express higher levels of CCR6 than antigen-specific T cells.* A) Radar plots summarizing the medians of $CD4^+$ AIM^+ activation markers in HD (top) and MS (bottom) patients across all viruses (EBV, Spike, CMV, H1N1). Medians from bystander (green) and antigen-specific (red) $CD4^+$ AIM^+ T cells are visually compared using dots connected by lines. B) $CD4^+$ AIM^+ activation marker plots separated by virus. Each dot represents the median plus interquartile range for each dataset subset. Dots are connected by lines to highlight differences. Bystander (green) and antigen-specific (red) data were compared using ordinary two-way ANOVA with Sidak's post-hoc correction. *P < 0.05; **P < 0.01; ***P < 0.001; ****P < 0.0001; no symbol = not significant. C) Radar plots summarizing the medians of $CD8^+$ AIM^+ activation markers in HD (top) and MS (bottom) patients across all viruses (EBV, Spike, CMV, H1N1). Medians from bystander (green) and antigen-specific (red) $CD8^+$ AIM^+ T cells are visually compared using dots connected by lines. D) $CD8^+$ AIM^+ activation marker plots separated by virus. Each dot represents the median plus interquartile range for each dataset subset. Dots are connected by lines to highlight differences. Bystander (green) and antigen-specific (red) data were compared using ordinary two-way ANOVA with Sidak's post-hoc correction. *P < 0.05; **P < 0.01; ****P < 0.0001; no symbol = not significant.

4.2 Bystander T cells possess inflammatory Th17 and Th1-17 phenotypes *in vitro* experiments

Sorted bystander T cells show lower levels of peptide-induced activation than sorted antigen-specific T cells in vitro

To confirm that bystander cells are not activated by the antigens used in our assay but rather in a TCR-independent manner, we set up an *in vitro* proliferation assay using sorted CD3 high (bystander) and CD3 low (antigen-specific) T cells derived from five HD. For each donor, an AIM assay was first performed on freshly isolated PBMCs stimulated with a pool of viral peptides (Peptides or PEP) composed of SARS-CoV-2 Spike, EBV consensus, CMV pp65 and H1N1 NP overlapping peptides. On the following day, $CD4^+$ and $CD8^+$ AIM^+ CD3 high, $CD69^+$ (which were also CD3 high), and AIM^+ CD3 low T lymphocytes were sorted and plated to generate cell lines, as detailed in Table 4 (Materials and Methods, Section 3.5).

Single-positive CD69 high CD4+ and CD8+ cells were included in the sorting strategy, as they represent a subset of early activated T cells. Because these cells do not express other canonical AIM-positive markers, such as CD154 or CD137, they are likely to contain fewer low-affinity antigen-specific T cells, which would remain CD3 high, and a higher proportion of bystander T cells.

CD3 high, CD69+ and CD3 low T cell lines were expanded for 14 days and then tested for their ability to proliferate in response to the same pool of peptides used for their initial activation, presented by irradiated autologous feeder cells. Unstimulated cultures (CTRL) and a polyclonal stimulus (PHA+IL-2) controls were included as negative and positive controls. Proliferation was assessed five days after restimulation by dye-dilution, using a CFSE-style assay with CellTrace Violet (CTV).

The gating strategy and representative CTV profiles for each condition are shown in Fig. 12A and B. A cell line was considered proliferative when more than one CTV peak was present and fluorescence intensity was reduced relative to its paired control.

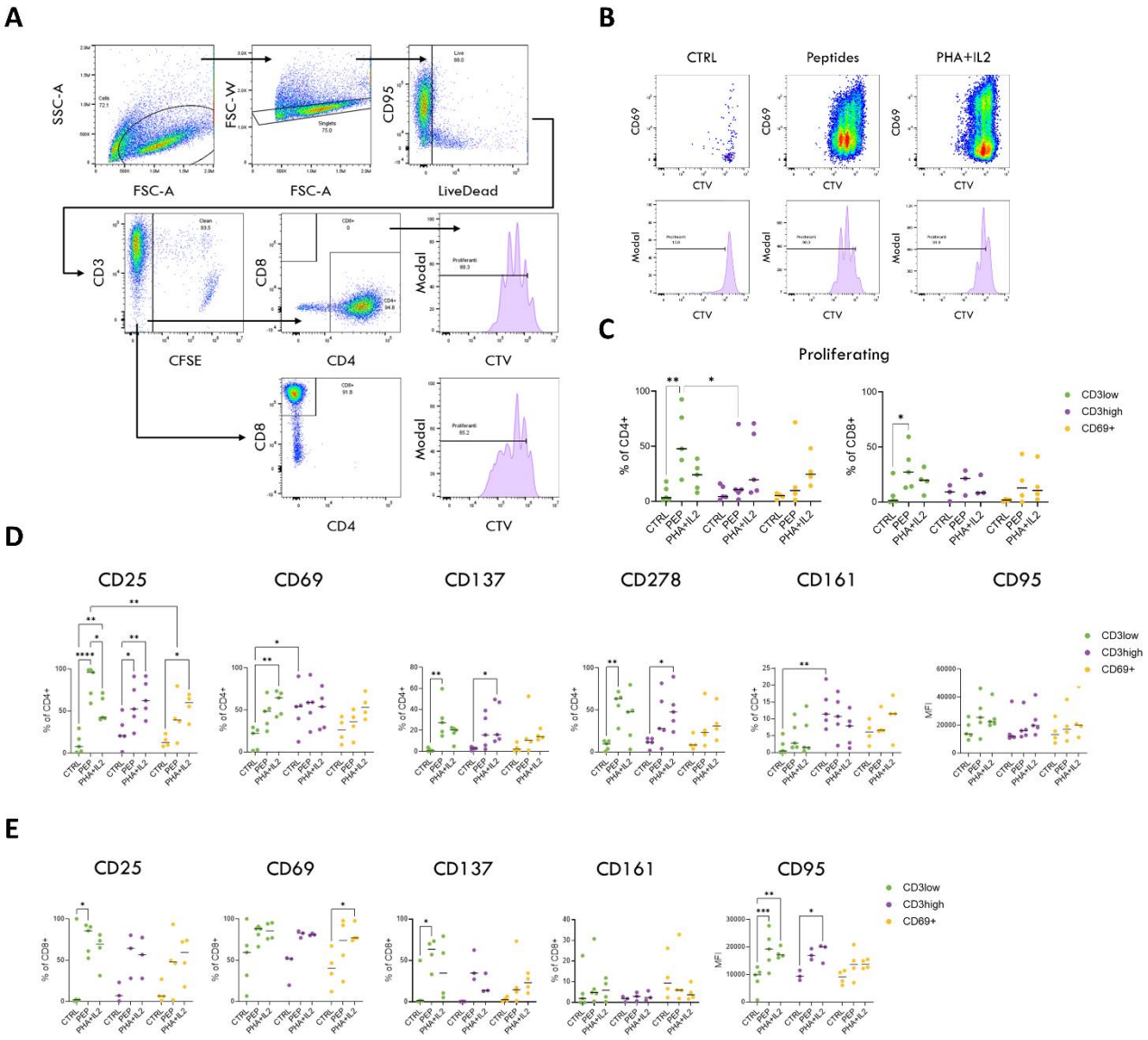

Figure 12. *Sorted bystander T cells show lower levels of activation to peptides than sorted antigen-specific T cells in vitro*. A) Gating strategy used to analyse CTV proliferation assay results. B) Representative plots showing CTV dilution in CTRL, Peptides, and PHA+IL-2 stimulation conditions. C) Dot plots representing the frequency of proliferating $CD4^+$ (left) and $CD8^+$ (right) cells, separated by stimulation condition (CTRL, Peptides/PEP, or PHA+IL-2) and coloured according to the original sorted subset (CD3 low in green, CD3 high in purple, $CD69^+$ in yellow). Each dot represents the average proliferation frequency for each HD and condition (CD3 low, CD3 high, and $CD69^+$ cell lines). Statistical analysis was performed using ordinary two-way ANOVA with Tukey's post-hoc test. *P < 0.05; **P < 0.01; no symbol = not significant. D) Expression of activation markers in $CD4^+$ CD3 low, CD3 high, and $CD69^+$ cell lines derived from each HD, separated by stimulation condition. Each dot represents the average frequency for each HD and condition. Statistical analysis was performed using ordinary two-way ANOVA with Tukey's post-hoc test. *P < 0.05; **P < 0.01; ****P < 0.0001; no symbol = not significant stellette. E) Frequencies of activation markers in $CD8^+$ CD3 low, CD3 high, and $CD69^+$ cell lines derived from each HD, separated by stimulation condition. Each dot represents the average frequency for each HD and condition. Statistical analysis was performed using ordinary two-way ANOVA with Tukey's post-hoc test. *P < 0.05; **P < 0.01; ***P < 0.001; no symbol = not significant.

Our data show that both $CD4^+$ and $CD8^+$ CD3 high and $CD69^+$ T cells showed minimal proliferation in response to the viral peptide pool, in contrast to CD3 low T cells (Fig. 12C), which proliferated robustly. Interestingly, PHA+IL-2 induced stronger proliferation in $CD4^+$ CD3 high and $CD69^+$ T cells, whereas CD3 low cells displayed a weaker response, when they were both compared with peptides. In $CD8^+$ T cells, PHA+IL-2 consistently drove a weaker proliferative response than Peptides, even in CD3 high cells.

We further confirmed peptide-induced T-cell activation by evaluating activation marker upregulation (Fig. 12D and E). CD25, CD137, and CD278 were markedly upregulated in peptide-stimulated CD3 low $CD4^+$ T cells, and also increased - though to a lesser degree - in CD3 high and $CD69^+$ subsets (Fig. 12E). Notably, CD3 high and, to a lesser extent, $CD69^+$ $CD4^+$ T cells exhibited high CD161 expression, an NK-associated receptor linked to the Th17 phenotype, as well as sustained CD69 expression across all conditions. In $CD8^+$ T cells, CD25, CD137, CD69, and CD95 were upregulated following both PEP and PHA+IL-2 stimulation, with CD3 high and $CD69^+$ subsets showing slightly lower expression levels than CD3 low T cells (Fig. 12E).

Overall, these data show that CD3 high T cell lines, as a population, fail to be robustly activated by the viral peptide pool, supporting the idea that most of them were initially activated through TCR-independent, bystander pathways. However, it is possible that this compartment also contains a fraction of peptide-specific T cells with low-avidity TCRs or suboptimal peptide recognition, which are not efficiently restimulated under our conditions. Thus, the bystander gate probably represents a mixture of truly TCR-independent bystander cells and weakly peptide-responsive T cells.

Bystander CD4+ T cells produce a set of cytokines compatible with Th17 and Th1-17 phenotypes

CD3 high, CD69+ and CD3 low cell lines were also tested for their cytokine production through stimulation with PMA and ionomycin in the presence of Brefeldin A to block secretion. Representative flow cytometry plots showing tested cytokines production are shown in Figure 13A. Intracellular cytokine staining revealed that $CD4^+$ CD3 high and $CD69^+$ T cells exclusively produced IL-17, IL-22, and IL-10, a cytokine profile corresponding to a Th17 phenotype (Fig. 13B). In contrast, CD3 low cells exhibited higher levels of IFN-γ compared with CD3 high and, in particular, compared to $CD69^+$ $CD4^+$ T cells. The presence of IFN-γ alongside Th17 signature cytokines suggests that CD3 high and $CD69^+$ $CD4^+$ T cells may also exhibit a Th1-17-like phenotype.

In $CD8^+$ T cells, differences among the three subsets were less pronounced, with only a slight increase in IL-22 production in CD3 high and $CD69^+$ cells compared with CD3 low cells (Fig. 13C). To further

confirm the Th17 phenotype of CD3 high and CD69^{+} CD4^{+} T cells, we stained CD3 high, CD69^{+}, and CD3 low CD4^{+} cell lines derived from three HD with a panel of fluorescent antibodies including CCR6 and CXCR3. Th17-like (CCR6^{+} CXCR3^{-}) and Th1-17-like (CCR6^{+} CXCR3^{+}) T cells were enriched, particularly in CD69^{+} cell lines (Fig. 13D). CD3 low cells appeared to consist predominantly of Th1-like (CXCR3^{+} CCR6^{-}) CD4^{+} T cells.

Thus, bystander CD3 high (and CD69^{+}) CD4^{+} T cells combine a Th17/Th1-17-biased cytokine repertoire with a CCR6^{+}CXCR3^{+}/CD161^{+} phenotype, a profile that has been linked to enhanced tissue homing and inflammatory potential and may therefore contribute to pathogenic responses in MS.

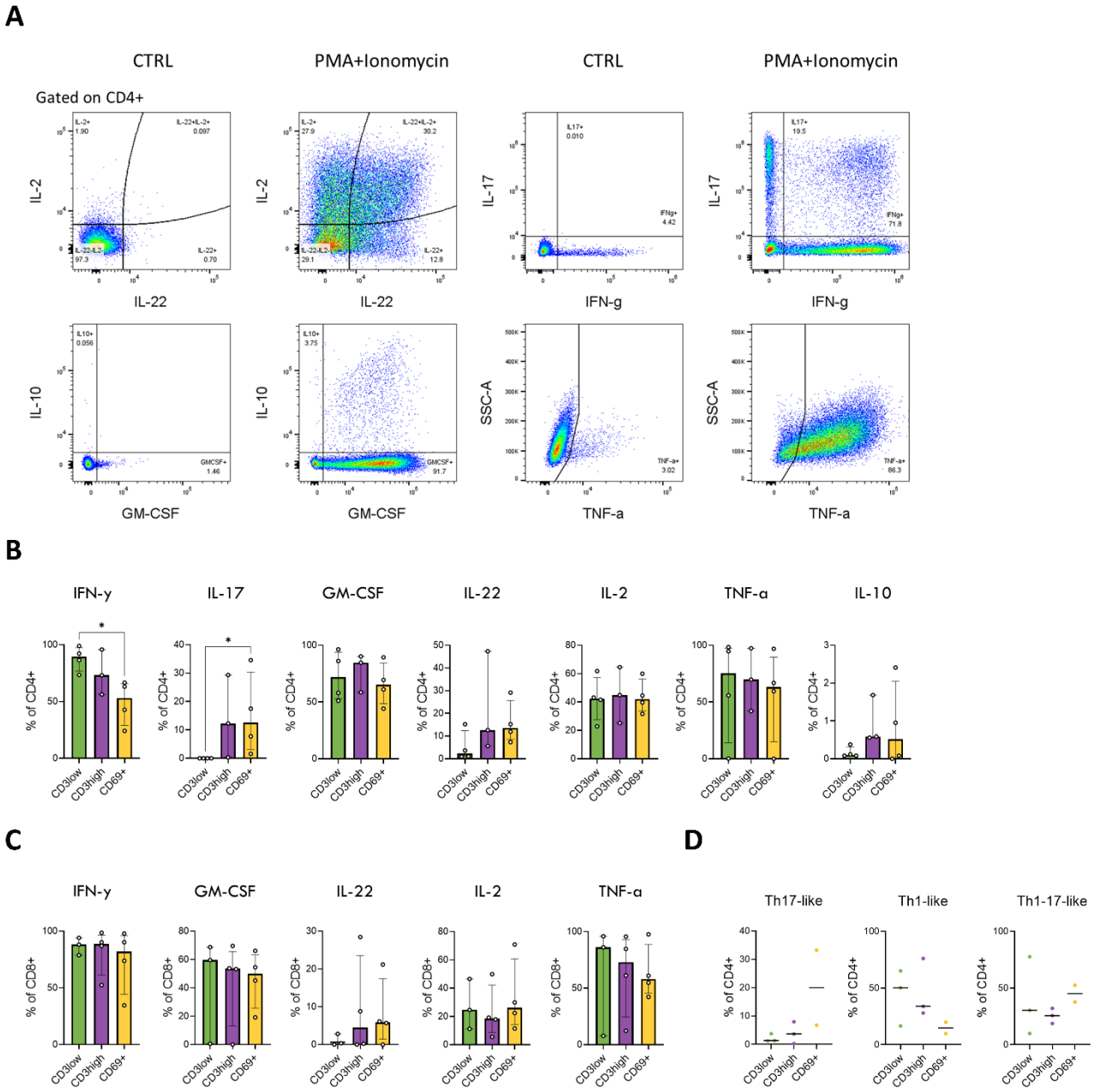

Figure 13. *Bystander CD4+ T cells produce a set of cytokines compatible to Th17 and Th1-17 phenotypes.* A) Representative flow cytometry plots showing tested cytokines production comparing unstimulated (CTRL) and PMA + Ionomycin stimulated conditions. B) Bar plots showing cytokine expression by $CD4^+$ T cells from each HD under each condition. Each dot represents the average frequency of a given cytokine for each HD and condition (CD3 low, CD3 high, and $CD69^+$ cell lines). Statistical analysis was performed using nonparametric Kruskal-Wallis test with Dunn's post-hoc correction. *P < 0.05; no symbol = not significant. C) Bar plots showing cytokine expression by $CD8^+$ T cells from each HD under each condition. Each dot represents the average frequency of a given cytokine for each HD and condition (CD3 low, CD3 high, and $CD69^+$ cell lines). Statistical analysis was performed using nonparametric Kruskal-Wallis test with Dunn's post-hoc correction. No symbol = not significant. D) Dot plots showing the frequencies of Th1, Th17, and Th1-17 $CD4^+$ T cells for each condition. Each dot represents the average frequency of each subset for each HD and condition (CD3 low, CD3 high, and $CD69^+$ cell lines). Statistical analysis was performed using nonparametric Kruskal-Wallis test with Dunn's post-hoc correction. No symbol = not significant.

4.3 Characterization of antigen-specific and bystander T cells in 3 HD and 3 naïve MS patients through scRNAseq

Acrtivated bystander T cells are contained within two clusters, characterized by inflammatory and interferon-driven gene expression.

To complete our characterization of bystander T cells, we performed a scRNA-seq experiment on 3 naïve MS patients and 3 HD from our cohort. First, we set up an AIM assay in which cells were stimulated with a pool of viral peptides composed of the Spike protein from SARS-CoV-2, EBV, CMV pp65, and H1N1 NP, in order to induce both bystander and antigen-specific activation. In addition, cells were stimulated with the previously-chosen homemade pro-inflammatory cytokine cocktail composed of IL-2, IL-12, and TNF-α at pre-optimized concentrations. A negative (unstimulated) control was also included in the experiment.

After 18 hours, cells were sorted and divided into four different samples-CTRL, Cytokines (Cyto), Peptides CD3 high (PEP CD3 high), and Peptides CD3 low (PEP CD3 low) - according to the gating strategy shown in Figure 14. Samples were then processed for the scRNA-seq experiment.

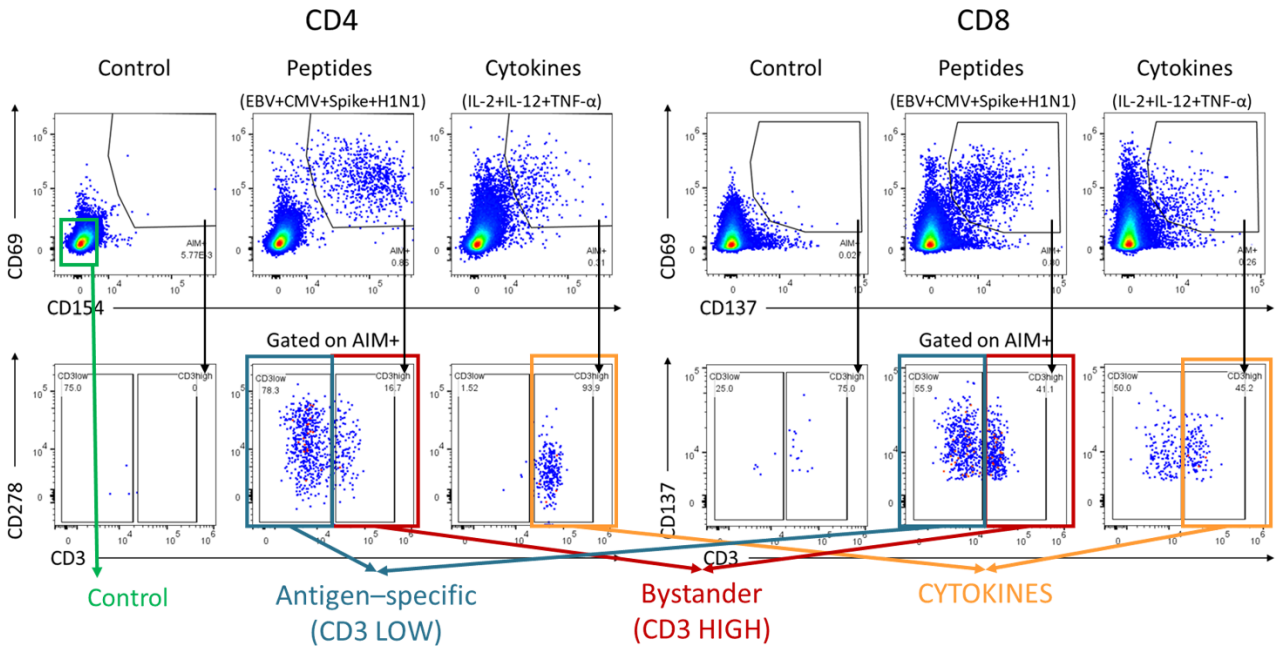

Figure 14. *Gating strategy used for scRNAseq experiments.* The four samples obtained from sorting are highlithed in different colours, green for control, blue for Peptides derived antigen-specific CD3 low T cells, red for Peptides induced bystander CD3 high T cells and yellow for cytokines.

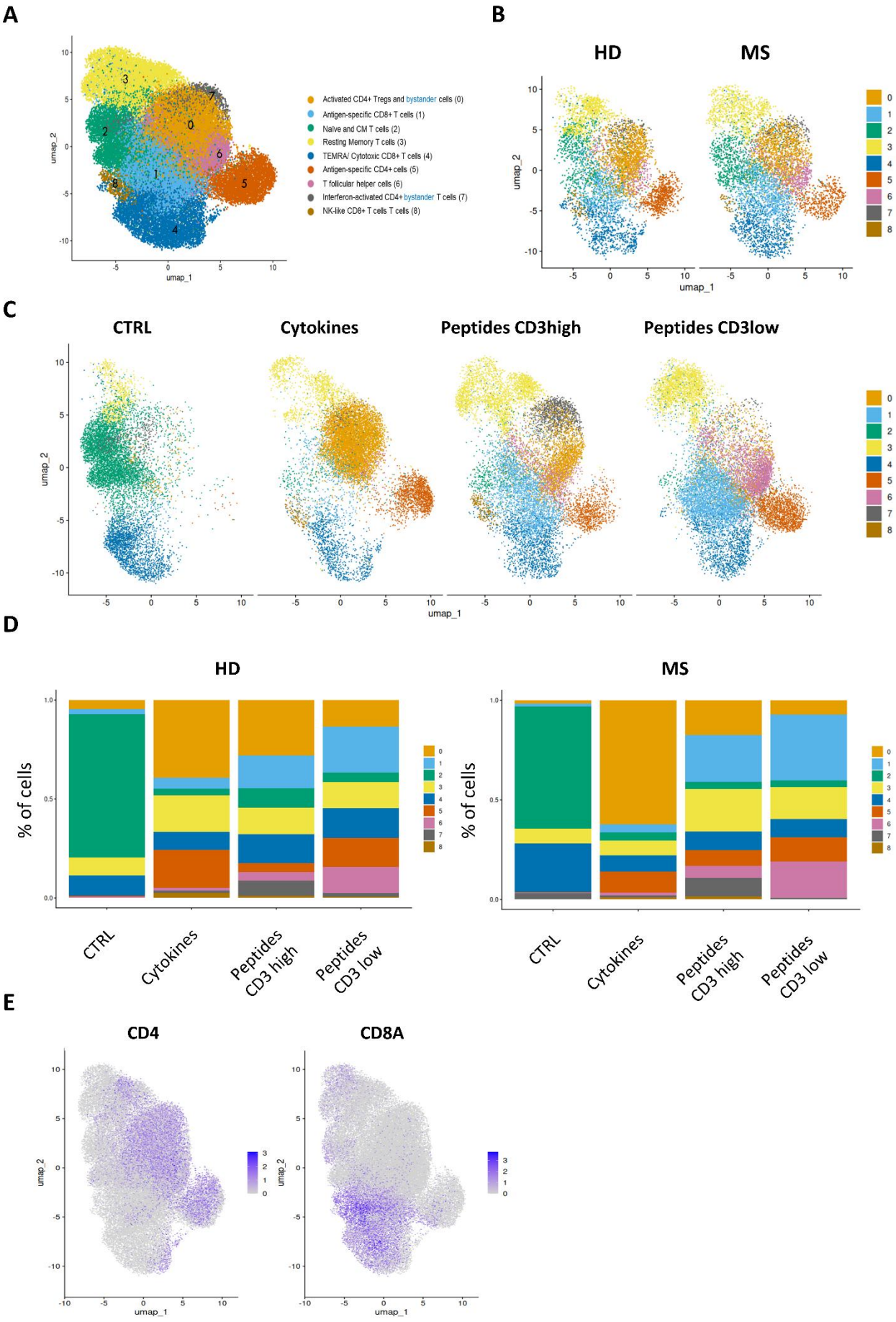
A
B
HD
MS
C
CTRL
Cytokines
Peptides CD3high
Peptides CD3low
D
HD
MS
% of cells
CTRL
Cytokines
Peptides CD3 high
Peptides CD3 low
E
CD4
CD8A
umap_1
umap_2
Activated CD4+ Tregs and bystander cells (0)
Antigen-specific CD8+ T cells (1)
Naive and CM T cells (2)
Resting Memory T cells (3)
TEMRA/ Cytotoxic CD8+ T cells (4)
Antigen-specific CD4+ cells (5)
T follicular helper cells (6)
Interferon-activated CD4+ bystander T cells (7)
NK-like CD8+ T cells T cells (8)

Figure 15. *Activated bystander T cells are contained within two clusters, characterized by inflammatory and interferon-driven gene expression.* A) Uniform Manifold Approximation and Projection (UMAP) representation of the complete scRNA-seq dataset, comprising all six donors and all stimulation conditions. Identified clusters are highlighted with distinct colors and numbered as indicated in the figure legend. B) UMAP plots of the scRNA-seq dataset stratified by HD and MS conditions. The MS dataset was downsampled to 6,000 cells to allow for clearer visualization. C) UMAP plots of the scRNA-seq dataset stratified by stimulation condition. D) Bar plots showing the frequency of cells in each cluster stratified by stimulation condition. HD (right) and MS (left) samples are shown separately. E) UMAP plots showing the differential distribution of *cd4* and *cd8α* gene expression across the scRNA-seq dataset.

Low-quality cells, highly stressed cells, and contaminating populations -such as monocytes, platelets, and B cells - were excluded from the analysis. We obtained 39,887 high-quality cells from MS patients and 5,838 cells from HD. To correct for batch effects between experiments, we applied CCA analysis and subsequently combined data from all conditions into a unified map (Fig. 15A).

Unsupervised clustering and gene enrichment analysis, performed using the Louvain algorithm at a resolution of 0.3 and the FindAllMarkers function, divided the map into 9 distinct clusters corresponding to several T-cell subtypes. Cluster annotation was performed using Gemini 3 Pro AI and verified manually.

Stratifying the dataset by disease condition did not reveal differences in cluster distribution in the UMAP (Fig. 15B). In contrast, the type of stimulation strongly influenced cluster enrichment or depletion across samples (Fig. 15C). We quantified these shifts by calculating the frequency of cells in each cluster, and visualizing their distribution. Data were also stratified by HD or MS condition (Fig. 15D).

The most striking differences included a strong depletion of cluster 2 in all stimulation conditions, an expansion of cluster 0 in both Cytokines and PEP CD3 high samples, a selective increase of cluster 7 in PEP CD3 high samples, and clusters 1, 5, and 6 being the most represented in PEP CD3 low samples.

We also observed that $CD4^+$ and $CD8^+$ T cells were differently distributed among clusters, with each cluster showing a predominance of either $CD4^+$ or $CD8^+$ T-cell subtypes (Fig. 15E).

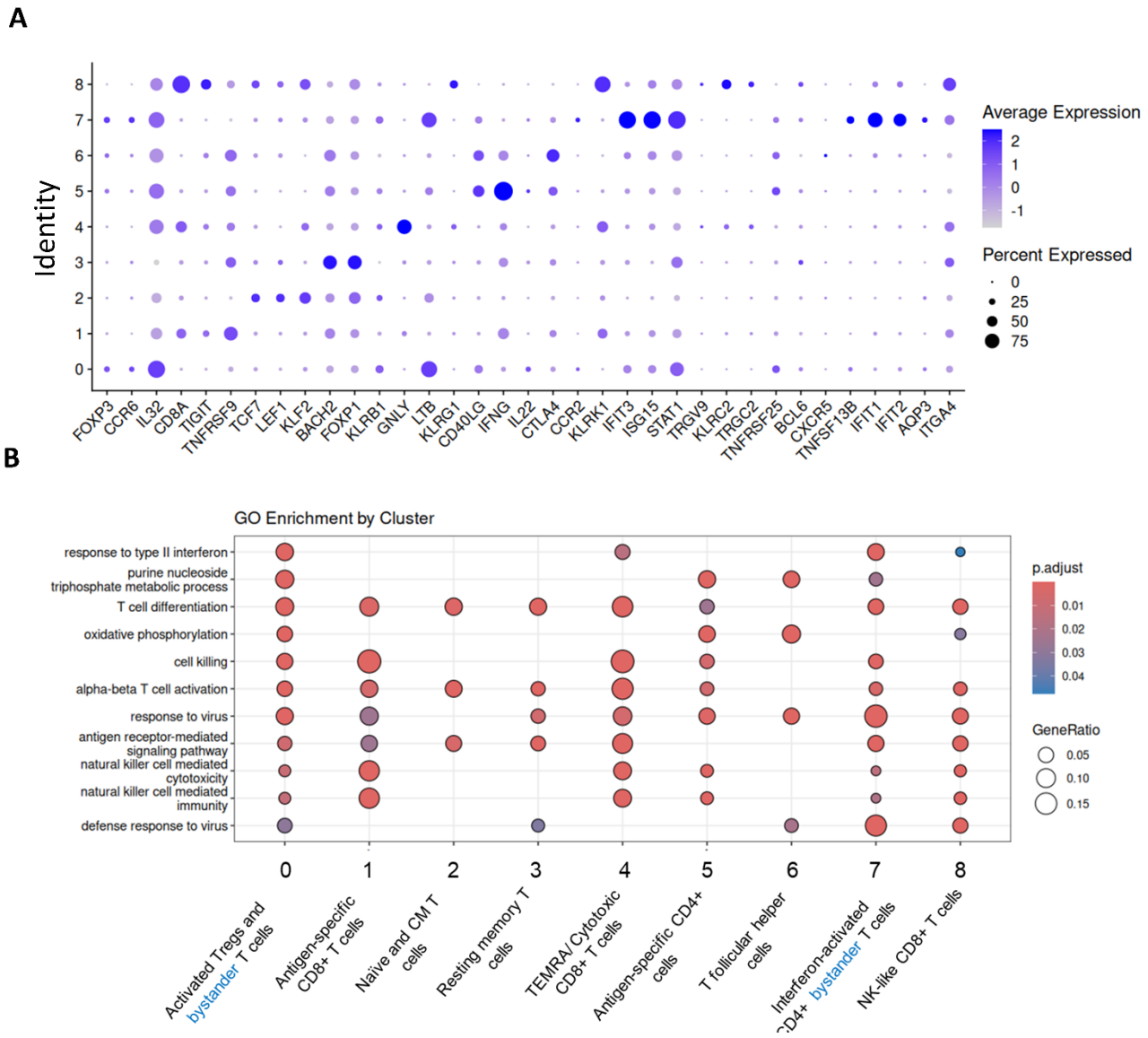

Figure 16. *Activated bystander T cells are contained within two clusters, characterized by inflammatory and interferon-driven gene expression.* A) Identity plot of each cluster, listed on the y-axis. The most representative genes for each cluster are shown on the x-axis. Average expression and percentage of expressing cells are indicated by the intensity of the blue color and the size of each dot, respectively. B) Gene Ontology (GO) enrichment analysis for each cluster. The most significant and relevant pathways are shown. Adjusted p values (p-adjust) and gene ratios (GeneRatio) are represented by a color gradient—from red (lower p values) to blue (higher p values)—and by dot size, respectively.

To annotate the transcriptional identity of each cluster, we examined the expression of canonical lineage and activation marker genes using a dot plot (Fig. 16A), where dot size indicates the fraction of cells expressing each gene and color intensity reflects average expression.

Cluster 0 was identified as activated, inflammation-driven Th cells, characterized by extremely high expression of *ltb*, *il-32*, and *stat1*, and by lower expression levels of *cd40lg* (CD154), *ccr6*, *il-22*, and *tnfsf13b* (BAFF) (Fig. 16A). Moreover, the presence of *foxP3* and *tnfrsf25* (GITR) suggested a Treg phenotype. Notably, cluster 7 shared some similarities with cluster 0, such as *ltb* and *il-32* expression;

however, it displayed markedly higher upregulation of IFIT genes (*ifit1*, *ifit2*, and *ifit3*) and *isg15*, suggesting a strong viral or interferon-induced activation.

We also identified a cluster of naïve and CM T cells (cluster 2), characterized by high expression of *tcf7*, *lef1*, and *klf2*, as well as a cluster of resting memory T cells (cluster 3), suggested by *bach2* and *foxp1* upregulation and the absence of activation markers.

Clusters 1 and 5 were annotated as antigen-specific $CD8^+$ and $CD4^+$ T cells, respectively, based on the expression of *tnfrsf9* (CD137), *cd40lg*, and *ifng*. Cluster 6 also contained activated $CD4^+$ T cells, identified as Tfh cells by their expression of *ctla4*, *bcl6*, and *cxcr5*.

Finally, two distinct clusters of cytotoxic and NK-like $CD8^+$ T cells—clusters 4 and 8—were identified by their characteristic signature genes, including *il-32*, *tigit*, *tnfrsf9*, *gnly*, *klrk1* (NKG2D), and *klrg1*.

We also performed a gene ontology (GO) enrichment analysis for each cluster, which confirmed predominantly interferon-driven activation in both clusters 0 and 7 (Fig. 16B). Interestingly, cluster 0 appeared to be more metabolically active compared to cluster 7.

Overall, the UMAP and frequency plots indicate that stimulation condition, rather than disease group, is the main driver of cluster composition in this cohort, with CTRL enriched for naïve/CM and resting memory states and activation conditions shifting cells into inflammatory/effector programs. Cytokines primarily induce the inflammatory bystander-like state (cluster 0) but also reproducibly generate an activated Th1-like CD4 cluster (cluster 5), in agreement with our premise that not all "activation-marker–high" clusters are peptide-dependent. In contrast, PEP CD3high most strongly enriches the interferon-driven bystander candidate (cluster 7) alongside cytotoxic/NK-like CD8 programs, supporting clusters 0 and 7 as the best candidates for activated bystander T cells in this dataset.

CD3 high and cytokine-stimulated samples show higher levels of pro-inflammatory genes

Our flow cytometry data from both HD and MS patients showed higher expression of CCR6 in activated bystander $CD4^+$ T cells. Conversely, antigen-specific $CD4^+$ T cells expressed higher levels of CD137. Moreover, our in vitro experiments on HD cell lines showed a slight upregulation of CD161 in sorted CD3 high cells. Interestingly, CCR6 expression is usually associated with CD161 expression in Th17 subsets[182]. To further validate these observations, we evaluated the expression of the corresponding genes -*ccr6*, *klrb1* (CD161), and *tnfrsf9* -across all stimulation conditions (Fig. 17A).

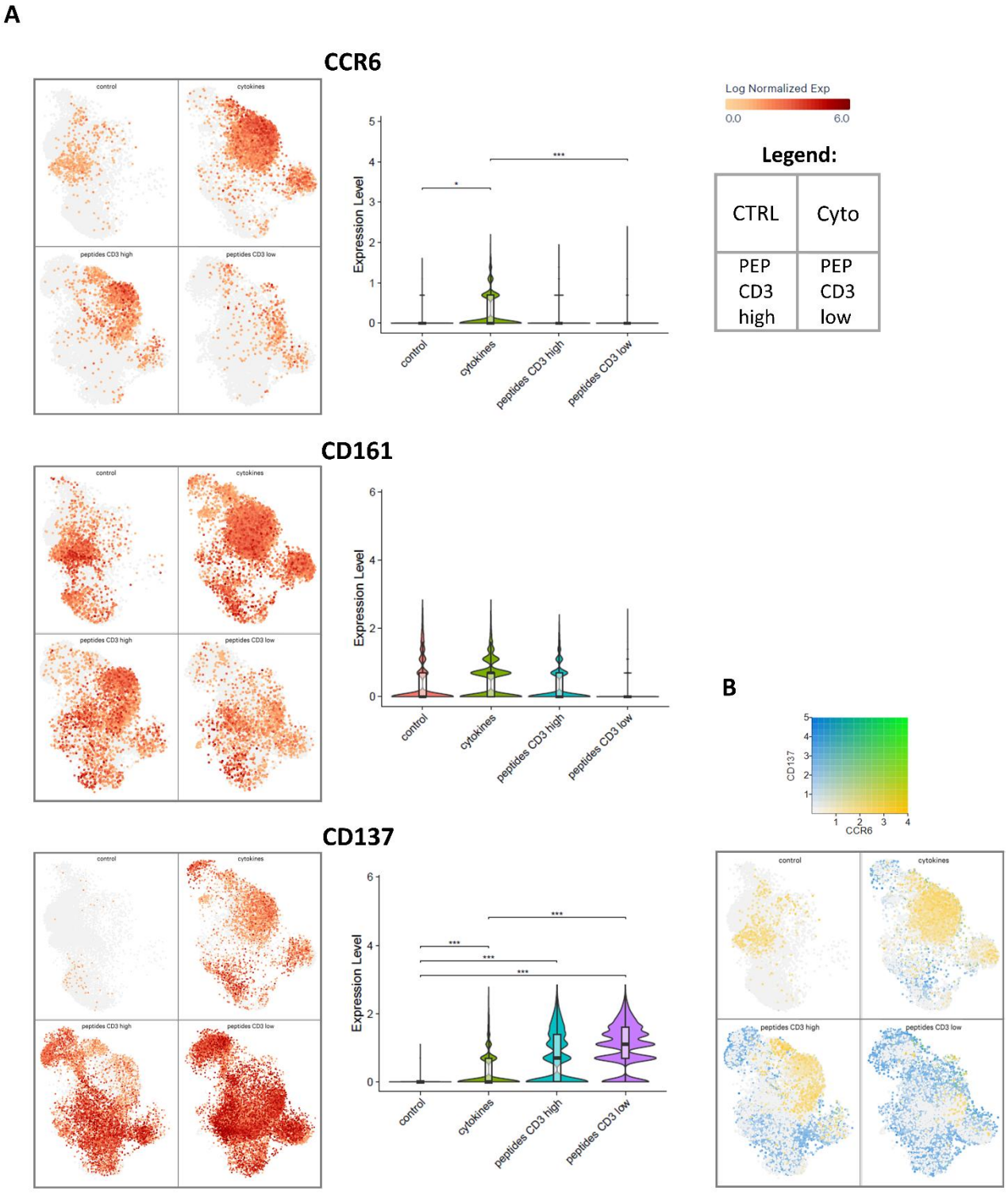

Figure 17. *CD3 high and cytokine-stimulated samples show higher levels of pro-inflammatory genes*. A) Paired UMAPs (right) and violin plots (left) showing *ccr6*, *klrb1* (CD161), and *tnfrsf9* (CD137) expression across the entire dataset, stratified by stimulation condition according to the figure legend (CTRL, Cyto, PEP CD3 high, PEP CD3 low). Statistical significance was assessed on pseudo-bulk data using DESeq2. $P < 0.05$; $^{**}P < 0.001$; no symbol indicates not significant. B) Representative UMAP of the entire dataset stratified by stimulation condition (CTRL, Cyto, PEP CD3 high, PEP CD3 low), showing the co-expression of *ccr6* and *tnfrsf9* (CD137).

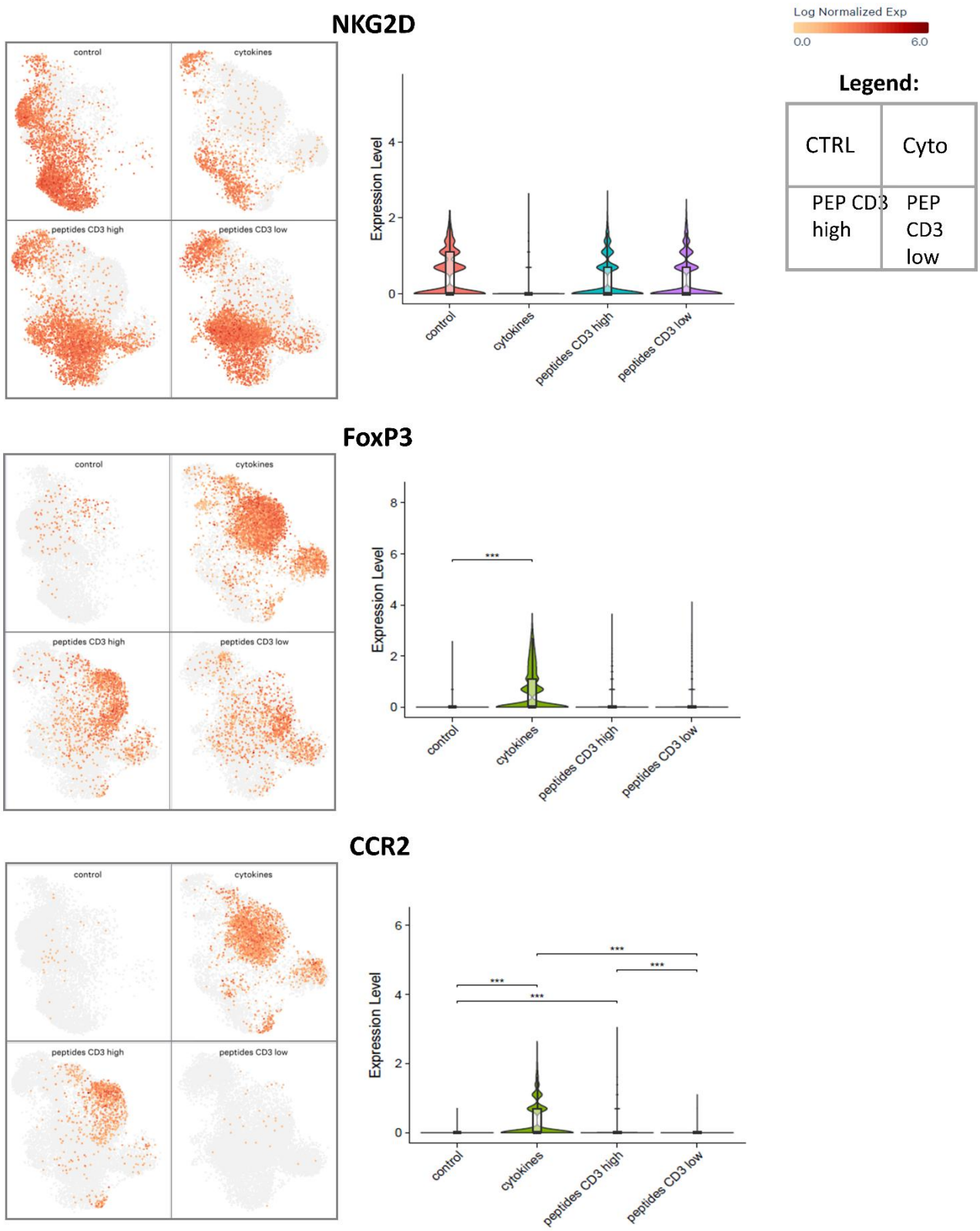

Figure 18. *CD3 high and cytokine-stimulated samples show higher levels of pro-inflammatory genes*. Paired UMAPs (right) and violin plots (left) showing *ltb*, *il-32*, and *il-22* expression across the entire dataset, stratified by stimulation condition according to the figure legend (CTRL, Cyto, PEP CD3 high, PEP CD3 low). Statistical significance was assessed on pseudo-bulk data using DESeq2. *P < 0.01; **P < 0.001; no symbol indicates not significant.

Crr6 gene expression was significantly upregulated in the cytokine condition, whereas *tnfrsf9* (CD137) expression was higher in the Peptides CD3 low condition. Visualization of *ccr6* and CD137 gene expression on the cumulative UMAP revealed an almost mutually exclusive expression pattern, particularly in clusters 0 and 7 (Fig. 17B). Notably, strong *ccr6* expression in these two clusters was observed only under cytokine and Peptides CD3 high stimulation conditions.

Furthermore, we evaluated the expression of additional pro-inflammatory genes enriched in clusters 0 and 7, specifically *ltb*, *il-32*, *ccr2*, and *il-22* (Fig. 18).

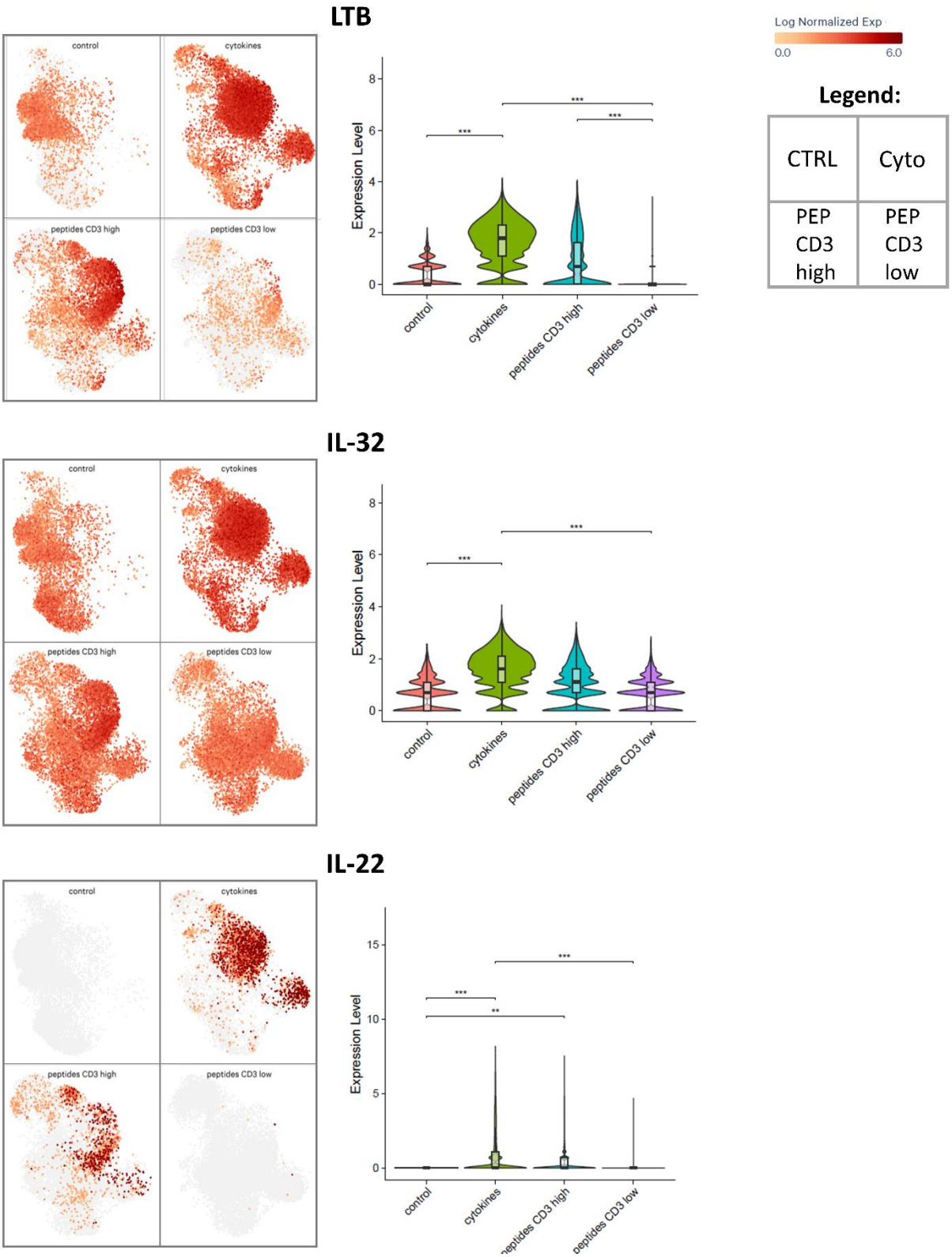

Figure 19. *CD3 high and cytokine-stimulated samples show higher levels of pro-inflammatory genes*. Paired UMAPs (right) and violin plots (left) showing klrk1 (NKG2D), foxP3, and ccr2 expression across the entire dataset, stratified by stimulation condition according to the figure legend (CTRL, Cyto, PEP CD3 high, PEP CD3 low). Statistical significance was assessed on pseudo-bulk data using DESeq2. **P < 0.001; no symbol indicates not significant.

Ltb and *il-22* genes were found to be highly expressed in the cytokine condition, followed by Peptides CD3 high. In contrast, *ltb* and *il-22* expression was almost absent in the Peptides CD3 low condition, suggesting their potential role as bystander activation markers.

Since bystander $CD8^+$ T cells are commonly described as expressing high levels of NKG2D, we assessed the expression of its corresponding gene in our dataset (Fig. 19).

Unexpectedly, *klrk1* expression was not increased in the CD3 high condition compared to the CD3 low counterpart. *FoxP3* gene expression was also evaluated and found to be significantly increased in the cytokine condition. Although *FoxP3* expression was detectable in both CD3 high and CD3 low conditions, no significant increase was observed compared to the control.

Finally, we examined the co-expression of two highly expressed pro-inflammatory genes in cluster 0, *ltb* and *il-32*, together with two genes typically associated with TCR-dependent stimulation, *ifng* and *cd40lg*, on the combined UMAP (Fig.20). As expected, *ltb* and *il-32* signals overlapped in cluster 0 and partially in cluster 7, whereas *ifng* and *cd40lg* were co-expressed in cluster 5, which is composed of antigen-specific $CD4^+$ T cells.

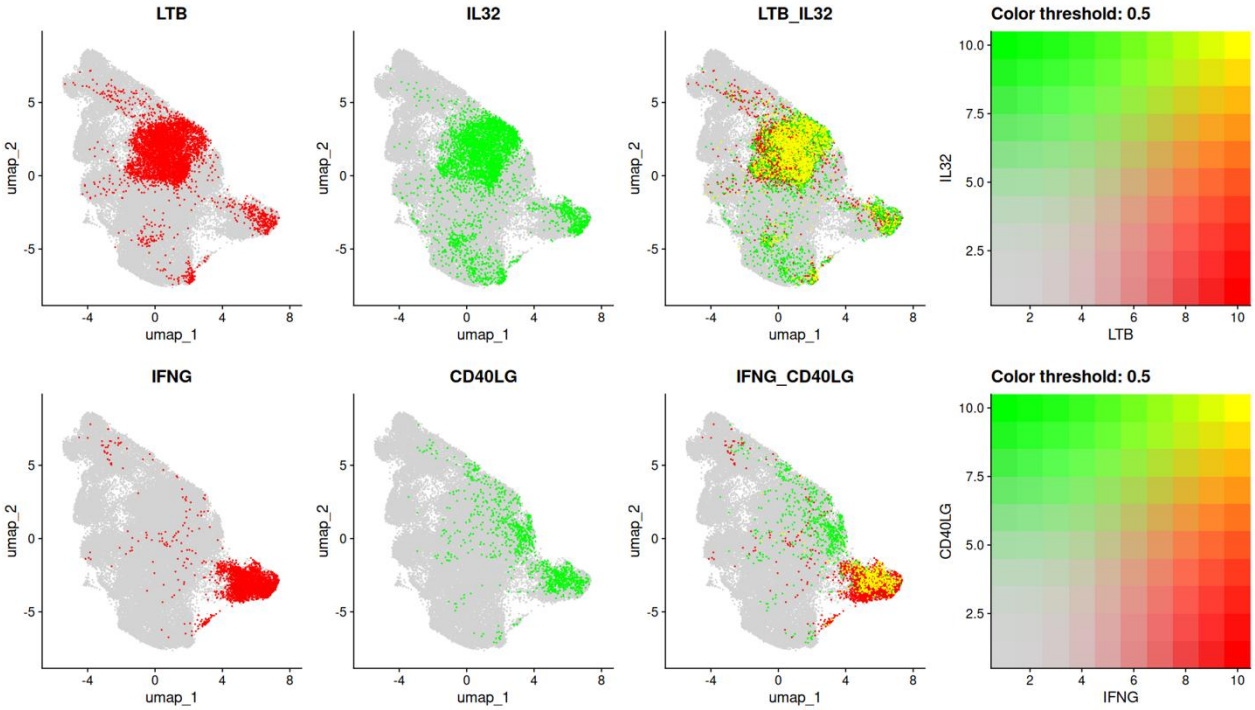

Figure 20. *CD3 high and cytokine-stimulated samples show higher levels of pro-inflammatory genes*. Representative UMAPs of the entire dataset showing co-expression of *ltb* and *il-32* (top) and of *ifng* and *cd40lg* (CD154) (bottom).

Together, these analyses show that bystander activation in our system corresponds to a cytokine- and CD3-high–linked inflammatory program enriched for *ccr6/klrb1* and *ltb/il-22* (with *il-32* as a broader

activation component), largely mapping to clusters 0 and 7, whereas antigen-specific activation is characterized by a TCR-dependent module marked by *tnfrsf9*/CD137 together with *ifng* and *cd40lg*, concentrated in cluster 5. The near-mutual exclusivity of *ccr6* and CD137 supports the existence of two separable activation trajectories (inflammation-driven vs TCR-driven), while the lack of a selective *klrk1*/NKG2D increase argues that the dominant bystander signal here is CD4-centered rather than a canonical bystander CD8/NK-like response.

MS patients possess some CDR3 sequences specific for myelin-associated proteins.

In addition to gene expression analysis, V(D)J sequencing of our scRNA-seq data was performed to investigate whether specific TCR clones were enriched in MS patients compared to HD. Moreover, we aimed to determine whether the different experimental conditions, listed as follows CTRL (CTR), Cytokines (CKs), bystander (CD3 high), and antigen-specific (CD3 low), shared similar or distinct clonalities and antigen specificities.

The first analysis focused on T-cell repertoire architecture, which is directly correlated with the breadth of antigen recognition. The greater the dissimilarity among TCR sequences, the broader the range of antigens that can be recognized, resulting in enhanced immune protection. T-cell repertoire architecture can be quantitatively assessed through network analysis.

We evaluated sequence similarity across all repertoires by determining, for each CDR3 sequence, whether it differed by a maximum of one amino acid from any other CDR3 within the same repertoire. We hypothesized that sequences differing by only one amino acid would represent clones with similar antigen-binding profiles. Different stimulation conditions resulted in distinct frequencies of connected clones in both MS patients and HD (Fig. 21A).

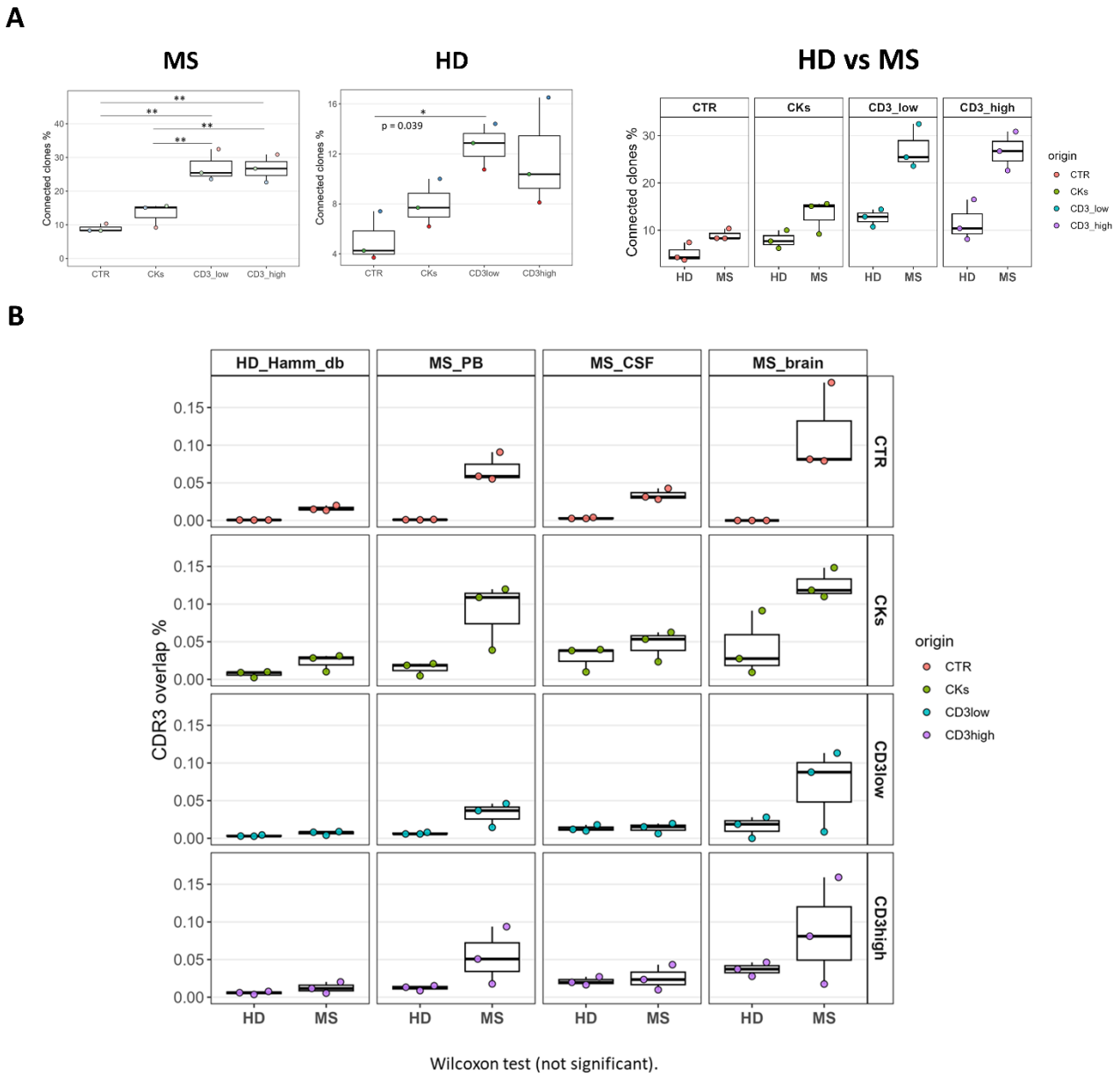

Figure 21. *MS patients possess some CDR3 sequences specific for myelin-associated proteins.* A) Graph showing clone network statistics reported as the percentage of connected clones in CTR, CKs, CD3 low, and CD3 high conditions in MS patients (n = 3, right), HD (n = 3, center), and in the combined dataset (left). Data are shown as mean ± SEM. One-way ANOVA followed by post hoc Tukey's test, or Wilcoxon test for MS versus HD comparisons, was performed. P values were adjusted for multiple comparisons ($P < 0.05$; $*P < 0.01$). B) Sequence overlap, reported as the percentage of overlapping CDR3 amino acid sequences, between samples from 3 HD individuals and 3 MS patients (CTR, CKs, CD3 low, CD3 high) and published TCR datasets from HD peripheral blood (HD_Hamm_dp) and MS peripheral blood (MS_PB), cerebrospinal fluid (MS_CSF), and brain lesions (MS_brain). Data are shown as mean ± SEM. Wilcoxon test was performed (not significant). C) Table showing CDR3 sequences shared between MS patients from our cohort and PMP-22– or MBP-specific TCRs. Source articles, amino acid matches, sample of origin, and IEDB associations are reported.

Notably, both CD3 high and CD3 low conditions showed higher frequencies of connected clones compared to unstimulated and CKs conditions. In particular, the frequency of connected clones in peptide-stimulated samples, both CD3 high and CD3 low, was higher in MS patients compared to HD (Figure 21B).

CDR3 sequences were then analyzed for overlap with public TCR datasets derived from HD PB (HD_Hamm_dp) and from MS PB (MS_PB), CSF (MS_CSF), and brain lesions (MS_brain) (see Materials and Methods, section 3.12).

Overall, the heatmap shows that these shared CDR3β sequences are more broadly represented in MS-derived repertoires than in healthy donors, with HD columns displaying only sporadic matches, whereas multiple sequences recur across MS columns (Fig. 22). Importantly, shared sequences were not confined to the CD3 low fraction (operationally defined as the antigen-engaged compartment in our assay), but were also detected within CD3 high repertoires and in the cytokine-cocktail (CKs) condition. This indicates that T cells carrying CDR3β sequences overlapping with public MS repertoires can be found among both antigen-driven and inflammation-driven (bystander-like) activated populations in our experimental system.

When stratifying the public MS repertoires by compartment of origin (PB, CSF, brain), several of the shared CDR3β sequences were detected across more than one compartment, and a subset overlapped with CSF and/or brain-derived repertoires.

Figure 22. *MS patients possess some CDR3 sequences specific for myelin-associated proteins.* This heatmap reports the top 50 most frequent shared CDR3s-a.a. between the three HD and MS with MS TCR repertoires retrieved from published studies. Public MS TCR data belong to PB, CSF, or brain lesions. The top 50 distribution is shown by group (red for MS, blue for HD), by MS compartment (dark gray for CSF, light orange for PB, light blue for brain) or by MS single-cell groups (light gray for CTR, purple for CKs, yellow for $CD3^{low}$, and green for $CD3^{high}$). The top 50 CDR3s-a.a. are listed on the y-axis.

Together, these observations support the presence, within our dataset, of CDR3β sequences that are repeatedly observed in MS across distinct tissue compartments, and they show that such sequences can be recovered from both CD3 low and CD3 high/CKs activation conditions in vitro.

Finally, CDR3 sequences from our scRNA-seq cohort were analyzed for potential antigen associations using publicly available TCR databases, including McPAS-TCR, VDJdb, and IEDB.

Interestingly, two out of three MS patients in our cohort harboured CDR3 sequences - CASSRTENYGYTF, CASSFGRNTEAFF, CASSPGLAGVADTQYF, CASSPNTEAFF, and CASSLGQNTEAFF -specific for peripheral myelin protein 22 (PMP-22), as reported by Súkeníková et al. (2024) in a study on peripheral blood–derived $CD4^+$ T cells from Guillain–Barré syndrome patients [183] (Fig.23A). These sequences were detected under different stimulation conditions in each MS patient, suggesting that PMP-22 specificity may be more closely related to disease status than to bystander activation.

A

Paper	Shared CDR3s	Specificity	Source	Amino acid match	Sample	IEDB association
PMID: 38233524	CASSPGLAGVADTQYF	PMP22	Peripheral blood CD4+ cells from Guillain-Barré patients	total	CTR, $CD3^{high}$ patient 1	
	CASSPNTEAFF				CTR, $CD3^{high}$ patient 1	SARS-CoV-2
	CASSRTENYGYTF				CKs, $CD3^{low}$ patient 4	
	CASSFGRNTEAFF				CKs, $CD3^{low}$ patient 4	
	CASSLGQNTEAFF				CKs, $CD3^{low}$ patient 4	SARS-CoV-2, EBV
PMID: 21199956	CATSALGDTQYF	MBP	TCR clone Hy.1B11 from a RRMS patient	1 a.a. apart (LD = 1) with CATSAEGDTQYF	$CD3^{high}$ patient 4	MBP, phosphomannomutase (*P. aeruginosa*), UL15 (HHV1)
	CATSAAGDTQYF					MBP

B

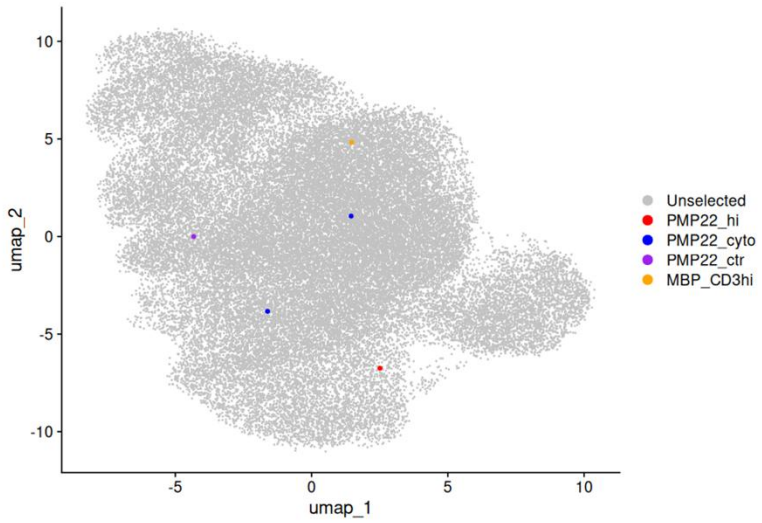

Figure 23. *MS patients possess some CDR3 sequences specific for myelin-associated proteins.* A) Table showing CDR3 sequences shared between MS patients from our cohort and PMP-22– or MBP-specific TCRs. Source articles, amino acid matches, sample of origin, and IEDB associations are reported. B) UMAP showing PMP-22 and MBP-specific CDR3s overlap on our scRNAseq clusters. Specific TCR clones are highlighted in different colours.

Moreover, one sequence -CATSAEGDTQYF -identified in the CD3 high condition from one MS patient in our scRNA-seq cohort differed by only one amino acid from a myelin basic protein (MBP)–specific CDR3 sequence previously described by Sethi et al. [184]. No CDR3 sequences from HD were found to be associated with MBP- or PMP-22-specific TCRs reported in the IEDB, McPAS-TCR, or

the study by Súkeníková et al. (2024)[183]. We examined which clusters our PMP-22 and MBP CDR3 sequence clones belonged to (Fig. 23B). Specifically, PMP-22-specific TCR clones from the control, cytokine-treated, and CD3 high-induced conditions overlapped with clusters 2, 0, and 4, respectively. Interestingly, the MBP CDR3 sequence from the CD3 high condition was derived from cluster 7.
Overall, these results suggest that virus-induced immune responses in MS patients may promote the expansion of pre-existing, potentially cross-reactive TCR clones specific for myelin proteins, thereby contributing to autoimmunity or disease exacerbation.

4.4 Phenotypization of brain-T cells in a mice model of Alzheimer's disease

During my research stay at Washington University in Marco Colonna's laboratory -an environment with strong expertise in neuroimmunology, brain-resident immune cells, and Alzheimer's disease mouse models - I aimed to extend my immunophenotyping skills to the CNS compartment and to learn how to integrate high-parameter flow cytometry with tissue imaging in a neurodegenerative setting. A central conceptual link with the broader theme of this thesis is compartmentalized inflammation: understanding whether immune cells detected in CNS preparations originate from the blood, from CNS-border tissues such as the meninges, or are truly embedded within the parenchyma is essential to interpret "CNS immunity" across diseases and homeostatic conditions. The origin of T cells responsible for neuroinflammation is particularly important, as differences in phenotype, function, and differentiation across compartments may lead to distinct immune responses[185]. Moreover, T cells are also present in the CNS under healthy conditions, and the characterization of these homeostatic CNS T-cell populations is still in its early stages[186–188].
For this reason, I established an experimental workflow to (i) map the anatomical accessibility/origin of brain T cells in healthy mice using dual in vivo CD45 labeling, and (ii) evaluate how neurodegenerative inflammation in the 5xFAD model influences T-cell recruitment, localization, and tissue-associated phenotypes using complementary confocal microscopy and flow cytometry.

Both CD4+ and CD8+ T cells are present in the brain parenchyma of WT mice

It is now well established that T cells are present in healthy brains, although their function remains largely understudied. To investigate whether brain-isolated T cells originate from the periphery, from the the meninges, or are truly tissue-resident within the brain parenchyma, we performed the following experiment. Three WT mice were injected in the intra-cisterna magna (ICM) with an anti-CD45 antibody conjugated to Alexa 647. One hour later, a second anti-CD45 antibody conjugated to

PE was injected intravenously (IV). Mice were then sacrificed, and brains were collected for flow cytometry analysis (Fig. 24A).

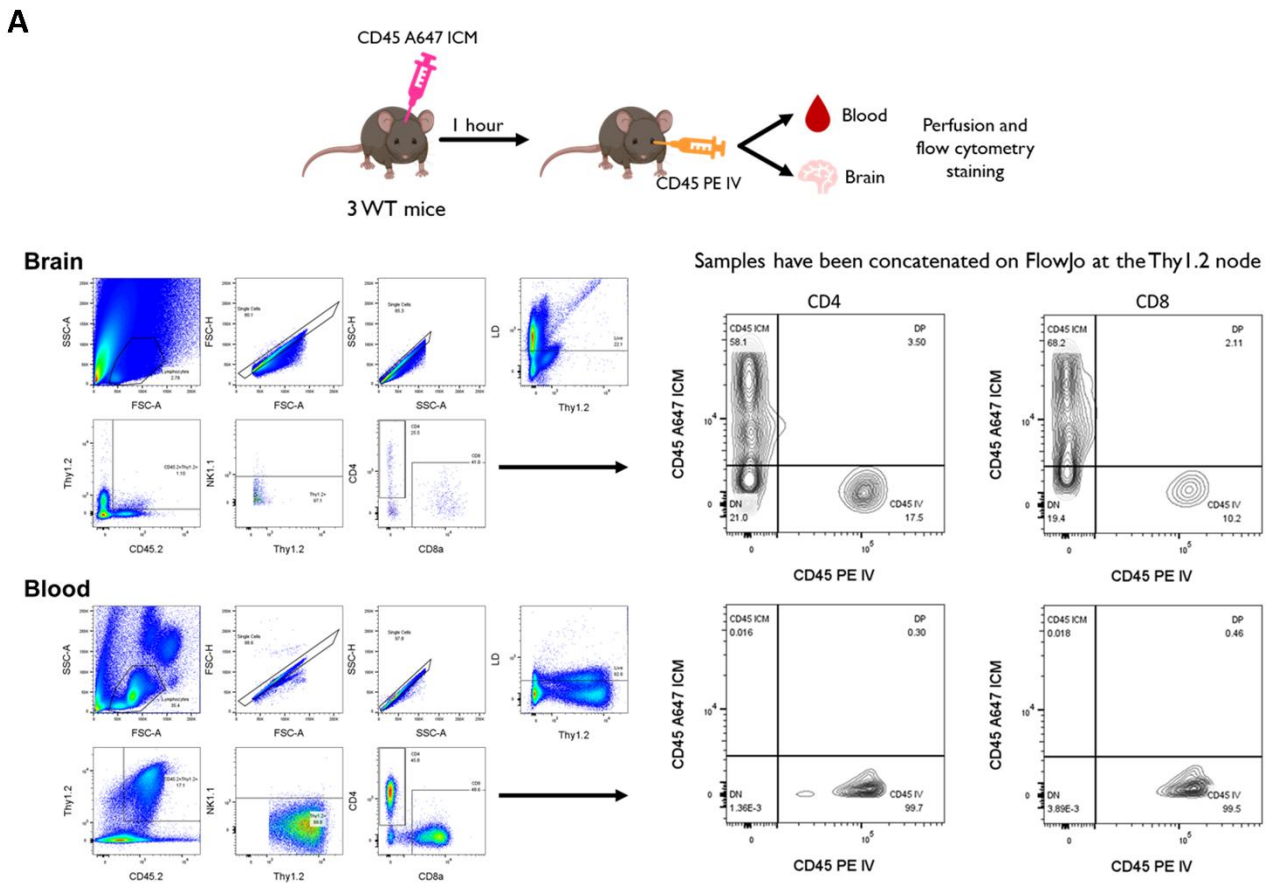

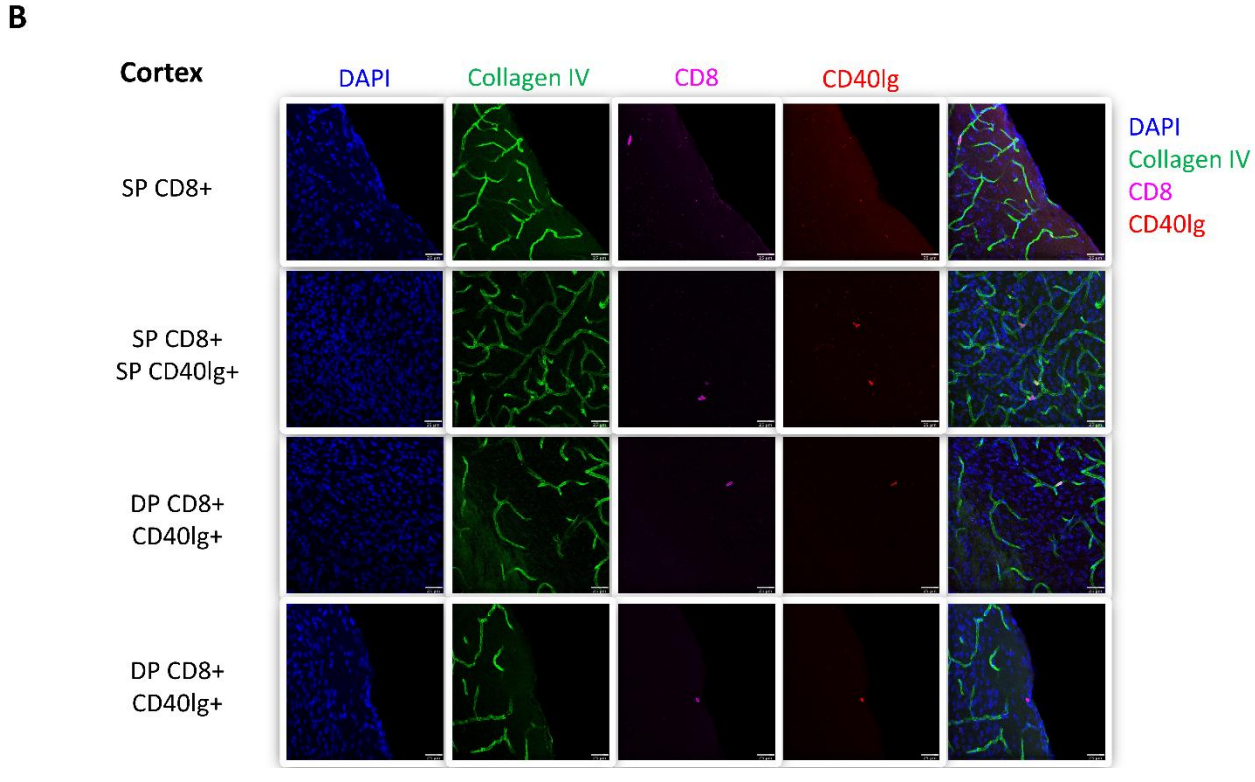

Figure 24. *Both CD4+ and CD8+ T cells are present in the brain parenchyma of WT mice*. A) Schematic representation of the experiment (top) to determine the origin of brain and whole blood T cells from three WT mice. CD45-Alexa 647 (A647) was injected into the intra-cisterna magna (ICM) of each mouse, followed by intravenous (IV) injection of CD45-PE prior to sacrifice. Blood and brains were collected for flow cytometry analysis. The bottom panels show the gating strategy (left) and concatenated results (right) of the experiment, separated by $CD4^+$ and $CD8^+$ T cells. B) Representative confocal images of the cortex from a Cd40lg-cre;Rosa26-tdTomato mouse stained with DAPI (nuclei, blue), Collagen IV (blood vessels, green), and CD8 (pink). SP = single positive for either $CD8^+$ or $CD40lg^+$; DP = double positive for both $CD8^+$ and $CD40lg^+$.

Whole blood was processed in parallel as a control. By concatenating events from all three mice, we observed that the majority of brain $CD4^+$ and $CD8^+$ T cells were single positive for CD45-Alexa 647 (58.1%-68.2%), consistent with a meningeal origin. Only a small fraction of brain T cells were single positive for CD45-PE (10.2%-17.5%), indicating a peripheral origin. Notably, a significant proportion of double-negative T cells (CD45-Alexa 647^- CD45-PE^-; 18.4%-21.0%) was detected, suggesting that some T cells are indeed resident within the brain parenchyma. Whole blood analysis confirmed assay functionality, with nearly all $CD4^+$ and $CD8^+$ T cells being CD45-PE single positive (99.5%-99.7%).

These results indicate that both $CD4^+$ and $CD8^+$ T cells are present in the brains of WT mice. To further validate this finding, we employed a Cd40lg-cre;Rosa26-tdTomato reporter mouse model, in which 100% of $CD4^+$ and 30% of $CD8^+$ T cells are labelled by tdTomato. Cortical brain sections from three Cd40lg-cre;Rosa26-tdTomato mice were stained for confocal microscopy using DAPI to visualize nuclei, Collagen IV to label blood vessels, and CD8 (Fig. 24B). This experiment confirmed the presence of $CD8^+$ single-positive, $CD40lg^+$ single-positive, and $CD40lg^+$ $CD8^+$ double-positive T cells within the brain parenchyma.

5xFAD mice show higher levels of CD8+ T cells infiltration in parenchyma of different brain regions

Considering our findings in WT mice, we next investigated whether the inflammation present in 5xFAD mouse brains would lead to increased recruitment of T cells. Whole hemibrain sections from three WT and three 5xFAD mice were prepared for confocal microscopy, using Methoxy-DAPI to identify Aβ plaques, along with Collagen IV and CD3 staining (Fig. 25A). Four brain regions were analysed: the cortex, corpus callosum, hippocampus, and olfactory bulb. The first three regions are relevant in 5xFAD studies due to the preferential accumulation of plaques, while the olfactory bulb is known to be an immune-enriched area in mice.

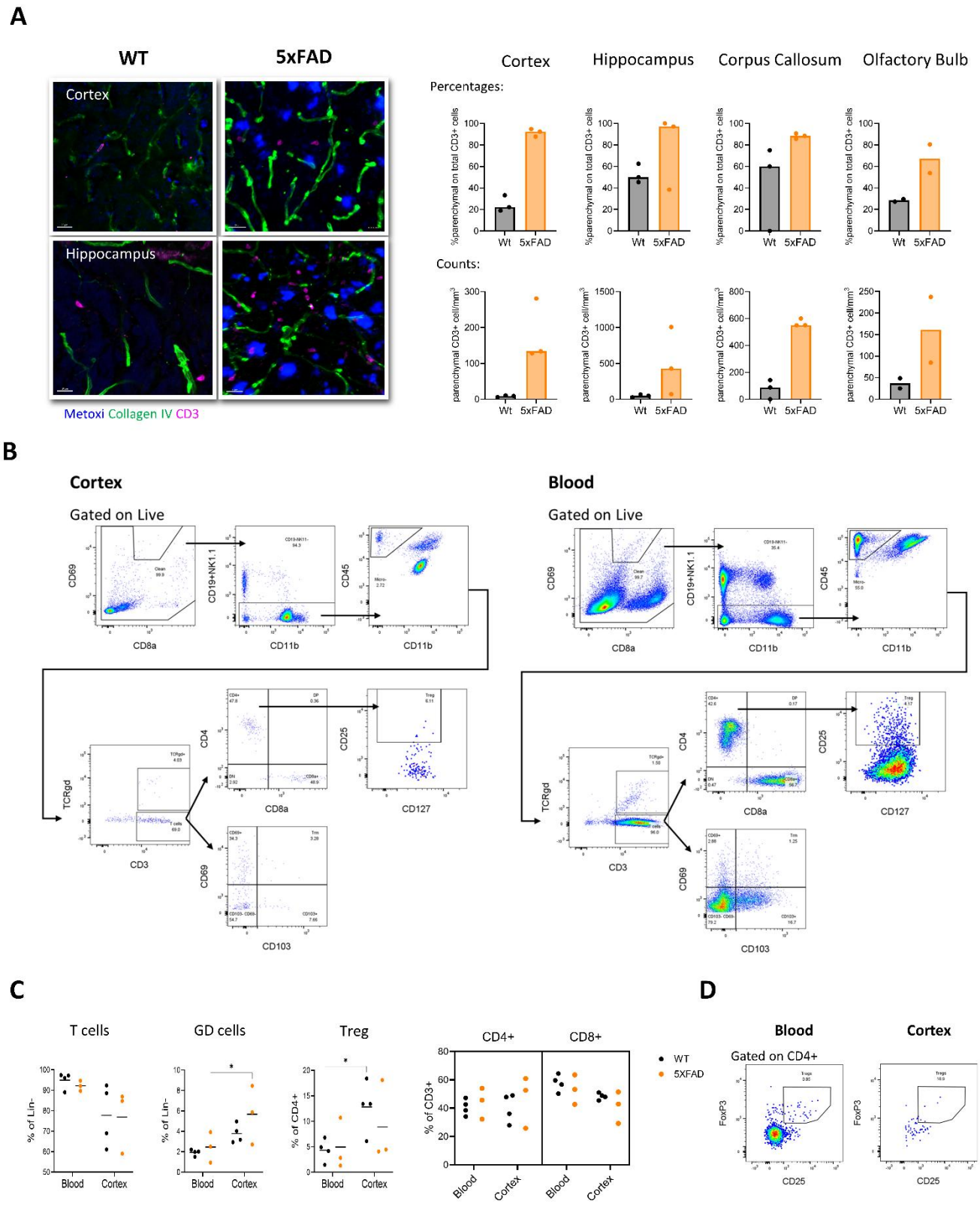
A
WT
5xFAD
Cortex
Hippocampus
Metoxi Collagen IV CD3
Cortex
Hippocampus
Corpus Callosum
Olfactory Bulb
Percentages:
%parenchymal on total CD3+ cells
Wt
5xFAD
Counts:
parenchymal CD3+ cell/mm3
B
Cortex
Blood
Gated on Live
CD69
CD19+NK1.1
CD45
CD8a
CD11b
TCRgd
CD3
CD4
CD25
CD127
CD103
C
T cells
GD cells
Treg
% of Lin-
% of CD4+
CD4+
CD8+
% of CD3+
Blood
Cortex
WT
5XFAD
D
Blood
Cortex
Gated on CD4+
FoxP3
CD25

Figure 25. *5xFAD mice show higher levels of CD8+ T cells infiltration in parenchyma of different brain regions.* A) Representative confocal images (left) of the cortex and hippocampus from WT and 5xFAD mice stained with Methoxy-DAPI (plaques and nuclei, blue), Collagen IV (blood vessels, green), and CD3 (pink). The right panels show quantification of $CD3^+$ T cells in four brain regions (cortex, hippocampus, corpus callosum, and olfactory bulb) comparing WT and 5xFAD mice. Statistical analysis was performed using the Mann-Whitney test. No symbol, not significant. B) Representative gating strategy used to phenotype T cells in brain cortex and blood from WT and 5xFAD mice. C) Comparison of different T cell subpopulations (conventional T cells, γδ T cells, Tregs, $CD4^+$ and $CD8^+$ T cells) in blood and brain cortex of four WT and three 5xFAD mice. Statistical analysis was performed using 2-way ANOVA with uncorrected Fisher's LSD multiple comparisons. *$P < 0.05$; no symbol, not significant. D) Flow cytometry plots showing the frequency of FoxP3+CD25+ Tregs cells in both blood and cortexes derived from 4 pooled samples of WT mice.

Quantification of confocal images revealed an enrichment in both the frequency and number of $CD3^+$ T cells in 5xFAD brains across all analysed regions. Notably, these T cells appeared particularly concentrated around plaques, suggesting a potential role in local inflammation.

To further characterize these T cells, we optimized a multi-colour flow cytometry panel and applied it to brain cortexes from four WT and three 5xFAD mice. We focused exclusively on the cortex to minimize contamination from other brain regions naturally enriched in T cells and to facilitate direct comparison with confocal data. Experiments were performed in parallel on both cortex and blood from each mouse (Fig. 25B).

Flow cytometry results indicated that the overall frequency of T cells was comparable between 5xFAD and WT mice (Fig. 25C). Interestingly, cortexes showed slight enrichment in γδ T cells and Tregs compared with blood, with γδ T cells being more abundant in 5xFAD and Tregs in WT. No significant differences were observed in $CD4^+$ and $CD8^+$ distribution between blood and cortex. To confirm the increase in Tregs in the cortex of WT mice, we repeated the staining by adding FoxP3 to the fluorescent antibody panel (Fig. 25D). Owing to the higher number of cells required for intracellular staining, blood and cortexes cells from four WT mice were pooled. Although these data support our previous flow cytometry results, the pooled cortexes samples showed a FoxP3+CD25+ Tregs frequency of 10.9 compared with 0.85 in pooled blood samples; however, the low number of events within the gate renders this result unreliable.

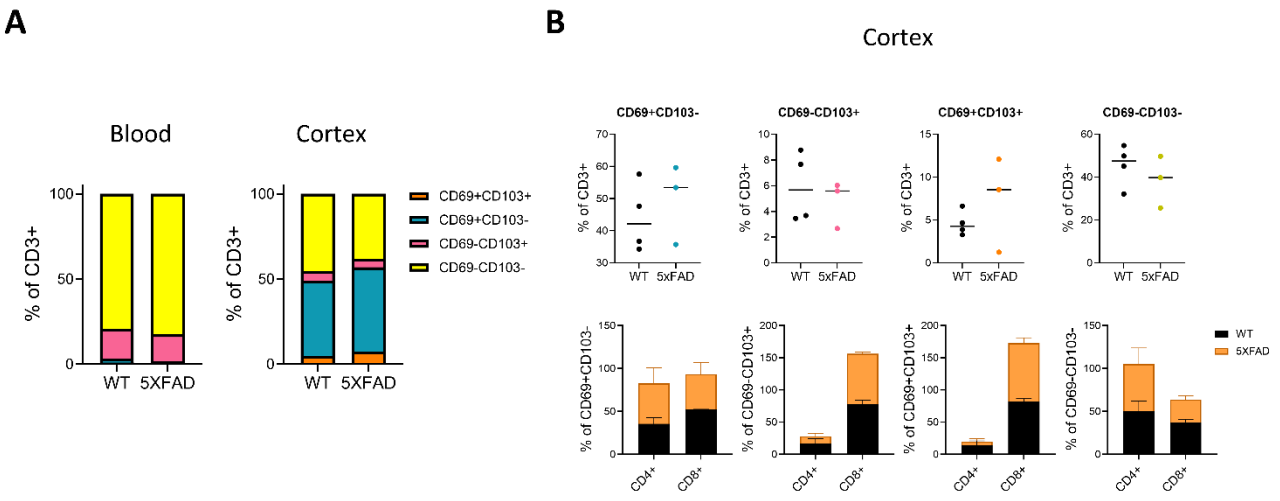

Figure 26. *5xFAD mice show higher levels of CD8+ T cells infiltration in parenchyma of different brain regions.* A) Cumulative bar plots showing the distribution of $CD3^+$ CD69/CD103 subpopulations in blood and brain cortex of WT and 5xFAD mice. B) Dot plots showing frequencies of $CD3^+$ CD69/CD103 subpopulations in brain cortex (top) and cumulative bar plots showing the proportion of $CD4^+$ and $CD8^+$ T cells within each CD69/CD103 subset for both WT and 5xFAD mice. Statistical analysis was performed using the Mann-Whitney test. No symbol, not significant.

Analysis of CD69 and CD103 expression allowed the identification of tissue-resident ($CD69^+CD103^+$) versus blood-derived ($CD69^-CD103^-$) T cells (Fig. 26A). Surprisingly, both WT and 5xFAD cortexes contained a substantial proportion of blood-derived T cells (WT 32.1–54.7%, 5xFAD 25.6–49.7%), while the most represented subset was $CD69^+CD103^-$ (WT 34.3–57.6%, 5xFAD 35.7–59.6%), indicating recent activation and likely extravasation. Tissue-resident $CD69^+CD103^+$ and $CD69^-CD103^+$ T cells were less frequent (WT 3.3–6.6% and 3.5–8.8%; 5xFAD 1.2–12.1% and 2.7–6.0%, respectively). In contrast, T cells from blood were mainly negative for both markers (WT 16.7–18.9%, 5xFAD 14.0–17.0%), although a considerable fraction of $CD69^-CD103^+$ cells was also observed (WT 76.6–80.1%, 5xFAD 79.9–85.0%).

Finally, the distribution of $CD4^+$ and $CD8^+$ T cells among CD69/CD103 subsets was evaluated (Fig. 26B). Tissue-resident $CD69^+CD103^+$ and $CD69^-CD103^+$ cells were predominantly $CD8^+$, whereas $CD69^+CD103^-$ cells exhibited a more balanced ratio of $CD4^+$ and $CD8^+$ T cells. Overall, WT and 5xFAD mice showed comparable frequencies across all subsets. These results indicate a preferential recruitment of $CD8^+$ over $CD4^+$ T cells in the brain cortex. However, using this flow cytometry approach, we could not confirm the confocal microscopy observation of increased T cell enrichment in 5xFAD compared with WT brains.

Overall, these experiments demonstrate that both $CD4^+$ and $CD8^+$ T cells are detectable in the brains of WT mice, and that this brain-associated T-cell pool is heterogeneous: most cells appear consistent

with a meningeal/CSF-accessible compartment, a smaller fraction is consistent with a blood-associated origin, and a substantial double-negative fraction suggests the presence of parenchyma-inaccessible (likely tissue-associated/resident) T cells. This conclusion was independently supported by reporter-based confocal imaging, which confirmed the presence of $CD8^+$ and CD40lg-labeled T cells within the brain parenchyma. In the 5xFAD neurodegenerative model, confocal microscopy across multiple regions indicated an apparent enrichment of $CD3^+$ T cells—often concentrated around Aβ plaques—supporting a spatial association with focal inflammatory pathology. In contrast, flow cytometry of dissociated cortex did not reveal a clear increase in total T-cell frequency, but it showed that cortex T cells are enriched for activation/retention-associated phenotypes ($CD69^+CD103^-$) and that the more tissue-associated subsets are predominantly $CD8^+$, suggesting preferential recruitment/retention of $CD8^+$ T cells in the inflamed CNS milieu. Taken together, the combined imaging and flow approach supports a model in which neurodegeneration may primarily alter T-cell localization and activation state, particularly plaque-proximal accumulation, rather than uniformly increasing total cortical T-cell abundance detectable by bulk dissociation.

5. Discussion and Conclusion

In this project, we aimed to unravel the role of viral infections in the context of MS, with a particular focus on T lymphocytes. Nonspecific bystander T-cell inflammation has been described in many autoimmune disorders, including MS, and its link to viral infection is undeniable[89]. In this cohort, our results showed that bystander T cells were not increased in frequency in treatment-naïve MS patients compared with HD. Moreover, $CD4^+$ and $CD8^+$ bystander T cells did not differ in any of the evaluated activation markers between HD and MS patients in our cohort, suggesting that bystander activation may be highly dependent on the inflammatory context.

An early study in the EAE mouse model suggested that a viral infection can prime animals for autoimmune diseases, which are then triggered by a nonspecific challenge or infection, even long after the initial infection has been eradicated [189]. At the same time, *Klebsiella pneumoniae*–induced bystander activation of $CD4^+$ Trm, previously generated in response to *Bordetella pertussis*, in lung and nasal tissues was shown to reduce bacterial burden through IL-17A production [190].
Together, these observations may explain why the precise role and characterization of bystander T cells remain elusive, likely due to the extreme functional heterogeneity these cells can acquire.

In both HD and MS cohorts, virus-induced bystander $CD4^+$ T cells expressed higher levels of CCR6 than their antigen-specific counterparts, which instead showed increased CD137 expression. CCR6 is a particularly relevant marker, as it is associated with Th17 and Th1-17 phenotypes and homing to inflamed tissues. Moreover, CCR6 depletion in the EAE mouse model blocked the early entry of pathogenic Th17 cells into the CNS [191]. CCR6 expression in Th17 cells has also been linked to other potentially pathogenic markers, such as CD161 and CCR2. Indeed, double-positive $CCR6^+CCR2^+$ $CD4^+$ T cells were shown to be pathogenic in MS patients and to produce high levels of IFN-γ and GM-CSF in response to pro-inflammatory cytokines [192].

CD161 deserves emphasis in this context since it is tightly linked to human IL-17-producing programs and commonly co-segregates with CCR6 and IL-23R in Th17-lineage cells. Importantly for MS, CD161high $CD8^+$ T cells have been reported to be enriched in pwMS, can migrate into the MS brain , and have been found within intralesional infiltrates and ectopic B-cell follicles-supporting the broader concept that innate-like/Th17-skewed $CD161^+$ T cells can participate in compartmentalized CNS inflammation[193,194].

In vitro proliferation experiments performed on pre-virus-activated, sorted bystander (CD3 high CD69^{+}) and antigen-specific (CD3 low) CD4^{+} T cells derived from five HD donors showed that bystander T cells did not efficiently proliferate in response to the same viral peptides. Moreover, bystander CD4^{+} T cells displayed lower expression of CD25, CD278, and CD137, but higher levels of CD69 and CD161, already under steady-state conditions. Functional assays performed on the same cell lines further revealed that, in contrast to antigen-specific CD4^{+} CD3 low cells—which predominantly produced IFN-γ, GM-CSF, and TNF-α, consistent with a Th1 phenotype—bystander CD4^{+} CD3 high cells also produced IL-17, IL-22, and IL-10, suggesting a skewing toward a Th17 or Th1-17 phenotype.

This pattern supports our central hypothesis that CD3 high cells contain a biologically distinct pool of bystander-activated T cells that can nonetheless be pathogenic: they are less classically activated (reduced CD25/CD137, limited peptide-driven proliferation) yet display a Th17/Th1-17-like effector potential (CCR6/CD161, IL-17/IL-22 ± IL-10). In MS, such cells could be particularly relevant at CNS borders, where cytokine-rich milieus may repeatedly license them independent of cognate antigen, thereby sustaining inflammation even when antigen-specific signals fluctuate.

Prompted by these encouraging results, we searched for this pro-inflammatory signature in our scRNAseq data. Our analysis identified nine clusters, two of which—cluster 0 and cluster 7—were enriched in cytokine-stimulated and PEP CD3 high conditions, respectively, in both HD and MS patients. Notably, CCR6 was significantly enriched in cytokine-stimulated conditions, and its expression largely overlapped with clusters 0 and 7 on the UMAP. Conversely, CD137 was predominantly expressed in the PEP CD3 low condition and showed an almost complementary expression pattern to CCR6. These data suggest that CD137 represents a robust marker of antigen specificity in CD4^{+} T cells and could be used to discriminate activated bystander CD4^{+} T cells.

Notably, cytokines alone can preferentially activate CD161+ T-cell populations (including MAIT-like and other innate-like T cells) via IL-12+IL-18 in a TCR-independent manner—providing a mechanistic bridge between our cytokine condition and the emergence of CD161-linked inflammatory states.

Furthermore, cluster 0, and to a lesser extent cluster 7, exhibited high expression levels of additional pro-inflammatory cytokines and molecules, including *ltb, ccr2, il-22, tnfsf13b* (BAFF) and *il-32*.

IL-32 is a particularly interesting cytokine, highly pro-inflammatory and implicated in the pathogenesis of several AIDs, especially those of a rheumatic nature[195]. Moreover, serum and plasma levels of IL-32 have been reported to be increased in MS and NMO, respectively[196,197].

Cluster 7 was instead characterized by very high expression of interferon-stimulated genes, such as *ifit1, ifit2, ifit3,* and *isg15,* indicative of a strong antiviral response. Interestingly, IFN-γ was mainly produced by clusters 5 and 6, which were identified as antigen-specific $CD4^+$ T cells and Tfh cells, respectively, with the latter being expanded exclusively in the PEP CD3 low condition. IFN-γ production almost completely overlapped with *cd40lg* (CD154) expression in these two clusters. However, CD154 was also detected, albeit at lower levels, in clusters 0 and 7, suggesting that this marker may be more promiscuous in identifying antigen-specific $CD4^+$ T cells.

Tertiary lymphoid tissues (TLTs) are aggregates of T and B cells that resemble secondary lymphoid organs and arise at sites of chronic inflammation, where they act as reservoirs for autoreactive lymphocytes. TLTs have been described in several autoimmune diseases, including RA, SLE, and Sjögren's syndrome. In MS, TLTs have been observed in the meninges of patients with secondary progressive MS, and recent evidence suggests that these structures may also be present at early stages of the disease[198,199]. Both Th17 cells and lymphotoxins A and B are known to be involved in TLT formation. In particular, LTA and LTB expression by Th17 cells appears to be required to initiate TLT organization in EAE [200]. BAFF is a crucial cytokine that regulates B-cell maturation, survival and differentiation which overexpression has been associated to several AIDs, including MS, and TLTs formations[201–203].

Mechanistically, the IL-17/IL-22 + lymphotoxin axis is particularly relevant for compartmentalized inflammation: IL-17 and IL-22 can promote meningeal stromal remodeling and support the development of lymphoid-like stromal networks, while the LT pathway helps organize and stabilize TLT architecture, together creating a niche that can perpetuate local Th17-skewed responses[200].

In addition, a study by Kaufmann et al. (2021) identified hybrid Th17-Tfh cells in newly natalizumab-treated MS patients, suggesting a potential role for these cells in disease pathogenesis. These Th17-Tfh cells were characterized by scRNAseq as expressing *ltb, klrb1*(CD161), *icos*(CD278), *aqp3, itga4*(VLA4), and *tnfrsf25* [204]. Strikingly, this gene signature closely resembles the top upregulated genes identified in our clusters 0 and 7 (Fig. 15A), suggesting that bystander T cells, likely represented within these clusters, may preferentially adopt this phenotype under certain

conditions. Moreover, the high expression of *ltb* and BAFF further suggests that bystander T cells may contribute to TLT formation in MS patients.

TCR analysis of our scRNAseq data revealed that MS patients shared a higher number of CDR3 sequences with MS-derived TCR datasets, particularly those obtained from brain lesions and peripheral blood. Notably, two out of three MS patients in our cohort -but none of the HD - harbored CDR3 sequences previously described as specific for PMP-22. One of these patients also possessed one additional CDR3 sequence highly similar (differing by only one amino acid) to sequences reported to recognize MBP. Case reports have described patients with Charcot–Marie–Tooth disease type 1A (CMT1A) who subsequently developed MS. In these cases, PMP-22 overexpression—the target protein in CMT1A—may have triggered CNS autoimmunity through molecular mimicry [205,206]. PMP-22 is involved in myelin formation and maintenance, and alterations in its gene cause several peripheral neuropathies [207]. MBP is the second most abundant protein in myelin and has long been proposed as a candidate autoantigen in MS, particularly in EAE models. However, in CIS patients, no correlation was found between serum anti-myelin antibodies (anti-MBP and anti-MOG) and subsequent demyelinating events. In contrast, cross-reactivity between MBP and Epstein–Barr virus (EBV) proteins, such as EBNA-1, has been demonstrated, suggesting that strong anti-EBV immune responses may also target myelin [208].

In conclusion, we identified the lack of CD3 downregulation upon stimulation and CCR6 upregulation as potential markers of bystander $CD4^+$ T cells. We also confirmed their potentially pathogenic Th17-like phenotype through both in vitro and scRNAseq analyses. Notably, clusters enriched in cytokine-stimulated and PEP CD3 high conditions displayed a distinct super-inflammatory signature—including *ltb, il-32, baff, ccr2, cd161,* and *il-22*—that may instruct CNS stromal cells to establish a pro-TLT niche. These findings suggest that activated bystander T cells may contribute to MS autoimmunity by promoting the formation of autoreactive TLTs.

Taken together, our data support the hypothesis that, in MS patients, CNS damage and inflammation, triggered by infection or other insults recall low-affinity autoreactive T and B cells that are already prone to nonspecific activation. Recent studies have demonstrated that activated marginal zone B cells (MZB), an IgM-producing B-cell subset, are the most efficient producers of IL-6 and TNF-α, two crucial cytokines driving Th17 phenotype skewing. MZB have emerged as key players in several AIDs, not only due to their pro-inflammatory cytokine secretion but also because of their high efficiency as self-APCs[209]. The local inflammatory milieu supported by MZB promotes bystander activation of T cells, followed by differentiation toward a Th17-like phenotype characterized by

CCR6, CCR2, IL-17, IL-22, IL-32, and CD161 expression. Moreover, LTβ and BAFF expression by these potentially pathogenic Th17 cells may instruct CNS stromal cells to establish a pro-TLT niche. Bystander-activated Th17 T cells and MZB would then cluster within TLTs, further exacerbating inflammation and predisposing to CNS autoimmunity or MS onset. Additionally, CNS damage would expose normally sequestered T-cell autoantigens, such as PMP-22 and MBP, thereby selecting more autoreactive clones or activating them through molecular mimicry. Targeting bystander T cells, MZB, and TLT formation may therefore represent a promising future therapeutic strategy for MS, interrupting the self-sustaining cycle of autoimmunity generated by interactions among these cell populations.

Further studies are required to complete the characterization of bystander T cells, and a comprehensive understanding of the mechanisms underlying MS onset and progression is still needed.

To broaden the relevance of these observations beyond MS, we also leveraged our Alzheimer's disease mouse model data as an independent CNS-compartment framework: by mapping the origin and activation state of brain-infiltrating T cells in a neurodegenerative setting, we could ask whether the same inflammation-driven, tissue-context-dependent principles that shape CD3 high bystander-like programs in MS also apply when immune activation occurs at CNS borders and within the parenchyma.

The characterization of brain-resident T cells under homeostatic conditions is critically important for understanding their role in neurological diseases. Our results showed that, in WT mice, the majority of brain-associated T cells originated from the meninges (approximately 63%), while only about 20% were likely parenchymal. Confocal microscopy data further suggested that most of these parenchymal T cells were of $CD8^+$ identity.

Interestingly, when comparing lymphocyte infiltration between WT mice and the 5xFAD mouse model, we observed an increased number of T cells in specific brain regions -including the cortex, corpus callosum, hippocampus and olfactory bulb - of 5xFAD mice. However, flow cytometry data did not fully support this observation, likely due to limitations associated with the T-cell isolation technique. In our experiments, most T cells were $CD4^+$ and did not co-express CD103 and CD69, which are canonical markers of tissue residency. In contrast, $CD8^+$ T cells were predominantly $CD103^+$, suggesting that $CD8^+$ lymphocytes represent the true parenchymal T-cell population, in line with our confocal microscopy findings in healthy mice.

This hypothesis is supported by a study by Su et al. (2023), which demonstrated preferential recruitment of peripheral blood $CD8^+$ T cells to plaque-associated regions in 5xFAD mice, mediated by CXCR6[210]. Moreover, Kedia et al. reported that $CD8^+$ T cells promote the progressive accumulation of aberrantly interferon-activated microglia with myelin-damaging activity in 5xFAD mice[211].

In conclusion, our data suggest a significant role for T cell–mediated inflammation in Alzheimer's disease. If confirmed in humans, targeting this immune component could represent a promising strategy to delay disease onset or slow its progression.

References

1. Buchmann, K. Evolution of Innate Immunity: Clues from Invertebrates via Fish to Mammals. *Front. Immunol.* **5**, (2014).
2. Desjardins, M., Houde, M. & Gagnon, E. Phagocytosis: the convoluted way from nutrition to adaptive immunity. *Immunol. Rev.* **207**, 158–165 (2005).
3. Dzik, J. M. The ancestry and cumulative evolution of immune reactions. *Acta Biochim. Pol.* **57**, (2010).
4. Schluter SF, M. J. 'Big Bang' emergence of the combinatorial immune system. *Dev. Comp. Immunol.* **23**, 107–111 (1999).
5. Matsunaga, T. & Rahman, A. What brought the adaptive immune system to vertebrates? - The jaw hypothesis and the seahorse. *Immunol. Rev.* **166**, 177–186 (1998).
6. Wang, R. *et al.* The interaction of innate immune and adaptive immune system. *MedComm* **5**, e714 (2024).
7. Marshall, J. S., Warrington, R., Watson, W. & Kim, H. L. An introduction to immunology and immunopathology. *Allergy Asthma Clin. Immunol.* **14**, 49 (2018).
8. Borregaard, N. Neutrophils, from Marrow to Microbes. *Immunity* **33**, 657–670 (2010).
9. Stone, K. D., Prussin, C. & Metcalfe, D. D. IgE, mast cells, basophils, and eosinophils. *J. Allergy Clin. Immunol.* **125**, S73–S80 (2010).
10. Merad, M., Sathe, P., Helft, J., Miller, J. & Mortha, A. The Dendritic Cell Lineage: Ontogeny and Function of Dendritic Cells and Their Subsets in the Steady State and the Inflamed Setting. *Annu. Rev. Immunol.* **31**, 563–604 (2013).
11. Guilliams, M., Mildner, A. & Yona, S. Developmental and Functional Heterogeneity of Monocytes. *Immunity* **49**, 595–613 (2018).
12. Lavin, Y., Mortha, A., Rahman, A. & Merad, M. Regulation of macrophage development and function in peripheral tissues. *Nat. Rev. Immunol.* **15**, 731–744 (2015).

13. Caligiuri, M. A. Human natural killer cells. *Blood* (2008).
14. Rebuffet, L. *et al.* High-dimensional single-cell analysis of human natural killer cell heterogeneity. *Nat. Immunol.* **25**, 1474–1488 (2024).
15. Vivier, E. *et al.* Innate Lymphoid Cells: 10 Years On. *Cell* **174**, 1054–1066 (2018).
16. Sun, L., Su, Y., Jiao, A., Wang, X. & Zhang, B. T cells in health and disease. *Signal Transduct. Target. Ther.* **8**, 235 (2023).
17. Cyster, J. G. & Allen, C. D. C. B Cell Responses: Cell Interaction Dynamics and Decisions. *Cell* **177**, 524–540 (2019).
18. Sun, L. *et al.* Innate-adaptive immunity interplay and redox regulation in immune response. *Redox Biol.* **37**, 101759 (2020).
19. Carpenter, S. & O'Neill, L. A. J. From periphery to center stage: 50 years of advancements in innate immunity. *Cell* **187**, 2030–2051 (2024).
20. Xu, Q., Tang, Y. & Huang, G. Innate immune responses in RNA viral infection. *Front. Med.* **15**, 333–346 (2021).
21. Yang, Q., Jeremiah Bell, J. & Bhandoola, A. T-cell lineage determination. *Immunol. Rev.* **238**, 12–22 (2010).
22. Staal, F. J. T., Wiekmeijer, A., Brugman, M. H. & Pike-Overzet, K. The functional relationship between hematopoietic stem cells and developing T lymphocytes. *Ann. N. Y. Acad. Sci.* **1370**, 36–44 (2016).
23. Dutta, A., Zhao, B. & Love, P. E. New insights into TCR β-selection. *Trends Immunol.* **42**, 735–750 (2021).
24. Rothenberg, E. V. The β-selection step shapes T-cell identity. *Nature* **613**, 440–442 (2023).
25. Mandl, J. N., Monteiro, J. P., Vrisekoop, N. & Germain, R. N. T Cell-Positive Selection Uses Self-Ligand Binding Strength to Optimize Repertoire Recognition of Foreign Antigens. *Immunity* **38**, 263–274 (2013).

26. Palmer, E. Negative selection — clearing out the bad apples from the T-cell repertoire. *Nat. Rev. Immunol.* **3**, 383–391 (2003).

27. Taniuchi, I. CD4 Helper and CD8 Cytotoxic T Cell Differentiation. *Annu. Rev. Immunol.* **36**, 579–601 (2018).

28. Shah, K., Al-Haidari, A., Sun, J. & Kazi, J. U. T cell receptor (TCR) signaling in health and disease. *Signal Transduct. Target. Ther.* **6**, 412 (2021).

29. Klebanoff, C. A., Chandran, S. S., Baker, B. M., Quezada, S. A. & Ribas, A. T cell receptor therapeutics: immunological targeting of the intracellular cancer proteome. *Nat. Rev. Drug Discov.* **22**, 996–1017 (2023).

30. Bettini, M. L. *et al.* Cutting Edge: CD3 ITAM Diversity Is Required for Optimal TCR Signaling and Thymocyte Development. *J. Immunol.* **199**, 1555–1560 (2017).

31. Mørch, A. M., Bálint, Š., Santos, A. M., Davis, S. J. & Dustin, M. L. Coreceptors and TCR Signaling – the Strong and the Weak of It. *Front. Cell Dev. Biol.* **8**, 597627 (2020).

32. Liu, H., Rhodes, M., Wiest, D. L. & Vignali, D. A. A. On the Dynamics of TCR:CD3 Complex Cell Surface Expression and Downmodulation. *Immunity* **13**, 665–675 (2000).

33. Sattler, A. *et al.* CD3 downregulation identifies high-avidity, multipotent SARS-CoV-2 vaccine– and recall antigen–specific Th cells with distinct metabolism. *JCI Insight* **9**, e166833 (2024).

34. Valitutti, S., Müller, S., Cella, M., Padovan, E. & Lanzavecchia, A. Serial triggering of many T-cell receptors by a few peptide–MHC complexes. *Nature* **375**, 148–151 (1995).

35. Qin, Z. & Xu, T. Deciphering the deterministic role of TCR signaling in T cell fate determination. *Front. Immunol.* **16**, 1562248 (2025).

36. Market, E. & Papavasiliou, F. N. V(D)J Recombination and the Evolution of the Adaptive Immune System. *PLoS Biol.* **1**, e16 (2003).

37. Elhanati, Y., Sethna, Z., Callan, C. G., Mora, T. & Walczak, A. M. Predicting the spectrum of TCR repertoire sharing with a data-driven model of recombination. *Immunol. Rev.* **284**, 167–179 (2018).

38. Gray, J. I., Westerhof, L. M. & MacLeod, M. K. L. The roles of resident, central and effector memory CD 4 T-cells in protective immunity following infection or vaccination. *Immunology* **154**, 574–581 (2018).

39. Masopust, D. *et al.* Guidelines for T cell nomenclature. *Nat. Rev. Immunol.* https://doi.org/10.1038/s41577-025-01238-2 (2025) doi:10.1038/s41577-025-01238-2.

40. Tian, Y. *et al.* Unique phenotypes and clonal expansions of human CD4 effector memory T cells re-expressing CD45RA. *Nat. Commun.* **8**, 1473 (2017).

41. Türk, L. *et al.* Cytotoxic CD8+ Temra cells show loss of chromatin accessibility at genes associated with T cell activation. *Front. Immunol.* **15**, 1285798 (2024).

42. Kamali, A. N. *et al.* A role for Th1-like Th17 cells in the pathogenesis of inflammatory and autoimmune disorders. *Mol. Immunol.* **105**, 107–115 (2019).

43. Toghi, M., Bitarafan, S. & Ghafouri-Fard, S. Pathogenic Th17 cells in autoimmunity with regard to rheumatoid arthritis. *Pathol. - Res. Pract.* **250**, 154818 (2023).

44. Plank, M. W. *et al.* Th22 Cells Form a Distinct Th Lineage from Th17 Cells In Vitro with Unique Transcriptional Properties and Tbet-Dependent Th1 Plasticity. *J. Immunol.* **198**, 2182–2190 (2017).

45. Jiang, Q. *et al.* Role of Th22 Cells in the Pathogenesis of Autoimmune Diseases. *Front. Immunol.* **12**, 688066 (2021).

46. Plitas, G. & Rudensky, A. Y. Regulatory T Cells: Differentiation and Function. *Cancer Immunol. Res.* **4**, 721–725 (2016).

47. Crotty, S. Follicular Helper CD4 T Cells (T_{FH}). *Annu. Rev. Immunol.* **29**, 621–663 (2011).

48. Koh, C.-H., Lee, S., Kwak, M., Kim, B.-S. & Chung, Y. CD8 T-cell subsets: heterogeneity, functions, and therapeutic potential. *Exp. Mol. Med.* **55**, 2287–2299 (2023).

49. St. Paul, M. & Ohashi, P. S. The Roles of CD8+ T Cell Subsets in Antitumor Immunity. *Trends Cell Biol.* **30**, 695–704 (2020).

50. Bishop, G. A. & Hostager, B. S. The CD40–CD154 interaction in B cell–T cell liaisons. *Cytokine Growth Factor Rev.* **14**, 297–309 (2003).

51. Poloni, C. *et al.* T-cell activation–induced marker assays in health and disease. *Immunol. Cell Biol.* **101**, 491–503 (2023).

52. Etxeberria, I., Glez-Vaz, J., Teijeira, Á. & Melero, I. New emerging targets in cancer immunotherapy: CD137/4-1BB costimulatory axis. *ESMO Open* **4**, e000733 (2019).

53. Li, W., Liang, L., Liao, Q., Li, Y. & Zhou, Y. CD38: An important regulator of T cell function. *Biomed. Pharmacother.* **153**, 113395 (2022).

54. Diedrich-Möhring, M., Epplen, J. T. & Schendel, D. J. Enhanced expression of HLA-class II molecules on activated human T lymphocytes following treatment with tumor necrosis factor alpha. *Hum. Immunol.* **31**, 286–292 (1991).

55. Salgado, F. J. *et al.* Interleukin-dependent modulation of HLA-DR expression on CD4 and CD8 activated T cells. *Immunol. Cell Biol.* **80**, 138–147 (2002).

56. Liu, K. *et al.* IL-15-Activated CD38+HLA-DR+CD8+ T cells induce liver injury in cirrhosis via JAK/STAT5 and PI3K/mTOR pathways. *Sci. Rep.* **15**, 17612 (2025).

57. Long, Q. *et al.* The CD38+HLA-DR+ T cells with activation and exhaustion characteristics as predictors of severity and mortality in COVID-19 patients. *Front. Immunol.* **16**, 1577803 (2025).

58. Simpson, T. R., Quezada, S. A. & Allison, J. P. Regulation of CD4 T cell activation and effector function by inducible costimulator (ICOS). *Curr. Opin. Immunol.* **22**, 326–332 (2010).

59. Timperi, E. & Barnaba, V. CD39 Regulation and Functions in T Cells. *Int. J. Mol. Sci.* **22**, 8068 (2021).

60. Jubel, J. M., Barbati, Z. R., Burger, C., Wirtz, D. C. & Schildberg, F. A. The Role of PD-1 in Acute and Chronic Infection. *Front. Immunol.* **11**, 487 (2020).

61. Saggau, C. *et al.* Autoantigen-specific CD4+ T cells acquire an exhausted phenotype and persist in human antigen-specific autoimmune diseases. *Immunity* **57**, 2416-2432.e8 (2024).

62. Theofilopoulos, A. N., Kono, D. H. & Baccala, R. The multiple pathways to autoimmunity. *Nat. Immunol.* **18**, 716–724 (2017).

63. Liblau, R. S., Latorre, D., Kornum, B. R., Dauvilliers, Y. & Mignot, E. J. The immunopathogenesis of narcolepsy type 1. *Nat. Rev. Immunol.* **24**, 33–48 (2024).

64. Baessler, A. & Vignali, D. A. A. T Cell Exhaustion. *Annu. Rev. Immunol.* **42**, 179–206 (2024).

65. Michot, J. M. *et al.* Immune-related adverse events with immune checkpoint blockade: a comprehensive review. *Eur. J. Cancer* **54**, 139–148 (2016).

66. Singh, R. P. *et al.* Th17 cells in inflammation and autoimmunity. *Autoimmun. Rev.* **13**, 1174–1181 (2014).

67. Sumida, T. S., Cheru, N. T. & Hafler, D. A. The regulation and differentiation of regulatory T cells and their dysfunction in autoimmune diseases. *Nat. Rev. Immunol.* **24**, 503–517 (2024).

68. Skowera, A. *et al.* β-Cell–Specific CD8 T Cell Phenotype in Type 1 Diabetes Reflects Chronic Autoantigen Exposure. *Diabetes* **64**, 916–925 (2015).

69. Wagner, C. A., Roqué, P. J., Mileur, T. R., Liggitt, D. & Goverman, J. M. Myelin-specific CD8+ T cells exacerbate brain inflammation in CNS autoimmunity. *J. Clin. Invest.* **130**, 203–213 (2019).

70. Lee, J. C. *et al.* Gene expression profiling of CD8+ T cells predicts prognosis in patients with Crohn disease and ulcerative colitis. *J. Clin. Invest.* **121**, 4170–4179 (2011).

71. Reich, D. S., Lucchinetti, C. F. & Calabresi, P. A. Multiple Sclerosis. *N. Engl. J. Med.* **378**, 169–180 (2018).

72. Boutitah-Benyaich, I. *et al.* Multiple sclerosis: molecular pathogenesis and therapeutic intervention. *Signal Transduct. Target. Ther.* **10**, 324 (2025).

73. Rolak, L. A. MS: The Basic Facts. *Clin. Med. Res.* **1**, 61–62 (2003).

74. Montalban, X. *et al.* Diagnosis of multiple sclerosis: 2024 revisions of the McDonald criteria. *Lancet Neurol.* **24**, 850–865 (2025).

75. Demir, S. Expanded Disability Status Scale (EDSS) in Multiple Sclerosis. *Cam Sakura Med. J.* **2**, 82–89 (2022).

76. Stadelmann, C., Franz, J. & Nessler, S. Recent developments in multiple sclerosis neuropathology. *Curr. Opin. Neurol.* **38**, 173–179 (2025).

77. Pukoli, D. & Vécsei, L. Smouldering Lesion in MS: Microglia, Lymphocytes and Pathobiochemical Mechanisms. *Int. J. Mol. Sci.* **24**, 12631 (2023).

78. Ciccarelli, O. *et al.* Using the Progression Independent of Relapse Activity Framework to Unveil the Pathobiological Foundations of Multiple Sclerosis. *Neurology* **103**, e209444 (2024).

79. Giovannoni, G. *et al.* Smouldering multiple sclerosis: the 'real MS'. *Ther. Adv. Neurol. Disord.* **15**, 17562864211066751 (2022).

80. De Silvestri, A. *et al.* The Involvement of HLA Class II Alleles in Multiple Sclerosis: A Systematic Review with Meta-analysis. *Dis. Markers* **2019**, 1–7 (2019).

81. Barrie, W. *et al.* Elevated genetic risk for multiple sclerosis emerged in steppe pastoralist populations. *Nature* **625**, 321–328 (2024).

82. Frau, J., Coghe, G., Lorefice, L., Fenu, G. & Cocco, E. Infections and Multiple Sclerosis: From the World to Sardinia, From Sardinia to the World. *Front. Immunol.* **12**, 728677 (2021).

83. D'Anca, M. *et al.* Why Is Multiple Sclerosis More Frequent in Women? Role of the Immune System and of Oral and Gut Microbiota. *Appl. Sci.* **13**, 5881 (2023).

84. Bjornevik, K. *et al.* Longitudinal analysis reveals high prevalence of Epstein-Barr virus associated with multiple sclerosis. *Science* **375**, 296–301 (2022).

85. Sundaresan, B., Shirafkan, F., Ripperger, K. & Rattay, K. The Role of Viral Infections in the Onset of Autoimmune Diseases. *Viruses* **15**, 782 (2023).

86. Vanderlugt, C. J. & Miller, S. D. Epitope spreading. *Curr. Opin. Immunol.* **8**, 831–836 (1996).

87. Fujinami, R. S., Oldstone, M. B., Wroblewska, Z., Frankel, M. E. & Koprowski, H. Molecular mimicry in virus infection: crossreaction of measles virus phosphoprotein or of herpes simplex virus protein with human intermediate filaments. *Proc. Natl. Acad. Sci.* **80**, 2346–2350 (1983).
88. Rojas, M. *et al.* Molecular mimicry and autoimmunity. *J. Autoimmun.* **95**, 100–123 (2018).
89. Pacheco, Y. *et al.* Bystander activation and autoimmunity. *J. Autoimmun.* **103**, 102301 (2019).
90. McRae, B. L., Vanderlugt, C. L., Dal Canto, M. C. & Miller, S. D. Functional evidence for epitope spreading in the relapsing pathology of experimental autoimmune encephalomyelitis. *J. Exp. Med.* **182**, 75–85 (1995).
91. Lanz, T. V. *et al.* Clonally expanded B cells in multiple sclerosis bind EBV EBNA1 and GlialCAM. *Nature* **603**, 321–327 (2022).
92. Van Aalst, S., Ludwig, I. S., Van Der Zee, R., Van Eden, W. & Broere, F. Bystander activation of irrelevant CD4+ T cells following antigen-specific vaccination occurs in the presence and absence of adjuvant. *PLOS ONE* **12**, e0177365 (2017).
93. Wahbeh, F. & Sabatino, J. J. Epstein-Barr Virus in Multiple Sclerosis: Past, Present, and Future. *Neurol. Neuroimmunol. Neuroinflammation* **12**, e200460 (2025).
94. Virtanen, J. O. & Jacobson, S. Viruses and Multiple Sclerosis. (2016).
95. Kalchschmidt, J. S. *et al.* Epstein-Barr virus nuclear protein EBNA3C directly induces expression of AID and somatic mutations in B cells. *J. Exp. Med.* **213**, 921–928 (2016).
96. Lünemann, J. D. *et al.* Elevated Epstein–Barr virus-encoded nuclear antigen-1 immune responses predict conversion to multiple sclerosis. *Ann. Neurol.* **67**, 159–169 (2010).
97. Lindsey, J. W., Hatfield, L. M. & Vu, T. Epstein–Barr virus neutralizing and early antigen antibodies in multiple sclerosis. *Eur. J. Neurol.* **17**, 1263–1269 (2010).
98. Munger, K., Levin, L., O'Reilly, E., Falk, K. & Ascherio, A. Anti-Epstein–Barr virus antibodies as serological markers of multiple sclerosis: a prospective study among United States military personnel. *Mult. Scler. J.* **17**, 1185–1193 (2011).

99. Gabibov, A. G. *et al.* Combinatorial antibody library from multiple sclerosis patients reveals antibodies that cross-react with myelin basic protein and EBV antigen. *FASEB J.* **25**, 4211–4221 (2011).

100. Goldacre, R. Risk of multiple sclerosis in individuals with infectious mononucleosis: a national population-based cohort study using hospital records in England, 2003–2023. *Mult. Scler. J.* **30**, 489–495 (2024).

101. Angelini, D. F. *et al.* Increased CD8+ T Cell Response to Epstein-Barr Virus Lytic Antigens in the Active Phase of Multiple Sclerosis. *PLoS Pathog.* **9**, e1003220 (2013).

102. Van Nierop, G. P. *et al.* Phenotypic and functional characterization of T cells in white matter lesions of multiple sclerosis patients. *Acta Neuropathol. (Berl.)* **134**, 383–401 (2017).

103. Elghali, M. *et al.* From infection to autoimmunity: can COVID-19 spark new auto-immune conditions? *Respir. Med. Case Rep.* **55**, 102216 (2025).

104. Xie, S., Wei, J. & Wang, X. The intersection of influenza infection and autoimmunity. *Front. Immunol.* **16**, 1558386 (2025).

105. Disease-Modifying Therapies. https://www.nationalmssociety.org/managing-ms/treating-ms/disease-modifying-therapies (2025).

106. Dello Russo, C., Scott, K. A. & Pirmohamed, M. Dimethyl fumarate induced lymphopenia in multiple sclerosis: A review of the literature. *Pharmacol. Ther.* **219**, 107710 (2021).

107. McGinley, M. P., Goldschmidt, C. H. & Rae-Grant, A. D. Diagnosis and Treatment of Multiple Sclerosis: A Review. *JAMA* **325**, 765 (2021).

108. Legroux, L. & Arbour, N. Multiple Sclerosis and T Lymphocytes: An Entangled Story. *J. Neuroimmune Pharmacol.* **10**, 528–546 (2015).

109. Siewert, K. *et al.* Unbiased identification of target antigens of CD8+ T cells with combinatorial libraries coding for short peptides. *Nat. Med.* **18**, 824–828 (2012).

110. Hemmer, B., Kerschensteiner, M. & Korn, T. Role of the innate and adaptive immune responses in the course of multiple sclerosis. *Lancet Neurol.* **14**, 406–419 (2015).

111. Kaskow, B. J. & Baecher-Allan, C. Effector T Cells in Multiple Sclerosis. *Cold Spring Harb. Perspect. Med.* **8**, a029025 (2018).

112. Bielekova, B. *et al.* Encephalitogenic potential of the myelin basic protein peptide (amino acids 83–99) in multiple sclerosis: Results of a phase II clinical trial with an altered peptide ligand. *Nat. Med.* **6**, 1167–1175 (2000).

113. Brucklacher-Waldert, V., Stuerner, K., Kolster, M., Wolthausen, J. & Tolosa, E. Phenotypical and functional characterization of T helper 17 cells in multiple sclerosis. *Brain* **132**, 3329–3341 (2009).

114. Ottum, P. A., Arellano, G., Reyes, L. I., Iruretagoyena, M. & Naves, R. Opposing Roles of Interferon-Gamma on Cells of the Central Nervous System in Autoimmune Neuroinflammation. *Front. Immunol.* **6**, (2015).

115. De Weerd, N. A. & Nguyen, T. The interferons and their receptors—distribution and regulation. *Immunol. Cell Biol.* **90**, 483–491 (2012).

116. Tzartos, J. S. *et al.* Interleukin-17 Production in Central Nervous System-Infiltrating T Cells and Glial Cells Is Associated with Active Disease in Multiple Sclerosis. *Am. J. Pathol.* **172**, 146–155 (2008).

117. Montes, M. *et al.* Oligoclonal myelin-reactive T-cell infiltrates derived from multiple sclerosis lesions are enriched in Th17 cells. *Clin. Immunol.* **130**, 133–144 (2009).

118. El-Behi, M. *et al.* The encephalitogenicity of TH17 cells is dependent on IL-1- and IL-23-induced production of the cytokine GM-CSF. *Nat. Immunol.* **12**, 568–575 (2011).

119. Van Langelaar, J. *et al.* T helper 17.1 cells associate with multiple sclerosis disease activity: perspectives for early intervention. *Brain* **141**, 1334–1349 (2018).

120. Saligrama, N. *et al.* Opposing T cell responses in experimental autoimmune encephalomyelitis. *Nature* **572**, 481–487 (2019).

121. Kuhlmann, T. Acute axonal damage in multiple sclerosis is most extensive in early disease stages and decreases over time. *Brain* **125**, 2202–2212 (2002).

122. Sinha, S., Boyden, A. W., Itani, F. R., Crawford, M. P. & Karandikar, N. J. CD8+ T-Cells as Immune Regulators of Multiple Sclerosis. *Front. Immunol.* **6**, (2015).

123. McCoy, L., Tsunoda, I. & Fujinami, R. S. Multiple sclerosis and virus induced immune responses: Autoimmunity can be primed by molecular mimicry and augmented by bystander activation. *Autoimmunity* **39**, 9–19 (2006).

124. Martino, G. Cytokines and immunity in multiple sclerosis: the dual signal hypothesis. *J. Neuroimmunol.* **109**, 3–9 (2000).

125. Doisne, J.-M. *et al.* CD8+ T Cells Specific for EBV, Cytomegalovirus, and Influenza Virus Are Activated during Primary HIV Infection. *J. Immunol.* **173**, 2410–2418 (2004).

126. Kim, J. *et al.* Innate-like Cytotoxic Function of Bystander-Activated CD8+ T Cells Is Associated with Liver Injury in Acute Hepatitis A. *Immunity* **48**, 161-173.e5 (2018).

127. Balint, E. *et al.* Bystander activated CD8+ T cells mediate neuropathology during viral infection via antigen-independent cytotoxicity. *Nat. Commun.* **15**, 896 (2024).

128. Li Causi, E. *et al.* Vaccination Expands Antigen-Specific CD4+ Memory T Cells and Mobilizes Bystander Central Memory T Cells. *PLOS ONE* **10**, e0136717 (2015).

129. Di Genova, G., Savelyeva, N., Suchacki, A., Thirdborough, S. M. & Stevenson, F. K. Bystander stimulation of activated $CD4^+$ T cells of unrelated specificity following a booster vaccination with tetanus toxoid. *Eur. J. Immunol.* **40**, 976–985 (2010).

130. Van Aalst, S., Ludwig, I. S., Van Der Zee, R., Van Eden, W. & Broere, F. Bystander activation of irrelevant CD4+ T cells following antigen-specific vaccination occurs in the presence and absence of adjuvant. *PLOS ONE* **12**, e0177365 (2017).

131. Paprckova, D., Salyova, E., Michalik, J. & Stepanek, O. Bystander activation in memory and antigen-inexperienced memory-like CD8 T cells. *Curr. Opin. Immunol.* **82**, 102299 (2023).

132. Kim, T.-S. & Shin, E.-C. The activation of bystander CD8+ T cells and their roles in viral infection. *Exp. Mol. Med.* **51**, 1–9 (2019).

133. Lee, H.-G., Cho, M.-J. & Choi, J.-M. Bystander CD4+ T cells: crossroads between innate and adaptive immunity. *Exp. Mol. Med.* **52**, 1255–1263 (2020).

134. Polakos, N. K. *et al.* Kupffer Cell-Dependent Hepatitis Occurs during Influenza Infection. *Am. J. Pathol.* **168**, 1169–1178 (2006).

135. Arleevskaya, M. I., Kravtsova, O. A., Lemerle, J., Renaudineau, Y. & Tsibulkin, A. P. How Rheumatoid Arthritis Can Result from Provocation of the Immune System by Microorganisms and Viruses. *Front. Microbiol.* **7**, (2016).

136. Meresse, B. *et al.* Coordinated Induction by IL15 of a TCR-Independent NKG2D Signaling Pathway Converts CTL into Lymphokine-Activated Killer Cells in Celiac Disease. *Immunity* **21**, 357–366 (2004).

137. Dai, Z. *et al.* Normally occurring NKG2D+CD4+ T cells are immunosuppressive and inversely correlated with disease activity in juvenile-onset lupus. *J. Exp. Med.* **206**, 793–805 (2009).

138. Lee, H.-G. *et al.* Pathogenic function of bystander-activated memory-like CD4+ T cells in autoimmune encephalomyelitis. *Nat. Commun.* **10**, 709 (2019).

139. Ferreira, T. B. *et al.* Different interleukin-17-secreting Toll-like receptor^{+} T-cell subsets are associated with disease activity in multiple sclerosis. *Immunology* **154**, 239–252 (2018).

140. Nogai, A. *et al.* Lipopolysaccharide Injection Induces Relapses of Experimental Autoimmune Encephalomyelitis in Nontransgenic Mice via Bystander Activation of Autoreactive CD4+ Cells. *J. Immunol.* **175**, 959–966 (2005).

141. Zhang, J. *et al.* Recent advances in Alzheimer's disease: mechanisms, clinical trials and new drug development strategies. *Signal Transduct. Target. Ther.* **9**, 211 (2024).

142. Chen, X. & Holtzman, D. M. Emerging roles of innate and adaptive immunity in Alzheimer's disease. *Immunity* **55**, 2236–2254 (2022).

143. Kamatham, P. T., Shukla, R., Khatri, D. K. & Vora, L. K. Pathogenesis, diagnostics, and therapeutics for Alzheimer's disease: Breaking the memory barrier. *Ageing Res. Rev.* **101**, 102481 (2024).

144. Kinney, J. W. *et al.* Inflammation as a central mechanism in Alzheimer's disease. *Alzheimers Dement. Transl. Res. Clin. Interv.* **4**, 575–590 (2018).

145. Jay, T. R. *et al.* TREM2 deficiency eliminates TREM2+ inflammatory macrophages and ameliorates pathology in Alzheimer's disease mouse models. *J. Exp. Med.* **212**, 287–295 (2015).

146. Bemiller, S. M. *et al.* TREM2 deficiency exacerbates tau pathology through dysregulated kinase signaling in a mouse model of tauopathy. *Mol. Neurodegener.* **12**, 74 (2017).

147. Dai, L. & Shen, Y. Insights into T-cell dysfunction in Alzheimer's disease. *Aging Cell* **20**, e13511 (2021).

148. Browne, T. C. *et al.* IFN-γ Production by Amyloid β–Specific Th1 Cells Promotes Microglial Activation and Increases Plaque Burden in a Mouse Model of Alzheimer's Disease. *J. Immunol.* **190**, 2241–2251 (2013).

149. Mittal, K. *et al.* CD4 T Cells Induce A Subset of MHCII-Expressing Microglia that Attenuates Alzheimer Pathology. *iScience* **16**, 298–311 (2019).

150. Zhang, J., Ke, K.-F., Liu, Z., Qiu, Y.-H. & Peng, Y.-P. Th17 Cell-Mediated Neuroinflammation Is Involved in Neurodegeneration of Aβ1-42-Induced Alzheimer's Disease Model Rats. *PLoS ONE* **8**, e75786 (2013).

151. Baruch, K. *et al.* Breaking immune tolerance by targeting Foxp3+ regulatory T cells mitigates Alzheimer's disease pathology. *Nat. Commun.* **6**, 7967 (2015).

152. Guillot-Sestier, M.-V. *et al.* Il10 Deficiency Rebalances Innate Immunity to Mitigate Alzheimer-Like Pathology. *Neuron* **85**, 534–548 (2015).

153. Yokoyama, M., Kobayashi, H., Tatsumi, L. & Tomita, T. Mouse Models of Alzheimer's Disease. *Front. Mol. Neurosci.* **15**, 912995 (2022).

154. Oakley, H. *et al.* Intraneuronal β-Amyloid Aggregates, Neurodegeneration, and Neuron Loss in Transgenic Mice with Five Familial Alzheimer's Disease Mutations: Potential Factors in Amyloid Plaque Formation. *J. Neurosci.* **26**, 10129–10140 (2006).

155. Guerrera, G. *et al.* BNT162b2 vaccination induces durable SARS-CoV-2–specific T cells with a stem cell memory phenotype. *Sci. Immunol.* **6**, eabl5344 (2021).

156. De Marco, L. *et al.* Assessment of T-cell Reactivity to the SARS-CoV-2 Omicron Variant by Immunized Individuals. *JAMA Netw. Open* **5**, e2210871 (2022).

157. D'Orso, S. *et al.* Primary and Recall Immune Responses to SARS-CoV-2 in Breakthrough Infection. *Vaccines* **11**, 1705 (2023).

158. Hao, Y. *et al.* Integrated analysis of multimodal single-cell data. *Cell* **184**, 3573-3587.e29 (2021).

159. Sturm, G. *et al.* Scirpy: a Scanpy extension for analyzing single-cell T-cell receptor-sequencing data. *Bioinformatics* **36**, 4817–4818 (2020).

160. Hafemeister, C. & Satija, R. Normalization and variance stabilization of single-cell RNA-seq data using regularized negative binomial regression. *Genome Biol.* **20**, 296 (2019).

161. Choudhary, S. & Satija, R. Comparison and evaluation of statistical error models for scRNA-seq. *Genome Biol.* **23**, 27 (2022).

162. Love, M. I., Huber, W. & Anders, S. Moderated estimation of fold change and dispersion for RNA-seq data with DESeq2. *Genome Biol.* **15**, 550 (2014).

163. R Core Team, R. C. T. R: A Language and Environment for Statistical Computing. *Vienna R Found. Stat. Comput.* https://www.r-project.org/ (2018).

164. Wickham, H. *Ggplot2: Elegant Graphics for Data Analysis*. (Springer International Publishing, Cham, 2016). doi:10.1007/978-3-319-24277-4.

165. Kassambara A, K. A. ggpubr: ggplot2 Based Publication Ready Plots. https://rpkgs.datanovia.com/ggpubr/index.html (2018).

166. Neuwirth, E. RColorBrewer: ColorBrewer Palettes. 1.1-3 https://doi.org/10.32614/CRAN.package.RColorBrewer (2022).

167. Csardi, G. & Nepusz, T. The igraph software package for complex network research. *InterJ Complex Syst* 1695:1–9 (2006).

168. Clarke, E., Sherrill-Mix, S. & Dawson, C. ggbeeswarm: Categorical Scatter (Violin Point) Plots. 0.7.2 https://doi.org/10.32614/CRAN.package.ggbeeswarm (2016).

169. Kolde, R. pheatmap: Pretty Heatmaps. 1.0.13 https://doi.org/10.32614/CRAN.package.pheatmap (2025).

170. Shannon, P. *et al.* Cytoscape: A Software Environment for Integrated Models of Biomolecular Interaction Networks. *Genome Res.* **13**, 2498–2504 (2003).

171. Amoriello, R. *et al.* The TCR Repertoire Reconstitution in Multiple Sclerosis: Comparing One-Shot and Continuous Immunosuppressive Therapies. *Front. Immunol.* **11**, 559 (2020).

172. Amoriello, R. *et al.* TCR repertoire diversity in Multiple Sclerosis: High-dimensional bioinformatics analysis of sequences from brain, cerebrospinal fluid and peripheral blood. *EBioMedicine* **68**, 103429 (2021).

173. Planas, R., Metz, I., Martin, R. & Sospedra, M. Detailed Characterization of T Cell Receptor Repertoires in Multiple Sclerosis Brain Lesions. *Front. Immunol.* **9**, 509 (2018).

174. Salou, M., Nicol, B., Garcia, A. & Laplaud, D.-A. Involvement of CD8+ T Cells in Multiple Sclerosis. *Front. Immunol.* **6**, (2015).

175. Hamm, DE, H., DE. immunoSEQ hsTCRB-V4b Control Data. *Adapt. Biotechnol. Seattle WA USA* https://clients.adaptivebiotech.com/pub/tcrbv4-control (2020).

176. Tickotsky, N., Sagiv, T., Prilusky, J., Shifrut, E. & Friedman, N. McPAS-TCR: a manually curated catalogue of pathology-associated T cell receptor sequences. *Bioinformatics* **33**, 2924–2929 (2017).

177. Shugay, M. *et al.* VDJdb: a curated database of T-cell receptor sequences with known antigen specificity. *Nucleic Acids Res.* **46**, D419–D427 (2018).

178. Xia, Y. *et al.* BCL6-dependent TCF-1+ progenitor cells maintain effector and helper CD4+ T cell responses to persistent antigen. *Immunity* **55**, 1200-1215.e6 (2022).

179. Altosole, T., Rotta, G., Uras, C. R. M., Bornheimer, S. J. & Fenoglio, D. An optimized flow cytometry protocol for simultaneous detection of T cell activation induced markers and intracellular cytokines: Application to SARS-CoV-2 immune individuals. *J. Immunol. Methods* **515**, 113443 (2023).

180. Ferragut, F. *et al.* Activation-induced marker assays for identification of *TRYPANOSOMA CRUZI* -specific CD4 or CD8 T cells in chronic Chagas disease patients. *Immunology* **169**, 185–203 (2023).

181. Reiss, S. *et al.* Comparative analysis of activation induced marker (AIM) assays for sensitive identification of antigen-specific CD4 T cells. *PLOS ONE* **12**, e0186998 (2017).

182. Maggi, L. *et al.* CD161 is a marker of all human IL-17-producing T-cell subsets and is induced by RORC. *Eur. J. Immunol.* **40**, 2174–2181 (2010).

183. Súkeníková, L. *et al.* Autoreactive T cells target peripheral nerves in Guillain–Barré syndrome. *Nature* **626**, 160–168 (2024).

184. Sethi, D. K. *et al.* A highly tilted binding mode by a self-reactive T cell receptor results in altered engagement of peptide and MHC. *J. Exp. Med.* **208**, 91–102 (2011).

185. Smolders, J., Van Luijn, M. M., Hsiao, C.-C. & Hamann, J. T-cell surveillance of the human brain in health and multiple sclerosis. *Semin. Immunopathol.* **44**, 855–867 (2022).

186. Liston, A., Dooley, J. & Yshii, L. Brain-resident regulatory T cells and their role in health and disease. *Immunol. Lett.* **248**, 26–30 (2022).

187. Smolders, J. *et al.* Tissue-resident memory T cells populate the human brain. *Nat. Commun.* **9**, 4593 (2018).

188. Smolders, J., Hsiao, C.-C., Huitinga, I. & Hamann, J. Resident T cells in the healthy and multiple sclerosis brain. *Trends Immunol.* S147149062500314X (2026) doi:10.1016/j.it.2025.12.006.

189. Diethilde J Theil, Ikuo Tsunoda, Fe. Viruses can silently prime for and trigger central nervous system autoimmune disease. *J. Neurovirol.* **7**, 220–227 (2001).

190. Cornelis, R. & Shulman, Z. Bystander activation of tissue-resident memory CD4 T cells: Getting by with a little help from unfamiliar T-cell friends. *Eur. J. Immunol.* **53**, 2350413 (2023).

191. Reboldi, A. *et al.* C-C chemokine receptor 6–regulated entry of TH-17 cells into the CNS through the choroid plexus is required for the initiation of EAE. *Nat. Immunol.* **10**, 514–523 (2009).

192. Parween, F. *et al.* Migration arrest and transendothelial trafficking of human pathogenic-like Th17 cells are mediated by differentially positioned chemokines. *Nat. Commun.* **16**, 1978 (2025).

193. Annibali, V. *et al.* CD161highCD8+T cells bear pathogenetic potential in multiple sclerosis. *Brain* **134**, 542–554 (2011).

194. Schirmer, L., Rothhammer, V., Hemmer, B. & Korn, T. Enriched $CD161^{high}$ $CCR6^{+}$ γδ T Cells in the Cerebrospinal Fluid of Patients With Multiple Sclerosis. *JAMA Neurol.* **70**, 345 (2013).

195. Kwon, O. C., Park, M.-C. & Kim, Y.-G. Interleukin-32 as a biomarker in rheumatic diseases: A narrative review. *Front. Immunol.* **14**, 1140373 (2023).

196. Morsaljahan, Z. *et al.* Association between interleukin-32 polymorphism and multiple sclerosis. *J. Neurol. Sci.* **379**, 144–150 (2017).

197. Wang, H. *et al.* Increased Plasma Interleukin-32 Expression in Patients with Neuromyelitis Optica. *J. Clin. Immunol.* **33**, 666–670 (2013).

198. Negron, A., Stüve, O. & Forsthuber, T. G. Ectopic Lymphoid Follicles in Multiple Sclerosis: Centers for Disease Control? *Front. Neurol.* **11**, 607766 (2020).

199. Kolz, A. *et al.* T–B cell cooperation in ectopic lymphoid follicles propagates CNS autoimmunity. *Sci. Immunol.* **10**, (2025).

200. Pikor, N. B. *et al.* Integration of Th17- and Lymphotoxin-Derived Signals Initiates Meningeal-Resident Stromal Cell Remodeling to Propagate Neuroinflammation. *Immunity* **43**, 1160–1173 (2015).

201. Kang, S. *et al.* BAFF Induces Tertiary Lymphoid Structures and Positions T Cells within the Glomeruli during Lupus Nephritis. *J. Immunol.* **198**, 2602–2611 (2017).

202. Li, L. *et al.* The role of B cell-activating factor system in autoimmune diseases: mechanisms, disease implications, and therapeutic advances. *Front. Immunol.* **16**, 1538555 (2025).

203. Steri, M. *et al.* Overexpression of the Cytokine BAFF and Autoimmunity Risk. *N. Engl. J. Med.* **376**, 1615–1626 (2017).

204. Kaufmann, M. *et al.* Identifying CNS-colonizing T cells as potential therapeutic targets to prevent progression of multiple sclerosis. *Med* **2**, 296-312.e8 (2021).

205. Koros, C., Evangelopoulos, M.-E., Kilidireas, C. & Andreadou, E. Central Nervous System Demyelination in a Charcot-Marie-Tooth Type 1A Patient. *Case Rep. Neurol. Med.* **2013**, 1–4 (2013).

206. Doğan, Y., Gül, Ş., Ceylan, A. C. & Kutsal, Y. G. A special association between Charcot-Marie-Tooth type 1A disease and relapsing remitting multiple sclerosis. *Mult. Scler. Relat. Disord.* **35**, 83–85 (2019).

207. Cesaroni, C. A. *et al.* PMP22-Related Neuropathies: A Systematic Review. *Genes* **16**, 1279 (2025).

208. Thomas, O. G. & Olsson, T. Mimicking the brain: Epstein-Barr virus and foreign agents as drivers of neuroimmune attack in multiple sclerosis. *Front. Immunol.* **14**, 1304281 (2023).

209. Palm, A.-K. E. & Kleinau, S. Marginal zone B cells: From housekeeping function to autoimmunity? *J. Autoimmun.* **119**, 102627 (2021).

210. Su, W. *et al.* CXCR6 orchestrates brain CD8+ T cell residency and limits mouse Alzheimer's disease pathology. *Nat. Immunol.* **24**, 1735–1747 (2023).

211. Kedia, S. *et al.* T cell-mediated microglial activation triggers myelin pathology in a mouse model of amyloidosis. *Nat. Neurosci.* **27**, 1468–1474 (2024).